Development of a Regional-Scale Numerical Environmental Multimedia Modeling (RNEMM) Approach to Assess Spatial Eco-Environmental Exposure Risk of Contaminants

Jinxin Dong

A Thesis

In the Department

of

Building, Civil and Environmental Engineering

Presented in Partial Fulfillment of the Requirements

For the Degree of

Doctor of Philosophy (Civil Engineering) at Concordia University

Montreal, Quebec, Canada

December 2020

CONCORDIA UNIVERSITY

School of Graduate Studies

This is to certify that the thesis prepared

By: Jinxin Dong

Entitled: Development of a Regional-scale Numerical Environmental Multimedia Modeling (RNEMM) Approach to Assess Spatial Eco-Environmental Exposure Risk of Contaminants

and submitted in partial fulfillment of the requirements for the degree of

Doctor of Philosophy (Civil Engineering)

Complies with the regulations of the University and meets the accepted standards with respect to originality and quality.

Signed by the final examining committee:

_____ Chair

Dr. Arash Mohammadi

_____ External Examiner

Dr. Zhiming Qi

_____ External to Program

Dr. Yong Zeng

_____ Examiner

Dr. Ali Nazemi

_____ Examiner

Dr. Biao Li

_____ Thesis Supervisor

Dr. Zhi Chen

Approved by _____

Dr. Ashutosh Bagchi, Chair of Department

16 December 2020

_____

Dr. Mourad Debbabi, Dean, Faculty of Engineering and Computer Science

ABSTRACT

Development of a Regional-Scale Numerical Environmental Multimedia Modeling (RNEMM) Approach to Assess Spatial Eco-Environmental Exposure Risk of Contaminants

Jinxin Dong, Ph.D.

Concordia University, 2020

Environmental multimedia models (EMMs) have been used in environmental risk assessment since they reflect the interactive transport and fate processes of chemicals within multi-compartmental environmental systems. However, these existing models are limited in their abilities to predict contaminant concentrations in the multimedia environment at a better temporal-spatial resolution, especially for regional scale site contamination problems.

A novel regional numerical multimedia environmental modeling (RNEMM) approach is developed in this thesis for the multimedia environment. RNEMM consists of a water quality simulation module for river network system, a gaseous phase simulation module, a mass balance analysis module for soil, a food web module and a health risk assessment module. Two key developments are achieved to integrate these modules into the entire system: integrating different modules with non-uniform boundary conditions and inter-media flux, and coupling the modules based on practical considerations of regional scale multimedia contamination problems. Importantly, four validations related to the RNEMM development are conducted. First, a new model in 1D and 2D are established through considering the non-uniform boundary conditions and inter-media flux. Numerical algorithms, including the finite element method (FEM) and finite volume method (FVM), are used to solve the governing equations. The measured results in two landfill cases are used to validate the spatial and temporal accuracy of predicted concentrations obtained from these models. Second, a regional spatial environmental multimedia model (RSEMM)

is developed by coupling the modules based on a different concept (i.e., a water quality model for the river network and a fugacity model) to provide predicted concentration profiles of contaminants at a regional scale. A third regional site validation is conducted through a case in the urban area of Tianjin City and reasonable results have been obtained through the comparison of simulated and measured results.

Subsequently, based on the two key developments, a regional numerical multimedia environmental modeling (RNEMM) approach is developed and tested by assessing spatial eco-environmental exposure risk of perfluorooctane sulfonate (PFOS) in the pearl river basin. The exposure risk assessment for children and adults is further conducted based on the integrated risk assessment model. In conclusion, the RNEMM can serve as a comprehensive management tool to assess and control the exposure risks associated with emerging contaminants on regional water, soil, and ecosystem at an adequate spatial-temporal resolution.

ACKNOWLEDGMENTS

I would like to express my great appreciation to my supervisor Dr. Zhi Chen for his patience, motivation and guidance throughout my Ph.D. study. He guided me into the fantastic world of scientific research and his academic opinions are essential for completing this dissertation. His suggestions and support for my research and future plan are invaluable. His good personality will affect my entire life.

My thanks also go to all the other members of my committee: Dr. Arash Mohammadi, Dr. Ali Nazemi, Dr. Yong Zeng, Dr. Biao Li and Dr. Zhiming Qi for contributing their time and providing valuable advice.

Foremost, I am greatly indebted to my parents. Their unconditional support and encouragement push me farther than I thought I could go. I would especially like to thank my girlfriend, Ziyang Zhang, who made this long journey much easier. Their love forms the root of my happiness.

Last but not least, I would like to express my appreciation to all my friends and group fellows: Zunaira Asif, Ali Zakar, Samia Ben Hammouda, Lu Chen, Yinying Zhu, Zhaoyang Yang, Chudi Wu and Yanbin Zhuang, who have helped me to complete this thesis.

TABLE OF CONTENTS

LIST OF TABLES

TABLE OF FIGURES

LIST OF SYMBOLS

A_x:	length (L)
A_y:	width (L)
ADI:	acceptable daily intake (M/M T)
AT:	averaging time (T)
b:	coefficient for each parameter *x*
BCF:	bioconcentration factor (L^3/M)
BW:	body weight of an adult or child (M/person)
C:	contaminant concentration
C^k:	contaminant concentration in the *k* zone (M/L^3)
C_0:	initial concentration in the source zone (M/L^3)
$\overline{C}_a$:	average air concentration (M/L^3)
$C_{B,i}$:	internal tissue concentration in functional group *i* (M/L^3)
C_{doc}, C_s, C_{ss}, C_t:	contaminant concentrations in DOC, sediment, suspended particulates and total water column (M/M)
C_r:	environmental criterion (M/L^3)
C_u:	upper boundary condition of the source zone (M/L^3)
C_w:	contaminant concentrations in water (M/L^3)
D:	effective diffusion coefficient (L^2/T)
D_a:	active sediment depth (L)
D_{ji}:	inter-compartmental transfer rate from compartment *j* to *i* (M/T Pa)
D_l:	longitudinal dispersion coefficient (L^2/T)
D_t:	vertical dispersion coefficient (L^2/T)
D_x, D_z:	longitudinal and vertical dispersion coefficient (L^2/T)
$D_{A,i}$:	transport rate in the subarea *i* of air compartment (M/T Pa)

D_A, D_E, D_G, D_M, D_W:	transformation rate for diet, egestion, growth dilution, metabolism and respiration (M/T Pa)
D_{Ti}:	total transport and transformation rate in compartment *i* (M/T Pa)
E:	output variable after the parameter perturbation
E_i:	source or sink (M/T)
ED:	exposure duration (T)
EF:	exposure frequency (T/T)
EDI:	estimated daily intake (M/M T)
f_i:	fugacity in compartment *i* (Pa)
f_L:	probability density function
$f_{r,i}$:	fugacity the in subarea *i* of air compartment (Pa)
$f_{w,\,i}$:	fugacity in the subarea *i* of water compartment (Pa)
f_A, f_B, f_w:	chemical fugacity in the food, tissue and water (Pa)
F:	concentration fluxes of deposition (M/L^3 T)
H:	average river depth (L)
I:	flow balance conditions (M/T)
IR_{DW}:	drinking water ingestion rate (L^3/T)
IR_F:	fish consumption rate (M/T)
J:	inter-media flux
k:	input parameter
$k_{a\text{-}s}$:	transfer rate from air to soil by wet and dry deposition (1/T)
k_{doc}:	partition coefficients in DOC (L^3/M)
k_{sdeg}:	degradation rate in soil (1/T)
k_{ss}:	partition coefficients in the suspended particulates (L^3/M)
$k_{s\text{-}a}$:	transfer rate in the soil to air by diffusion (1/T)

$k_{s\text{-}w}$:	transfer rate from soil to freshwater by erosion in the suspended solid and liquid phase (1/T)
$k_{w\text{-}a}$:	transfer rate from water to air by diffusion (1/T)
K_1, K_2:	decay coefficient in the water and sediment zone (1/T)
K_d:	distribution coefficient (L^3/M)
K_e, K_l:	runoff rates of dissolved phase and solids in soil (L/T)
K_{se}, K_w:	degradation rates in the sediment and water zone (1/T)
K_x, K_z:	longitudinal and vertical hydraulic conductivity (L/T)
KEC:	known environmental criteria
L:	locations of the lower boundary for each medium in the *z*-direction (L)
M_a:	contaminant masses in corresponding air zone (M)
M_s:	contaminant masses in soil zone (M)
n:	number of parameters
PEC:	predicted environmental concentration
PNEC:	predicted no-effect concentration
RfD:	reference dose (M/M T)
Q:	discharge (L^3/T)
Q_w:	flow rate (L^3/T)
R:	retardation factor
R^2:	square of the multiple correlation coefficient between model output (Y) and input parameter (x_i)
R_{aw}:	diffusion rate from air to water (L/T)
R_s:	probability of system failure
R_{sa}:	diffusion rate from soil to air (L/T)
R_{wa}:	diffusion rate from water to air (L/T)
RQ:	risk quotient

S:	concentration fluxes of emission (M/L^3 T)
T:	the rate of mass transport (M/T)
$T_{a\text{-}s}$:	inter-media fluxes from air to soil (M/T)
$T_{s\text{-}a}$:	flux from soil to each air cell (M/T)
$T_{w\text{-}a}$:	mass transfer rates between water and air media (M/T)
$T_{w\text{-}s}$:	inter-media mass transfer process from water to soil (M/T)
u_s:	sediment resuspension velocity (L/T)
u_{ss}:	sedimentation velocity (L/T)
v_{dry}:	dry deposition velocity to water (L/T)
v_{wet}:	wet deposition velocity to water (L/T)
V:	velocity (L/T)
V_d:	darcy velocity (L/T)
V_i:	volume of compartment i (L^3)
V_s:	sediment bed velocity (L/T)
V_{un}:	average velocity of fluid in unsaturated zone (L/T)
V_x:	river velocity (L/T)
V_L:	pore water velocity (L/T)
x, y, z:	x-, y- and z-direction, respectively
x_i:	parameter i
Y:	output variable
Z_i:	fugacity capacity in compartment i (M/L^3 Pa)
Z_{sa}, Z_{so}, Z_{un}:	depth of saturated, source and unsaturated zone (L)
Δ_i:	step size of parameter x
ρ:	bulk density (M/L^3)
ρ_{doc}:	concentrations of suspended DOC in the water column (M/L^3)
ρ_s:	bulk density of the active sediment (M/L^3)

ρ_{sa}:	bulk density in saturated zone (M/L^3)
ρ_{so}:	bulk density in source zone (M/L^3)
ρ_{ss}:	concentrations of suspended particulates in the water column (M/L^3)
ρ_{un}:	bulk density in unsaturated zone (M/L^3)
φ_a, φ_w:	volumetric air and water content
φ_{sa}, φ_{so}, φ_{un}:	effective porosity in saturated, source and unsaturated zone
θ:	volumetric moisture content of the soil
μ:	degradation rate (1/T)
μ^*:	absolute mean
σ:	standard deviation

LIST OF ACRONYMS

ADE:	Advection-Dispersion Equation
ADI:	Acceptable Daily Intake
AERMOD:	American Meteorological Society/EPA Regulatory Model
AFFFs:	Application of Aqueous Fire-Fighting Foams
As:	Arsenic
BETR:	Berkeley-Trent
CAFO:	Concentrated Animal Feeding Operations
CEMC:	Canadian Environmental Modelling Centre
Cr:	Chromium
D5:	Decamethylcyclopentasiloxane
D6:	Dodecamethylcyclohexasiloxane
DJB:	Dongjiangbei
DJN:	Dongjiangnan
DOC:	Dissolved Organic Carbon
EMMs:	Environmental Multimedia Models
FDM:	Finite Difference Method
FEM:	Finite Element Method
FVM:	Finite Volume Method
G-CIEMS:	Geo-referenced Multimedia Environmental Fate Model
g-HCH:	g-hexachlorocyclohexane
GIS:	Geographic Information System
KEC:	Known Environmental Criteria
MCM:	Monte Carlo Method
MEC:	Measured Environmental Concentration
MT3DMS:	Modular 3-D Multi-Species Transport Model

MUM:	Multimedia Urban Model
NSE:	Nash-Sutcliffe Efficiency
OAT:	One Step at A Time
PAHs:	Polycyclic Aromatic Hydrocarbons
PBIAS:	Percent Bias
PCBs:	Polychlorinated Bipheny
PCDDs:	Polychlorinated Dibenzodioxins
PDFs:	Probability Density Functions
PEC:	Predicted Environmental Concentration
PFASs:	Perfluoroalkyl and Polyfluoroalkyl Substances
PFOA:	Perfluorooctanoic Acid
PFOS:	Perfluorooctane Sulfonate
POPs:	Persistent Organic Pollutants
PPCPs:	Pharmaceuticals and Personal Care Products
PRZM-3:	Root Zone Model Version 3
QHD:	Qianhaidao
RNEMM:	Regional-scale Numerical Environmental Multimedia Modeling
RSEMM:	Regional Spatial Environmental Multimedia Model
RSR:	RMSE-observations Standard Deviation Ratio
SA:	Sensitivity Analysis
SDZ:	Sulfadiazine
SOCs:	Semi-Volatile Organic Compounds
TNT2:	Agro-hydrological Model
UA:	Uncertainty Analysis
WHO:	World Health Organization
WWTPs:	Wastewater Treatment Plants

ZJZG: Zhujiangzhudao

Chapter 1 Introduction

1.1 Background

Environmental pollution unfavorably changes our surroundings mainly as a byproduct of human activities (Rai, 2016). The global pollutant problems have been attracting public attention for their severe long-term consequences. Between 1930 and 2000, anthropogenic chemicals' global production has increased 400 times from 1 million to 400 million tons (World Wide Fund for Nature, 2015) and over 50 % of them are environmentally harmful compounds (Gavrilescu et al., 2015). Many pollutants, including polycyclic aromatic hydrocarbons (PAHs), perfluoroalkyl and polyfluoroalkyl substances (PFASs), as well as pharmaceuticals and personal care products (PPCPs) have widespread occurrences in water, sediment, soil, and atmosphere (Liu et al., 2015; Liu et al., 2014; Zhang et al., 2015) and present highly variable spatial exposure profiles (Hodges et al., 2014; Z. Liu et al., 2017). Furthermore, the pollutants, taking PFASs as an example, are also found in the organism of humans and animals, such as fish, birds and marine mammals (Lanza et al., 2017; S. Liu et al., 2019). A great deal of these pollutants is toxic and has potential long-term impacts on human health. S. Liu et al. (2019) found that perfluorooctane sulfonate (PFOS) and perfluorooctanoic acid (PFOA) harmed the appropriate expression of CD90 (a surface antigen) and promoted adipogenesis. Additionally, these two contaminants, even at very low doses, were proved to affect the early stages of human pancreatic progenitor cell specification (Liu et al., 2018).

To evaluate the ecological and human health risks of a chemical, a commonly used method is comparing exposure and effect levels (Ao et al., 2019). However, the existing environmental monitoring methods presenting exposure levels are not available for all contaminants. Furthermore, regular monitoring alone cannot be applied to determine the magnitude of different sources (Lindim et al., 2016). The limitations of monitoring methods can be addressed by applying environmental multimedia models (EMMs) that can estimate the fate and transport of contaminants and identify the transport pathways between or in the media (Pistocchi et al., 2010;

Su et al., 2019).

EMMs are useful tools for health and ecological risk assessment since they can reflect the transport and fate processes of contaminants in the multimedia environment. One of the main types of EMMs is multimedia compartment models based on the fugacity concept or the first-order mass balance equations (Su et al., 2019). Different media are treated as "well-mixed" with uniform environmental properties and mass transfer coefficients. The classical EMMs, including SimpleBox (Hollander et al., 2016) and USEtox (Fantke et al., 2017), have been widely employed because they are relatively simple to execute with affordable data requirements (Csiszar et al., 2013). However, traditional EMMs are generally not able to address spatial variations of contaminant transport in different media (Kim et al., 2010). To further investigate spatial patterns of contaminant distribution, some models divide the study area into many subareas in which the mass balance is calculated considering the mass transport intra- or inter-media (Huang et al., 2019; Liu et al., 2014; Su, Lu, et al., 2018). For instance, STREAM-EU (Lindim et al., 2016) integrates the Delft3D-WAQ and a level IV fugacity model for establishing an irregular subdivision of the domain in sub-catchments and establishes mass balance in all subareas. These attempts assess the spatial distribution of contaminants. However, the spatial resolution for large field scale applications can be further investigated (Zhao et al., 2017).

Another type of EMMs applying the advection-dispersion equation (ADE) for environmental compartments is considered as a realistic numerical approach (Pistocchi et al., 2010). Both analytical and numerical algorithms can solve the ADE for applicable environmental media, like the aquatic environment (Csiszar et al., 2013; Gusev et al., 2005), while fugacity methods or analytical solutions are used for the other compartments (e.g., atmospheric environment) (Csiszar et al., 2014; Regens et al., 2002). Generally, fugacity and analytical methods are incapable of considering the temporal and spatial effects (Chen & Yuan, 2009), and inappropriate consideration of mass fluxes between different models may bring some errors (Pistocchi et al., 2010). Given the importance of water environment, there has been a lack of focus on the river systems affected by

various emission sources (Gusev et al., 2005; Travnikov & Ilyin, 2005). Particularly, a lot of emerging pollutants like PPCPs and PFASs are usually disposed via wastewater treatment systems after use, which often shows a highly variable spatial distribution of contaminants concentration (Franco et al., 2017).

Recent studies have focused on integrating the models with Geographic Information System (GIS) to provide an effective method for geophysical properties and spatial pollutant distributions (Jolliet et al., 2020; Sakurai et al., 2019). Taking G-CIEMS as an example, it is a geo-referenced dynamic multimedia environmental fate model based on GIS and further applied to investigate the multimedia behavior of decamethylcyclopentasiloxane (D5) and dodecamethylcyclohexasiloxane (D6) in the catchment basin of Tokyo Bay, Japan (Sakurai et al., 2019; Suzuki et al., 2004). The GIS is often applied as a pre-processor for the processing of the model input for the environment modeling program (Font et al., 2019). It is also used to analyze and visualize the result data by mapping modeled exposure levels of contaminants (Huang et al., 2017). Thus, the integration of GIS and EMMs could provide some benefits for providing a more realistic environmental assessment and management process.

Consequently, the development of a regional-scale numerical environmental multimedia modeling (RNEMM) approach is proposed and applied to the multimedia study cases with complex conditions. The RNEMM is developed based on the numerical integration of a river network simulation module, a numerical air contaminant transport module, a mass balance analysis module for soil compartment, as well as a food web analysis module, and all modules further combine with GIS. The uncertainties of RNEMM are handled by using Monte Carlo simulation while the health risk assessment method is applied to evaluate the spatial risk quotient of human health. Moreover, this model has a graphical user interface and share standard data storage.

1.2 Research Objectives

The main objective of this study is to develop a regional-scale numerical environmental

multimedia modeling (RNEMM) approach and implement it to the regional study case for exploring the feasibility of this approach. In RNEMM, the pollutant transport model (including river network, air, and soil modules), food web model and health risk assessment model are integrated and combined with the ArcGIS Engine. This modeling approach is capable of providing the spatial distribution of contaminant concentrations in the multimedia environment, making environmental quality predictions and the related health risk assessments. The objectives of this research can be itemized as follows:

1. Develop an approach to integrate different modules with non-uniform boundary conditions and inter-media flux and establish a new model with this developed method to validate this approach.
2. Develop a method to couple the modules based on different computational schemes and generate an environmental multimedia model (EMM) which is then applied to a study case at regional scale for the method verification.
3. Based on the above two developed methods, establish the RNEMM approach, including the pollutant transport model (including river network, air, and soil modules), food web model and health risk assessment model, and visualizing the fate and transport of pollutants through ArcGIS.
4. Develop the graphical user interface for RNEMM and conduct it to the study case in the Pearl River Basin for testing the entire system.

1.3 Thesis Organization

This dissertation is organized into eight chapters as shown in Figure 1-1. Their summary is provided as follows:

Chapter 1 introduces the research background of environmental multimedia models, states the limitations of existing models and research problems, and specifies the research objectives.

Chapter 2 provides a literature review regarding the existing models, the sensitivity analysis methods and the risk assessment studies for the environment and human health.

Chapter 3 describes the methodologies for developing the regional-scale numerical environmental multimedia modeling (RNEMM) approach. Two key developments are introduced: integrating different modules with non-uniform boundary conditions and inter-media flux, and coupling the modules based on various concepts. Besides, it also introduces the sensitivity analysis and risk assessment methods, which are developed and applied in this novel modeling system.

Chapter 4 presents the implementation of the model in 1D version with non-uniform boundary conditions and inter-media flux. This model is applied to a landfill case study in Alberta, Canada, and validated by comparing it to the measured results and the simulated results from analytical solutions.

Chapter 5 depicts the case study validation for the extending model in 2D version which uses Alternating Direction Implicit method for simulation. Furthermore, the risk assessment is conducted to evaluate the long term impact of the contaminant on human health.

Chapter 6 represents the implementation of the model coupling the modules based on different concepts and the further regional scale validation through the comparison between simulated and measured results. Then the spatial health risk assessments for adults and children are presented.

Chapter 7 describes the RNEMM approach to simulate the spatial distribution of PFOS and assess the consequent exposure risks for an essential water basin region of the Pearl River in China. In this chapter, the validation of the field data and the spatial distribution of contaminant and hazard quotient in the multimedia environment are presented.

Chapter 8 summarizes the main conclusions and contributions and addresses the recommendations for further research.

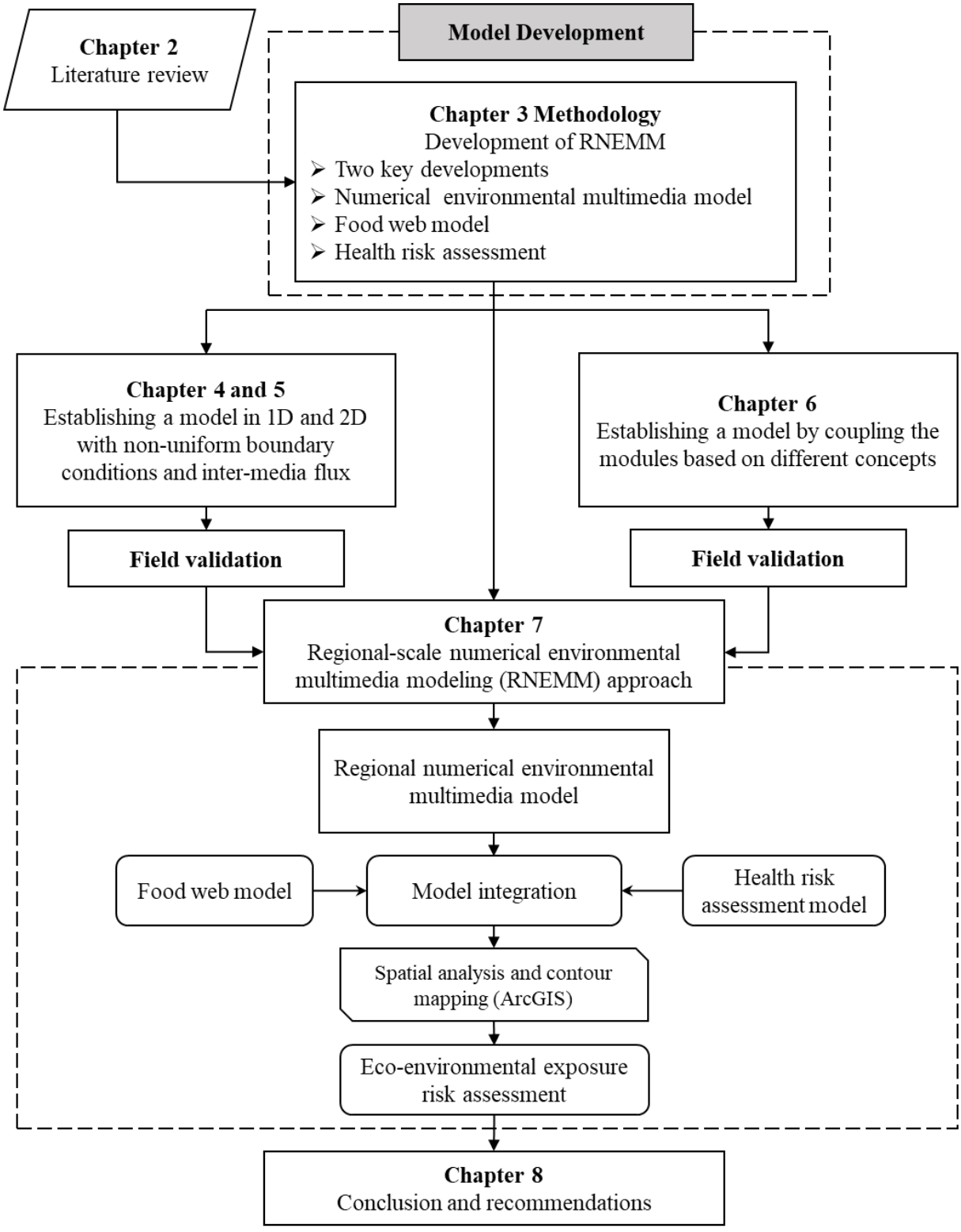

Figure 1-1 Thesis organization

Chapter 2 Literature Review

2.1 Pollution Problems in the Multimedia Environment

Environmental pollution problems have commenced many decades ago and are mainly caused by the adverse consequence of human activities like industry, agriculture, and urbanization (Trevors, 2010). The global production of anthropogenic chemicals has risen by 400 times between 1930 and 2020 (WWF, 2015). Over 50 % of the production of chemicals is regarded as environmentally harmful compounds (Gavrilescu et al., 2015). Many environmental pollutants, including heavy metals, persistent organic pollutants (POPs) and some emerging pollutants, have a ubiquitous presence (Berk et al., 2014).

In recent years, both type and content of heavy metals in the multimedia environment, including soil, water and groundwater, have increased due to human activities and resulted in the deterioration of the environment (Kumar et al., 2019; Su et al., 2014; Waseem et al., 2014). Kumar et al. (2019) assessed the concentrations of heavy metals in the global surface water from 1994 to 2019. Their research indicates that the average concentration of Cr, As and Cd are 413, 3981 and 180 μg/L, which are much higher values than the highest acceptable value for drinking water. Based on the contamination indices, such as heavy metal toxicity load, they further concluded that it is required to remove 99 % of As, 97 % of Co, 99% of Cr and 61 % of Mn for making the water suitable for human purpose. Furthermore, heavy metal pollutants have been detected in the urban and agriculture soils (Su et al., 2014; Waseem et al., 2014). Taking China as an example, Wei and Yang (2010) reviewed the studies related to the heavy metal contaminants in several cities in China, from 2000 to 2010. The results reveal that most concentrations of the heavy metal (e.g., Cr, Ni, Cu, Pb and Cd) are higher than their background levels of soil and these contaminants are widespread in urban soils and road dust. Over 65% of the cities selected in this study have high or extremely high contamination levels, especially the ones whose economy concentrate in the heavy industry, such as Changchun, Shenyang and Changsha (Wei & Yang, 2010). The heavy metal

contaminants are also detected in the atmosphere worldwide (Bajpai et al., 2011; Duan & Tan, 2013; Khamesi et al., 2020). In China, the average concentrations of atmospheric As, Mn, Ni, Cr and Cd are 1.2 to 8 times higher than the air quality standards of China and the World Health Organization (WHO) (Duan & Tan, 2013). The presence of heavy metal contaminants in the multimedia environment can be a severe problem because these pollutions are covert, irreversible and persistent. They can degrade the quality of the environment and also pose a significant threat to human health (Z. Li et al., 2014). Among them, Cd and As are potentially mutagenic, while Pb and Hg are fetal toxic for human beings (Duan & Tan, 2013). For instance, chronic exposure to Cd can cause bone demineralization, kidney dysfunction and increase the potential risk of lung cancer (Bernard, 2008).

PFASs recognized as emerging persistent organic pollutants have been noted to cause several critical environmental problems because of their occurrences and properties (Kunacheva et al., 2012). PFOS and PFOA are the most commonly used PFASs. They are not only detected in surface water and sediment (Kaboré et al., 2018; Pan et al., 2020) but also in soil and groundwater (Rankin et al., 2016; Szabo et al., 2018). They are present in both developing and developed countries, including Brazil (Schwanz et al., 2016), China (B. Liu et al., 2019; Liu et al., 2015), and North America (Rankin et al., 2016; Vedagiri et al., 2018). Furthermore, they are also found in the livers and blood samples of humans and of many animals (e.g., birds, fishes and marine mammals) (Lanza et al., 2017; S. Liu et al., 2019). Taking the Great lakes as an example, a large body of evidence demonstrates the accumulation of PFOS and PFOA in the multimedia environment of the Great Lakes, especially Lake Ontario. In 2010, the mean concentrations of PFOS and PFOA in Lake Ontario reached 5.51 and 4.31 ng/L, respectively (De Silva et al., 2011), and they remained stable in 2017 due to their chemical stability (Gewurtz et al., 2019). Moreover, the PFOS concentrations in Lake Ontario sediment ranged from 0.026 to 20.305 ng/g in 2010, and the estimated total loads of PFOS and PFOA present in the sediment of Lake Ontario can reach 4.90 and 2.68 tonnes (Christensen et al., 2019). Codling et al. (2018) have estimated the temporal trends of PFASs identified in sediment cores in Lake Ontario from 1800 to 2014. It indicates that the

concentrations in many samples increased, especially from 2000 to 2014. PFOS and PFOA are also found in the food web, including Lake trout, Brown trout, Carp and Chinook salmon (McGoldrick & Murphy, 2016; Stahl et al., 2014). The mean PFOS concentrations of fish in Lake Ontario reached 53.6 ng/g (McGoldrick & Murphy, 2016). PFOS and PFOA are toxic and have potential long-term impacts on humans. For instance, exposure to PFOS and PFOA could have a negative influence on the estrogen homeostasis during pregnancy (Wang et al., 2019) and they could act as endocrine disruptors to affect the sexual steroids functions (Chaparro-Ortega et al., 2018).

As introduced above, the pollutions in the multimedia environment have significant adverse impacts on human health and the ecosystem. Thus, it is essential to make the environmental risk assessment for these contaminants and assess their potential multimedia environmental impact. Characterizing and reaching a comprehensive understanding of pollutant behavior in the environment using multimedia models is crucial for environmental risk assessment and the management of contaminated sites.

2.2 Existing Environmental Multimedia Models

Environmental multimedia models (EMMs) are able to comprehensively identify the transport processes of contaminants in multimedia and compile a comprehensive pattern of their environmental behavior (MacLeod et al., 2010). These models are widely employed on screening exposure and risk assessment because the simulated outputs could identify relatively higher-risk regions and provide technical support for contaminant control and management (Su, Song, et al., 2018). These models can be classified as non-spatial and spatial EMMs based on whether they can provide spatial resolution. According to the different methods applying to these models, they can be further classified. The details will be discussed in the following sections.

2.2.1 Non-spatial EMMs

Among the non-spatial EMMs, those based on the fugacity concept are the most prevailingly employed. Mackay firstly suggested that applying the fugacity approach is a good method to quantify the transport behavior of contaminants in the multimedia environment and then established the fugacity models, which describe the transfer behavior of contaminants by degradation, partition, diffusion and non-diffusion processes (Mackay, 1979, 2001; Mackay et al., 1985). In the fugacity concept, fugacity (*f*) is applied to express the driving forces for mass transfer among media instead of the concentration (*C*) (Kong et al., 2018). They also assume that all environmental compartments are well mixed, which means the compartment characteristics are uniform (Diamond et al., 2001). The fugacity model has been developed and improved by many researchers to satisfy the demands under different conditions. One of the representative developments is adding the vegetation compartments into the model for considering the deposition and transpiration of chemicals through plant roots (Su et al., 2019).

A typical fugacity model, the multimedia urban model (MUM), is developed by Diamond et al. (2001). The MUM includes six compartments encompassing surface water, sediment, air, soil, vegetation and organic film, which aims to assess the fate of the movement of semi-volatile organic compounds (SOCs) in an urban environment. The organic film was defined as a new compartment that can efficiently capture the particle and gas phase of SOCs partition (Diamond et al., 2000). Diamond et al. (2001) applied this model to quantify the fate and transport of two PAHs and three polychlorinated dibenzodioxins (PCDDs) in the lower Don River watershed. They successfully obtained the concentrations of these contaminants at steady state. ChemCAN, developed by the Canadian Environmental Modelling Centre (CEMC), is another representative model (Webster et al., 2004). It focuses on 24 regions of Canada and evaluates the fate of chemicals at steady state. This model provides the average concentrations of chemicals in seven compartments and the mass flows from these media as its outputs (Zhang et al., 2012). In recent years, this kind of model is still employed for estimating the fate and transport of many contaminants, such as PAHs,

antibiotics and perfluoroalkyl acids at a regional scale, like a lake and city (Chen et al., 2018; Domínguez-Morueco et al., 2016; Gewurtz et al., 2019; Huang et al., 2019). In brief, for this kind of model, versatility, small input data requirements and simplicity of operation are vital ingredients for their widespread application. However, they fail to consider the spatial variance in chemical fate in the environment and the mass exchange between different regions.

2.2.2 Spatial EMMs

Some recent models have attempted to improve EMMs based on the fugacity concept by considering the spatial distribution processes and describing the region as a more refined grid of subareas. For instance, the Berkeley-Trent (BETR) model developed by Macleod (MacLeod et al., 2001) is a regionally segmented chemical fate model. The study areas are divided into a number of segments according to geographic features and political boundaries. It increases spatial resolution by increasing the number of individual segments and connecting them by inter-regional flows. Similarly, with other fugacity models, each segment consists of seven homogeneous compartments. Song et al. (2016) extended the BETR model as the BETR-Urban-Rural model based on different emission rates within urban and rural areas.

Furthermore, to improve the spatial resolution, hydrological database or hydrodynamic models are used to describe the river-network structure and establish the irregular horizontal subdivision of the model domain (Lindim et al., 2016; Sakurai et al., 2019; Wannaz et al., 2018). These domain subdivisions are further subdivided in compartments, and fugacity concept models or mass balance models are applied. Taking G-CIEMS as an example, Suzuki et al. (2004) divided the river network structure into basins according to the Japanese river-networking database. Each of the basins contains multiple unit catchments that include the corresponding river segment and the other compartments as well as the other models. These geo-referenced approaches can provide a more accurate exposure estimation compared to the results from the monitoring method (Suzuki et al., 2004).

These spatial EMMs based on the fugacity concept have been successfully applied to estimate the behavior of chemicals like PAHs, PFOS and Polychlorinated biphenyl (PCBs) on various scales (Liu et al., 2014; MacLeod et al., 2011; Su, Lu, et al., 2018). Despite their wide applications, they have some weaknesses. Although some attempts have been made for improving spatial resolution, most of these models are more suitable for low spatial and temporal resolution applications and highly simplify the spatial variation of landscape and environmental parameters (Zhao et al., 2017). Moreover, the assumption that the intra- and inter- transfer rates are set as constant in time has a strong negative influence on the accuracy of assessing these transfer processes.

On the other hand, some studies have included the advection-dispersion equation (ADE), which is considered as the practical method for environmental compartments (Pistocchi et al., 2010). These models applying ADE with complex structure have been developed, such as MSCE-POP (Gusev et al., 2005) and DEHM-POP (Hansen et al., 2004). For instance, MSCE-POP is a multi-compartment hemispheric three-dimensional model and consists of six environmental media: sea water, sea ice, snow, atmosphere, soil and vegetation. The atmosphere and seawater modules are considered as three-dimensional models by solving ADE. For soil, the ADE is solved in one dimension. Lammel et al. (2007) stated that traditional EMMs might overestimate the sink of contaminants and underestimate long-range transport in the multimedia environment. Shin et al. (2011) attempted to link several environmental fate and transport models, including the American Meteorological Society/EPA Regulatory Model (AERMOD), Pesticide Root Zone Model Version 3 (PRZM-3), BreZo, Modular Three-Dimensional Groundwater Flow Model (MODFLOW), and Modular 3-D Multi-Species Transport Model (MT3DMS), most of which are based on the ADE and apply the numerical method to solve the equations. However, this coupled modeling system has extensive computational requirements and takes a week per run for a regional scale case (Shin et al., 2011). Furthermore, since the input format of each model component is different, the extensive data processing is required to integrate the above mentioned models.

Such complex ADE based models can overcome these limitations and ascertain the significance of these processes. However, these complicated models also have their limitations (Pistocchi et al., 2010). Firstly, all numerical solutions to the ADE bring some unavoidable artifacts such as numerical dispersion. Secondly, many empirical correctors are used in parameter calibration due to the lack of experimental data. Thirdly, they are overwhelmingly data-demanding and computation-intensive.

Some "hybrid" models combine the ADE module with other concept-based modules. Most of them apply ADE and solve them through numerical methods in single compartment or in some compartments (e.g., atmosphere or groundwater media) (Csiszar et al., 2013; Shin et al., 2011). For the other compartments, fugacity models (Csiszar et al., 2013) or analytical solutions (Regens et al., 2002) are applied, whereas both of them often fail to consider the temporal and spatial effects. Apart from that, to integrate different kinds of models, the fluxes between models have to be modified to bring some errors.

To conclude, despite their usefulness, these existing models are limited in their abilities to predict contaminant concentrations in the multimedia environment. Therefore, there is a need for a numerical multimedia model system simulating contaminant mass fluxes and concentration profiles, applying the appropriate method for various media including air, soil, water, sediment and biota media, and connecting them with the real non-uniform conditions.

2.3 Input Data Preparation in EMMs

With the increasing input data requirement and complexity of models, one of the key concerns in EMMs is the input data preparation that requires considerable time and effort. Because the input data needed by EMMs are usually obtained from distributed sources and are semantically heterogeneous (Jolliet et al., 2020; Sakurai et al., 2019). The other modeling studies, such as geographic and hydrological modeling, also confront this problem and many different data preparation methods have been applied (Hou et al., 2019; Panhalkar, 2014). For geographic

modeling, they are classified into three categories: Manual, (semi-) automatic, and intelligent (Hou et al., 2019). The first one is the dominant method and usually uses software, like Geographic Information System (GIS), to reduce data manipulations and simplify data transformations (Dile et al., 2016). For EMMs, GIS is also widely applied for collecting, storing and displaying the spatial characteristics of a system (e.g., hydrologic and land use data) (Wang et al., 2013) and often used as a pre-processor for processing the model input for the environment modeling program (Font et al., 2019).

Additionally, GIS can also be used to analyze and visualize the result data by mapping the modeled exposure levels of contaminants (Huang et al., 2017). Recently, the GIS application has gained popularity in environmental multimedia modeling because GIS acts as an integrative approach for the entire process (Jolliet et al., 2020; Wannaz et al., 2018). Vizcaíno and Pistocchi (2010) developed the MAPPE GIS model for producing a quantitative description of the fate and transport of g-hexachlorocyclohexane (g-HCH) in Europe. Song and Xu (2011) combined the traditional fugacity model and GIS and validated it through a hypothetical small region case. A geo-referenced dynamic multimedia environmental fate model (G-CIEMS) is also developed on the GIS method and further applied to investigate the multimedia behavior of D5 and D6 in the catchment basin of Tokyo Bay, Japan (Sakurai et al., 2019; Suzuki et al., 2004). Thus, the EMMs can be improved by further combining with GIS, and this combination could become a promising approach to assess the potential impacts of contaminants and provide more realistic assessments (Pistocchi et al., 2010).

2.4 Sensitivity Analysis and Uncertainty Analysis

With the increase of computing power, the EMMs have become complicated and require abundance of data, aiming to consider more transport and transfer processes and provide a higher resolution. However, this development means much more data requirement as model inputs while these data are usually not well-known (Saltelli et al., 2019). Thus, it is crucial to evaluate the impact of these uncertainties on the output. Sensitivity analysis (SA) and Uncertainty analysis (UA)

are two major methods to explore the uncertainty of models. Saltelli and Annoni (2010) highlighted that UA aims to characterize the uncertainty in model prediction and SA aims to identify the factors which cause this uncertainty. Thus, SA is intended as the complement of UA instead of the alternative.

SA methods can be classified as local and global methods (Ferretti et al., 2016). Local SA focus on the effects of uncertain inputs around a point or the base case. The one-step-at-a-time (OAT) method is the most frequently used approach in the modeling studied (Cho et al., 2016). In OAT, one parameter is perturbed while the others are held constant and the sensitivity is evaluated by computing partial derivatives of the output functions for the parameters. However, using the local method cannot always identify which parameters are more influential because there are interactions between the input parameters, and the sensitivity results will also depend on the remaining parameters. Furthermore, the results are affected by the non-linearities present in the model, which means if the model is non-linear, the results will change based on the range of the input parameter chosen to measure (Song et al., 2015).

On the contrary, global SA techniques explore the impact of factors through the full multi-dimensional space. Therefore, they are well suitable for analyzing non-linear relationships and factor interactions (Yi et al., 2016). Currently, several global methods like the screening method, regression analysis and variance-based method have been widely applied in the environmental models (Borgonovo & Plischke, 2016). The screening method aims to evaluate the contribution of input variables and identify the ranking of them in terms of their significance. The Morris screening method proposed by Morris (1991) is one of the most commonly applied screening methods. Its fundamental assumption is that the system model is $Y(x) = Y(x_1, x_2, \ldots, x_n)$, where n is the number of parameters. The values of x_i are standardized with their minimal and maximal values to vary in (0,1). These intervals are then divided into p levels. As the i-th parameter x_i varies by the magnitude of step Δ_i which is $1/(p-1)$, the elementary effect of a change Δ_i of the parameter x_i can be calculated through the variance of the model output divide the change Δ_i. The mean and standard deviation

of the elementary effects can indicate the overall influence of the input parameters on the output and the interaction between parameters or the non-linearities of the model (Shin et al., 2013). The Morris screening method has a lower computational requirement than the other methods, and it is easy to execute. Thus, many kinds of models, especially hydrological models, apply this method for ranking the parameter sensitivity (Fraga et al., 2016; Song et al., 2013). For instance, Song et al. (2013) analyzed the sensitivity of hydrological factors for the Xin'anjiang model by using the Morris screening method. Moreau et al. (2013) implemented this method to evaluate the impact of input factors on output variables for the agro-hydrological model (TNT2). However, this method cannot quantify the effects of parameters on outputs and can only provide the overall interaction of one factor with the others (Song et al., 2015).

Regression analysis is another global SA method that uses standardized regression coefficients to measure the sensitivity and fits a linear regression to the model response (Saltelli & Annoni, 2010). The typical form of a regression method is that $Y=b_0+b_1x_1+b_2x_2+\ldots+b_nx_n+\varepsilon$ where b is the coefficient for each parameter x, and Y is the output variable. Moreover, the model coefficient of determination R^2 is defined as the square of the multiple correlation coefficients between Y and x. The lower R^2 means the higher non-linearity of the model (Cariboni et al., 2007). The regression method is simple to execute and has a relatively low computation cost. When the model response is linear, it can evaluate the sensitivity of each factor, even though all factors affect the output at the same time (Song et al., 2015). Variance-based methods (e.g., the Fourier Amplitude Sensitivity Test (FAST) (Fang et al., 2003) and Sobol' method (Sobol, 1993) are also commonly employed for the sensitivity analysis, which uses a variance ratio to evaluate the significance of factors. The first-order variance for parameters and the parameter interactions can represent the total variance of the model output. Therefore, two indices can be calculated: the first-order sensitivity index of parameter x_i and the total-order sensitivity index of x_i. The interaction of parameter x_i with others can be measured based on the difference between these two indices (Massmann & Holzmann, 2012). These methods have some advantages: (1) they can work for the models with different characteristics, like linear or non-linear and non-monotonic; (2) they can capture interaction effects

between parameters; and (3) they can treat a set of parameters as a single one (Song et al., 2015). However, it is not proper for complicated models with a large number of factors due to the extensive model evaluations.

In general, SA and UA are often coupled and applied in many study cases (Saltelli et al., 2019). The UA methods include the Monte Carlo Method (MCM), the first-order reliability method and the first-order second-moment analysis, etc. In the applications of environmental multimedia modeling, uncertainty analysis is usually conducted by MCM (Chen et al., 2018; Kim et al., 2017; Kong et al., 2018; Song et al., 2016; Wang et al., 2017). In this methodology, the parameter values are selected randomly from the specific probability distributions and then input into the model to calculate the probability distribution of model output. Although MCM may not be quite efficient if the parameter uncertainty is poorly described and the models require intensive simulation, this method provides great versatility in the researches related to uncertainty analysis (Mishra, 2009).

2.5 Health Risk Assessment

Human health risk assessment is the process of estimating the environment and the probability of the current and/or potential impacts on human health by exposure to contaminants in the multimedia environment (Ruiz et al., 2013). It aims to provide quantitative analysis for the risks associated with environmental pollutants and a better understanding of those risks (Cote et al., 2019). The results of health risk assessments can technically help environmental management for adverse impacts.

The potential risks to the human health of various types of contaminants can be classified as carcinogenic and non-carcinogenic effects. For carcinogenic risk assessment, the lifetime cancer risk for pollutants, including heavy metals and volatile organic chemicals, represents the probability of developing cancer during one's lifetime (Sarigiannis et al., 2011; Zuo et al., 2020). The cancer risk can be calculated by the cancer slop factor multiplying the chronic daily intake of contaminants (Sharafi et al., 2019). This probability carcinogenic risk assessment method has been

adopted by many researchers for quantifying the potential risks (Pan et al., 2018; Yang et al., 2018; Zuo et al., 2020). For example, Yang et al. (2018) investigated the heavy metal concentrations in soils of more than 400 industrial sites and more than 1000 agricultural sites in China and estimated the carcinogenic risk of arsenic (As). The results show that the majority of As risks are between 10^{-5} and 10^{-4}, which is relatively unacceptable. This is because the lifetime cancer risk exceeding 10^{-4} is regarded as posing significant health effects. Another assessment is non-carcinogenic risk assessment. Non-carcinogenic hazard quotients are typically represented by the hazard quotient, which is calculated as the ratio of the estimated daily intake and a reference dose. This method provides an indicator of the risk level associated with contaminant exposure, which has recently been applied for many different sites and pollutants (N. Li et al., 2014; X. Liu et al., 2017; Pan, Zhao, et al., 2014; Zhao et al., 2011). This method considers the possible exposure pathways for humans. For instance, the exposure pathways of airborne heavy metals include direct inhalation, ingestion due to deposition and dermal absorption of particles (Dahmardeh Behrooz et al., 2021). Both of these two assessments have been shown to be valid and useful to identify and evaluate the adverse effects on human health.

Recently, some researchers attempted to use the simulated results from EMMs for health risk assessment (Chen et al., 2018; Tobiszewski et al., 2017; Zhu et al., 2019). However, most of them can only provide the risk quotients of contaminants for the whole study area. Therefore, it is necessary to develop a new model approach containing both new EMM and appropriate risk assessment methods to an integrated tool for providing the risk assessment with sufficient spatial resolution.

2.6 Summary

In this chapter, the problems caused by different kinds of pollutants, like heavy metal and PFASs, are studied. The investigation results indicate that these environmental pollutants have a ubiquitous presence in the multimedia environment and have significant adverse impacts on human health and the ecosystem. Thus, it is crucial to assess the fate and transport of these

contaminants and their related risks. The environmental multimedia models are efficient tools to identify the transport processes and their environmental behavior comprehensively. These models can be divided based on whether they can provide spatial resolution. For the spatial EMMs, they can be further classified according to the concept they apply. However, the majority of them have many limitations. These spatial EMMs based on the fugacity concept are more suitable for low spatial and temporal resolution applications and highly simplify the spatial variation of landscape and environmental parameters. Furthermore, assuming the intra- and inter- transfer rates as constant in time harms the accuracy of assessing the transfer processes. On the other hand, some models that apply the advection-dispersion equation can provide higher spatial resolution and ascertain the significance of these processes, whereas they demand extensive data and intensive computation, and some unavoidable artifacts are carried by the numerical solutions.

The potential of GIS in the field of environmental multimedia modeling is also investigated. The combination of EMMs and GIS could provide a new way to assess the potential impacts of contaminants and provide more realistic assessments. Moreover, due to the increasing computing power, the EMMs have become complicated and required the abundance of data. There is a need to evaluate the impact of the uncertainties on the output. Sensitivity analysis and Uncertainty analysis are two major methods to explore the uncertainty of models. Last but not least, the methods of health risk assessment of humans by exposure to the contaminants are summarized. Carcinogenic and non-carcinogenic risk assessment methods are proved to be valid and useful. However, only a few studies attempted to combine the EMMs and these health risk assessments.

In conclusion, it is expected that the new RNEMM simulates contaminant mass fluxes and concentration profiles, applies the appropriate method for various media and connects them with the real non-uniform conditions. In addition, the new RNEMM incorporates the sensitivity analysis, uncertainty analysis and health risk assessment to illustrate the risks associated with contaminant transport into the multimedia environment.

Chapter 3 Methodology

For mitigating the limitations and challenges described in Chapter 2, a novel regional numerical environmental multimedia model (RNEMM) will be developed in this study. Two key developments, integrating different modules with non-uniform boundary conditions and inter-media flux and coupling the modules based on different concepts, will be introduced in the following sections 3.1 and 3.2. After accomplishing these two developments and applying them into the RNEMM, this modeling system will provide good spatial and temporal resolutions for estimating the distribution of contaminant concentrations in the multimedia environment (air, soil, surface water, sediment and biota), which are crucial in identifying the exposure risk level for human health to hazardous pollutants.

3.1 Development of a numerical EMM in 1D and 2D with Non-uniform Boundary Conditions and Inter-media Flux

In this section, a new EMM in 1D and 2D with non-uniform boundary conditions and inter-media flux will be introduced, which is developed to include emission source zone and more environmental media for complex contamination sites. The conceptual model in 1D and 2D is provided in Figure 3-1. It is intended to estimate the impact of the source zone on the surrounding environment. In the case described in Chapters 4 and 5, this model focuses on the source, unsaturated and groundwater zone since the target chemical is heavy metal. The released leachate into the soil surrounding source zone is expressed as the non-uniform flux in z- and/or x-directions.

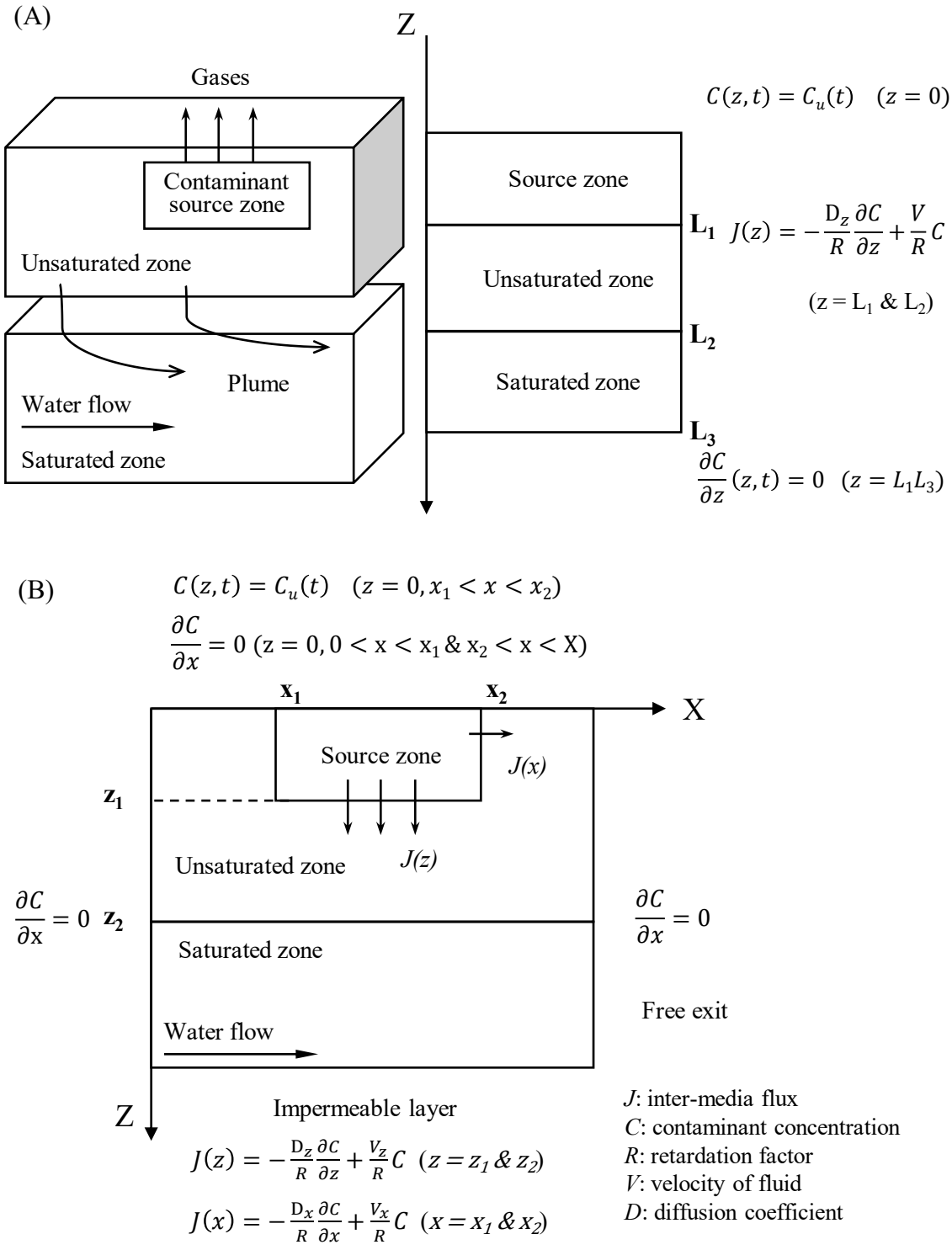

Figure 3-1 The conceptual model for the proposed approach in (a) 1D and (b) 2D

3.1.1 Governing Equations

Initially, the multimedia model is formulated by considering physical transport, sink and sorption processes. In the one dimensional version, it only considers the vertical direction (*z*-direction). The governing equation is given by Chen and Yuan (2009) and Van Genuchten and Alves (1982):

$$\frac{\partial C^k}{\partial t} = \frac{1}{R^k}\left(D_x^k \frac{\partial^2 C^k}{\partial x^2} + D_z^k \frac{\partial^2 C^k}{\partial z^2} - V_x^k \frac{\partial C^k}{\partial x} - V_z^k \frac{\partial C^k}{\partial z} \right) \tag{3-1}$$

$$R = 1 + K_d \frac{\rho}{\theta} \tag{3-2}$$

where C^k is the contaminant concentration in the k zone (g/m^3), subscript x and z are the x- and z-direction, V is the effective solute velocity (m/d), D is the effective diffusion coefficient (m^2/d), R is the retardation factor, ρ is the bulk density of the soil (g/m^3), K_d is the distribution coefficient (m^3/g) and θ is the volumetric moisture content of the soil.

Flux transfer between each module

The mass transport of heavy metal can be expressed as the flux in the aqueous phase. In the boundary section, we set the pollution flux percolating through this section as F_t into the aquifer:

$$F_t = -\frac{D_i}{R}\frac{\partial C}{\partial x_i} + \frac{V_i}{R}C \tag{3-3}$$

where i means different direction, and all the other parameters are detailed above.

3.1.2 Initial and Boundary Conditions

The governing equations for the three compartments deal with similar general transport mechanisms. All of them consider not only advection and transformation in a specific medium, but also inter-media mass transfer. The consideration of non-uniform and non-steady conditions is required to develop an integrated system. The following equations give the integrated boundary and initial conditions in 1D as shown in Figure 3-1a:

$$C(z,0) = C_0(z) \tag{3-4}$$

$$C(0,t) = C_u(t) \tag{3-5}$$

$$\partial C / \partial z = 0 \quad (z = L_3) \tag{3-6}$$

where L_1, L_2 and L_3 are the locations of the lower boundary for each medium in the z-direction (m), C_0 is the initial concentration in the source zone (g/m^3) and C_u is the upper boundary condition of the source zone (g/m^3).

In the 2D version, the pollutant source is conceptualized as leachate entering into the soil beneath the sources in x- and z-direction and it simultaneously achieves the mass balance between the source and the surrounding media. The main initial and boundary conditions are given in Figure 3-1b, which is similar to that in the 1D version. Moreover, some assumptions are considered: (1) Groundwater flow is steady and uniform, which is following the x-direction; (2) Dispersion is assumed as a Fickian process; (3) The principal axes of the dispersion tensor are assumed to cohere with the paralleled and transverse directions to groundwater flow. More detailed case studies will be provided in the later chapters.

3.1.3 Solution Techniques for Governing Equations

The finite difference method (FDM) and finite element method (FEM) are two of the most widespread numerical solutions for solving differential equations. FDM has been applied by many models (MODFLOW, MSCE-POP, etc.) because of its simplicity and efficiency (Bailey et al., 2013; Gusev et al., 2005). On the contrary, FEM is flexible in dealing with complex geometries and irregular shapes and implementing higher-order approximation, while it is more complicated and has higher simulation requirements (Albani & Albani, 2019; Sheu & Chen, 2002). Both of them are applied to resolve the governing equations and the calculation details are shown in Appendix A. Furthermore, the 1D version model is applied for a landfill case and the results are compared to that from the analytical solutions which are also provided in Appendix A.

3.2 Development of an Integrated EMM for Multimedia River Network System

3.2.1 Model Framework

As summarized in Chapter 2, it is crucial to apply the appropriate method for various media including air, soil, water, sediment and biota media, and connect them with the real non-uniform conditions. Another key development, coupling the modules based on different computational schemes (e.g., ADE and fugacity concept), is applied for establishing a regional spatial environmental multimedia model (RSEMM). The modeling framework of the RSEMM is shown in Figure 3-2. The river network system in the study area is divided into sections based on junction nodes (Figure 3-3a). The fate and transport of contaminants in the water and sediment are simulated for each section. Additionally, the study area is divided into individual subareas, each of which contains air, soil and water compartments. The water compartments are linked to the river network system. Meanwhile, the inter-media flux of contaminants is considered to be an additional source or sink for the river network system. The components of the modeling system are described in the following sections.

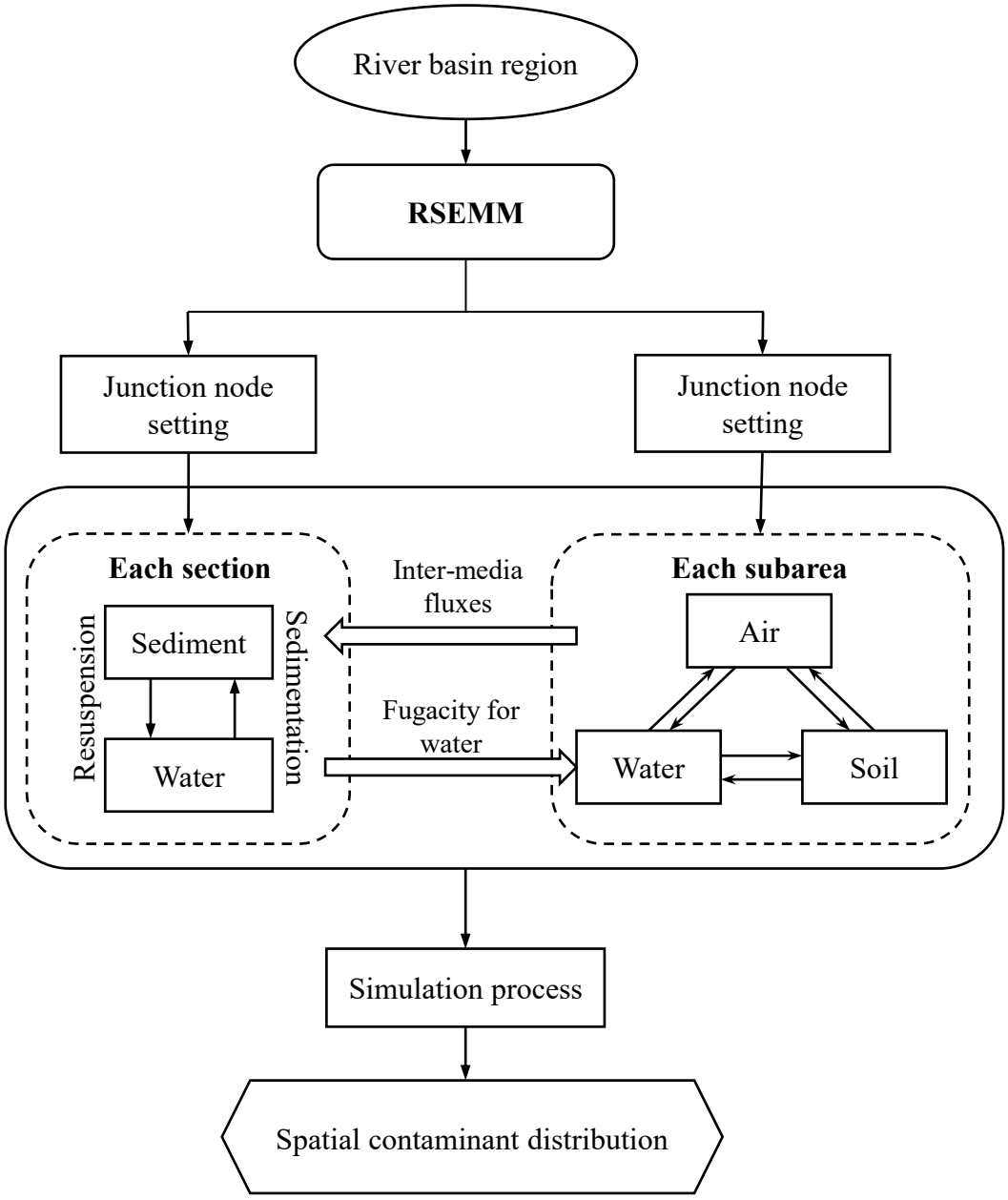

Figure 3-2 RSEMM modeling framework

3.2.2 Water and Sediment Module

River network system

A typical river basin system with multiple streams is conceptualized as depicted in Figure 3-3a. The system can be divided into sections based on junction nodes. If there are n+1 points in a single section, there are thus n segments. These are written for n segments and yield 2n-2 equations with 2n+2 unknowns. Using four equations which represent the upstream and downstream conditions in the water and sediment zones, 2n equations can be solved for the upstream channel. The upstream and downstream conditions can be described as follows:

Upstream conditions: $$C_t(0,t) = C_{t0} \qquad C_s(0,t) = C_{s0} \tag{3-7}$$

Downstream conditions: $$\frac{\partial C_t}{\partial x} = 0 \qquad \frac{\partial C_s}{\partial x} = 0 \tag{3-8}$$

where subscript t and s mean total water column and sediment; C_{t0} and C_{s0} represent the boundary condition of water and sediment zone.

If the channel is located downstream, the upstream boundary conditions are generated by Equation (3-9) (Zhang et al., 2008). The concentrations of contaminants in the junction node are assumed to be thoroughly mixed, which means the outflow concentrations are uniform. The water depth in the junction node is estimated to be stable.

$$\sum_{i=1}^{n} Q_i C_i - \sum_{j=1}^{m} Q_{out,j} C_{out} = 0 \tag{3-9}$$

where Q is the discharge (m^3/h), which can be obtained from the flow velocity multiplying flow area. After applying Equation (3-9), the upstream conditions are obtained. The distribution of contaminants in each downstream channel can be simulated.

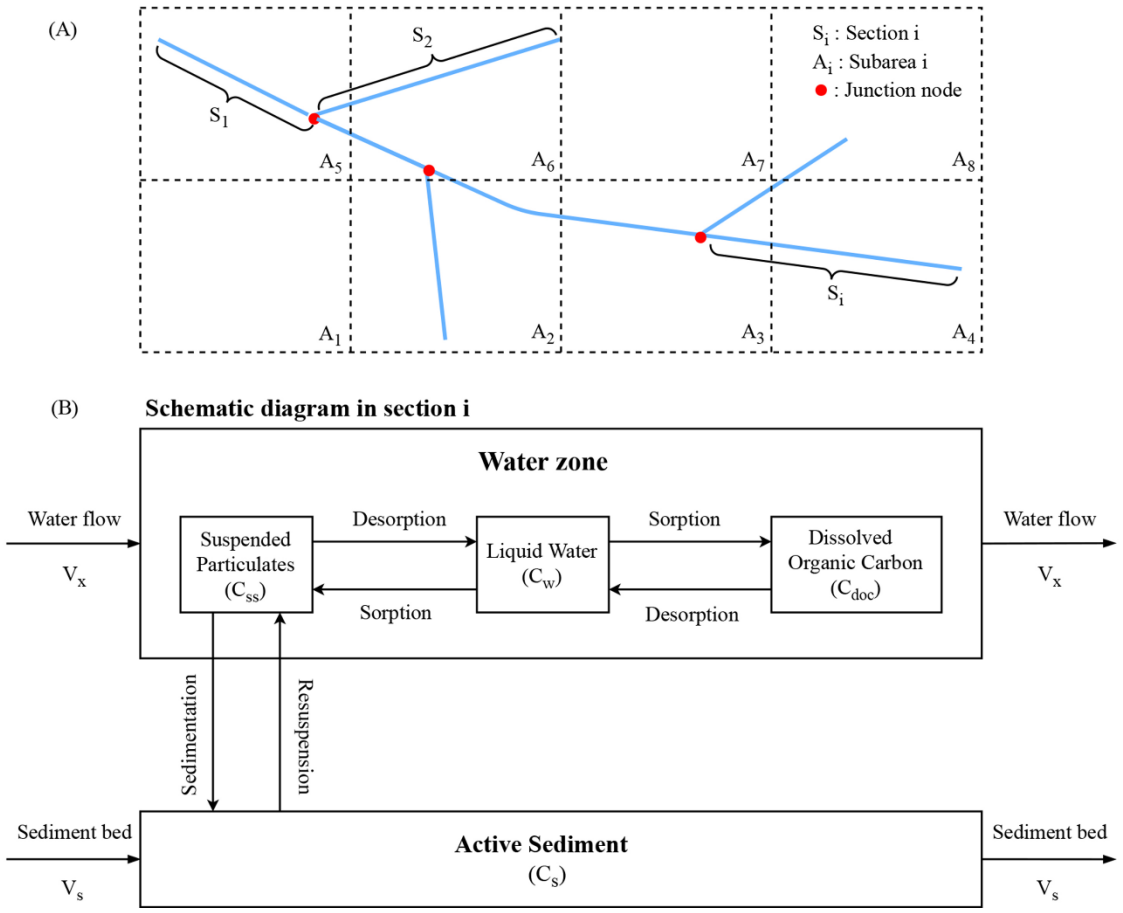

Figure 3-3 (a) Conceptual application of the river basin system and (b) Schematic diagram in section *i*.

Water quality model in a single section

The water-sediment system is divided into two compartments, the water column and the sediment, as shown in Figure 3-3b. The water zone is further divided into three sub-compartments: suspended particulates, liquid water and dissolved organic carbon (DOC).

Water compartment

The dissolved and sorbed contaminants are estimated to be in linear equilibrium. Therefore, the total concentration of contaminant in the water column can be expressed as (Giri et al., 2001):

$$C_t = C_w + C_{doc} + C_{ss} = C_w\left[1 + K_{doc}\rho_{doc} + K_{ss}\rho_{ss}\right] \quad (3\text{-}10)$$

where C_t, C_w, C_{doc} and C_{ss} are the contaminant concentrations in the total water column (g/m^3), water (g/m^3), DOC (g/g) and suspended particulates (g/g) respectively; ρ_{ss} and ρ_{doc} are respectively the concentrations (g/m^3) of suspended particulates and DOC in the water column; k_{ss} and k_{doc} (m^3/g) are the partition coefficients in the suspended particulates and DOC.

The water zone is assumed to gain contaminants through sediment resuspension and lose them through the sedimentation of suspended particulates. The degradation of contaminants in the water compartment is taken into account. The sedimentation and resuspension processes are assumed to reach equilibrium states. The governing equation is given as follows (Feng et al., 2016; Giri et al., 2001):

$$\frac{\partial C_t}{\partial t} + V_x \frac{\partial C_t}{\partial x} = D_x \frac{\partial}{\partial x}\left(\frac{\partial C_t}{\partial x}\right) - K_1 C_t - \frac{C_{ss}\rho_{ss}u_{ss}}{H} + \frac{C_s \rho_s u_s}{H} + S \tag{3-11}$$

$$\rho_{ss}u_{ss} = \rho_s u_s \tag{3-12}$$

where H is the average river depth (m), D_x is the dispersion coefficient (m^2/h), V_x is the river velocity (m/h), K_1 is the decay coefficient in the water zone (1/h), ρ_s is the bulk density of the active sediment (kg/m^3), C_s is the concentration in the sediment (g/kg), u_{ss} is the sedimentation velocity (m/h), u_s is the sediment resuspension velocity (m/h) and S is the contaminant source in the water zone (g/m^3 h).

Sediment zone

The active sediment gains mass through sedimentation but loses it through resuspension and sediment burial. The governing equation for sediment zone is given (Giri et al., 2001):

$$\frac{\partial\left(C_s\rho_s\right)}{\partial t} + V_S \frac{\partial\left(C_s\rho_s\right)}{\partial x} = \frac{C_{ss}\rho_{ss}u_{ss} - C_s\rho_s u_s}{D_a} - K_2 C_s \tag{3-13}$$

where D_a is the active sediment depth (m), V_s is the sediment bed velocity (m/h) and K_2 is the decay coefficient in the sediment zone (1/h). The other parameters are mentioned above.

By simplifying equations (3-10) to (3-13), the final model equations can be given as follows:

$$\frac{\partial(C_t)}{\partial t}+V_x\frac{\partial(C_t)}{\partial x}=D_x\frac{\partial}{\partial x}\left(\frac{\partial C_t}{\partial x}\right)-K_1C_t-\frac{\rho_{ss}u_{ss}}{H}\left[\frac{K_{ss}C_t}{1+K_{doc}\rho_{doc}+K_{ss}\rho_{ss}}-C_s\right]+S \tag{3-14}$$

$$\frac{\partial(C_s\rho_s)}{\partial t}+V_s\frac{\partial(C_s\rho_s)}{\partial x}=\frac{\rho_{ss}u_{ss}}{\rho_sD_a}\left[\frac{K_{ss}C_t}{1+K_{doc}\rho_{doc}+K_{ss}\rho_{ss}}-C_s\right]-K_2C_s \tag{3-15}$$

3.2.3 Air and Soil Module

As shown in Figure 3-3a, the study area is divided into subareas of appropriate size. Each subarea consists of three discrete and homogeneous compartments: air, soil and water. A level IV fugacity model is used to describe the unsteady-state behavior of the contaminants. By considering all processes, the unsteady-state mass balance of contaminants in the three compartments is described with the following system of linear differential equations (Chen et al., 2018; Kong et al., 2018):

$$V_iZ_i\frac{df_i}{dt}=E_i+\sum_{i\neq j}D_{ji}f_j+D_{ti}f_i\ ,\ i=s,a,w \tag{3-16}$$

where V_i, Z_i, f_i, E_i and D_{Ti} are the volume (m^3), fugacity capacity (mol/m^3 Pa), fugacity (Pa), source or sink (mol/h) and transport and transformation rate (mol/h Pa); D_{ji} is the inter-compartmental transfer rate from compartment j to i.

3.2.4 Integrated Model Development

To couple the two modules, the water compartment in the fugacity multimedia model is linked to the water-sediment system. The sections in each subarea are regarded as water compartments in the fugacity model. The fugacity concentration in each subarea's water compartment is calculated by the following equation:

$$f_{w,i}=\frac{C_{w,i}}{Z_w}=\frac{\sum\int C_jA_jdx}{Z_w\sum A_jL_j} \tag{3-17}$$

where subscript *w* represents the water compartment, *i* represents the subarea, *j* represents the channel in that subarea and *L* represents the length of the channel.

The flow balance conditions *I* for the inter-regional movement of the air compartment (Wang et al., 2017) are as follows:

$$I_{r,i} = D_{A,j} f_{r,j} \tag{3-18}$$

where $D_{A,i}$ is the air advection D-value (mol/h Pa) for subarea *i*, $f_{r,i}$ is the air fugacity (Pa) in subarea *i* and the subscript *j* refers to the subarea *j*.

The RSEMM is coupled by running the two components mentioned above separately for a given time step as follows and this process is repeated for the whole simulation period:

1. As the contaminant source enters the water media, the water-sediment module calculates the distribution of contaminant concentrations in the water and sediment zones.
2. The fugacity value in the water compartment is obtained from the previous results. The multimedia model then runs by Δt.
3. The fugacity in other media (soil and air) and the inter-media flux for the water compartment are analyzed. These inter-media fluxes are considered to be another source or sink and input for the next time step into the water-sediment module.

3.3 Development of Regional-scale Numerical Environmental Multimedia Modeling (RNEMM) Approach

The framework of the developed regional numerical multimedia environmental modeling (RNEMM) approach is shown in Figure 3-4. The contaminant like PFASs is mainly releasing into surface water through wastewater treatment plants (WWTPs). At the same time, a part of them emits into the atmosphere and soil from industrial sites. Therefore, the typical study region is divided into three parts including river network, atmosphere and soil compartments, for which

different modeling processes are applied. The RNEMM consists of a water quality simulation module for river network system, a numerical air contaminant transport module and a mass-balance based calculation module for soil. These modules are integrated based on mass conservation and mass-flux linkages of modules. Based on simulation results from water, air, and soil modules, an ecological calculation module is then coupled to determine further the concentration of pollutants in the food web system of the study region. The health risk assessment is finally conducted based on the results from the above-mentioned air, water, soil, and ecosystem simulation modules. The computational modules of RNEMM are introduced in the following sections.

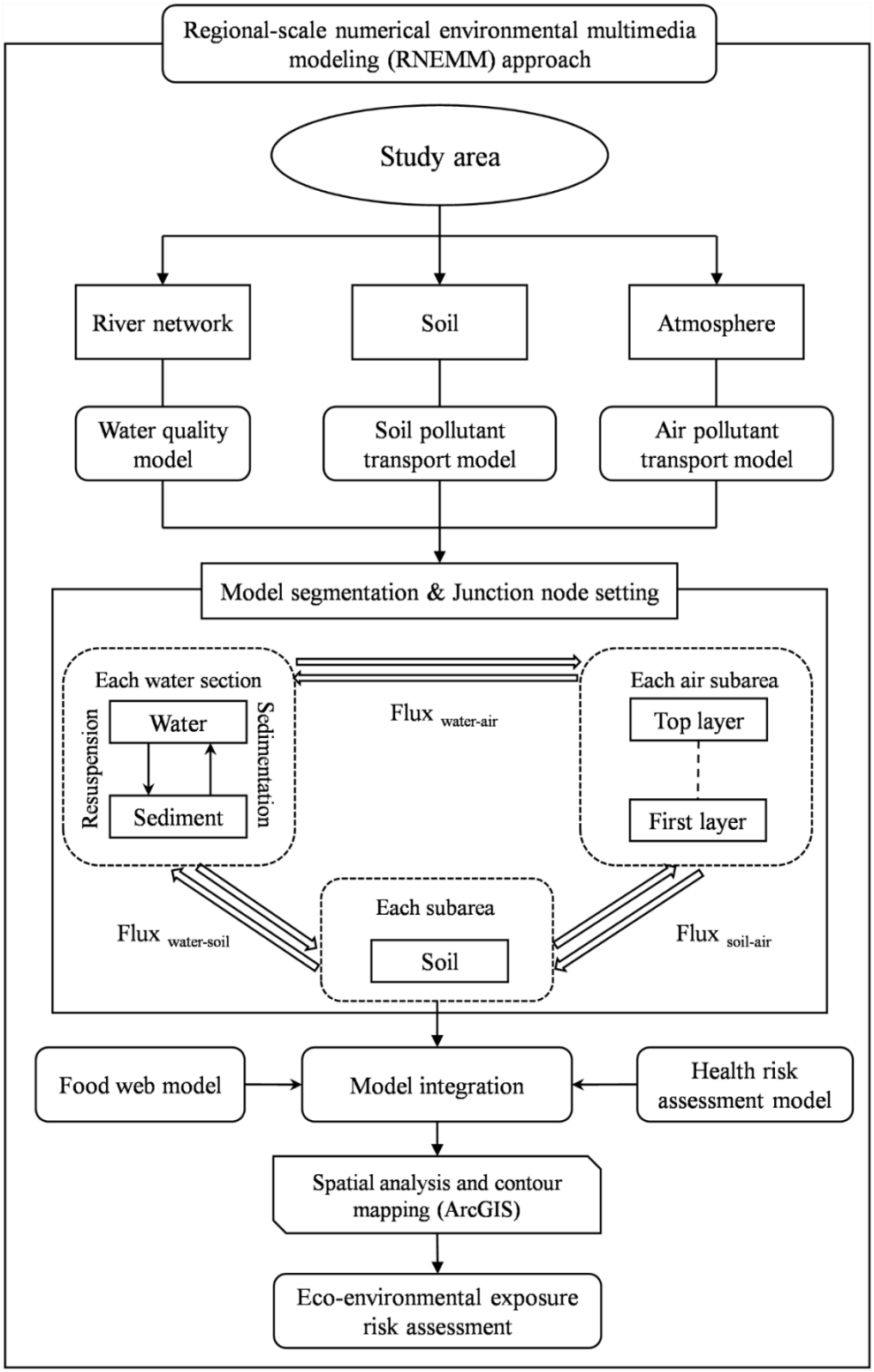

Figure 3-4 Framework of the regional numerical environmental multimedia modeling system

(RNEMM)

3.3.1 Regional Numerical Environmental Multimedia Modeling

The conceptual model of the RNEMM is presented in Figure 3-5. The water basin area includes a river network system consisting of a number of river sections separated by junction nodes. In each section, the fate and transport of contaminant in water and sediment zones is simulated. Additionally, atmosphere and soil zones are divided into individual subareas to be assessed by soil and air modules with the required spatial resolution (i.e., grid subareas in Figure 3-5). The inter-media mass fluxes of contaminants are considered as the contaminant source or sink for each medium zone.

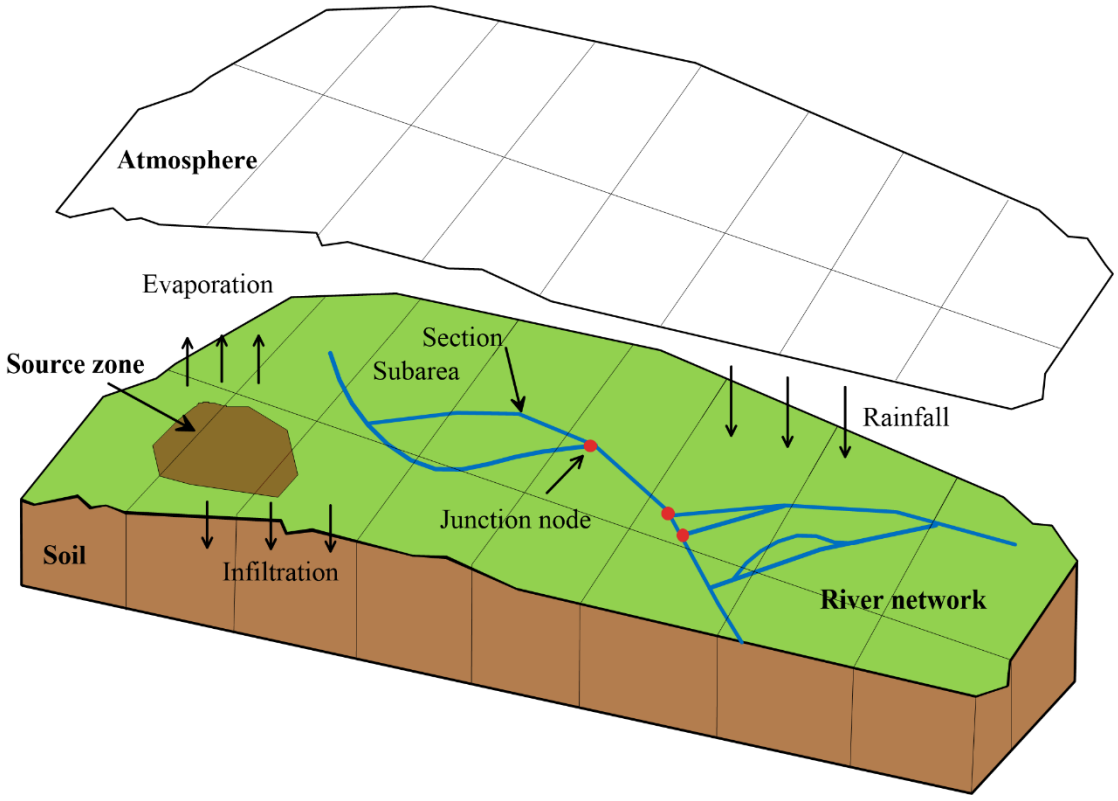

Figure 3-5 The conceptual model of the RNEMM

River network module

The river network module has been described in section 3.2.2. The same approach is also

applied in this modeling system for simulating the fate and transport of contaminants in surface water and sediment zone. Furthermore, the surface water seepage rate is considered to reflect the impact of groundwater.

Atmosphere module

Contaminants are usually released through vapor phase emissions from the source area and coagulated in the atmosphere under lower ambient temperatures and settled down the ground surface by wet or dry deposition. Thus, this air module is established by considering the transport, sorption and deposition processes. The governing equation is described as the following equation (Csiszar et al., 2013; Daggupaty et al., 2006). Further more, finite volume method (FVM) is applied to solve this governing equation and the details are provided in Appendix A.

$$\frac{\partial C_a}{\partial t} = D_x \frac{\partial^2 C_a}{\partial x^2} + D_y \frac{\partial^2 C_a}{\partial y^2} + D_z \frac{\partial^2 C_a}{\partial z^2} - V_x \frac{\partial C_a}{\partial x} - V_y \frac{\partial C_a}{\partial y} - V_z \frac{\partial C_a}{\partial z} - \mu C_a + S_a - F_a \tag{3-19}$$

where subscript a, x, y and z represent the air zone, x-, y- and z-direction, respectively, D is the diffusion coefficient (m^2/day), V is the wind velocity (m/day), μ is the degradation rate (1/day), S and F are concentration fluxes (g/m^3 day) due to emission and deposition, respectively.

Soil module

First-order rate coefficients are used to reflect the chemical transports in the soil zone and between compartments in different media. The unsteady-state mass balance of contaminant in the soil compartment is given (Pennington et al., 2005):

$$\frac{d(C_s V)}{dt} = \frac{dM_s}{dt} = -M_s \left(k_{s\deg} + k_{s-w} + k_{s-a} \right) + M_a k_{a-s} + S_s \tag{3-20}$$

where M_s and M_a are the contaminant masses in soil zone and corresponding air zone (g), $k_{s\text{-}w}$, $k_{s\text{-}a}$, $k_{a\text{-}s}$ and k_{sdeg} represents transfer rate from soil to freshwater by erosion in the suspended solid and liquid phase, soil to air by diffusion, from air to soil by wet and dry deposition and the

degradation rate in soil (1/day). All of these transfer rate are modified as the same unit (1/day) based on the parameters of the related process.

3.3.2 Module Integration

To couple water-sediment and atmosphere modules, the river network system is separated based on the mesh of atmosphere, corresponding to soil subareas in Figure 3-5 at a different spatial resolution. The contaminant mass and water volume of each grid cell are estimated, and the mass transfer rates between water and air media are calculated:

$$T_{w-a} = k_{w-a} M_w = R_{wa} \sum \int_0^L C_{w,j} A c_j dx \tag{3-21}$$

$$T_{a-w} = k_{a-w} M_a = (v_{dry} + v_{wet}) A_w C_{a,i} + R_{aw} C_{a,i} A_w \tag{3-22}$$

where subscript a and w represent air, water compartments, i and j represent air gird cell i and water section j, T is the rate of mass transport (g/day), $k_{w\text{-}a}$ means the transfer rate from water to air by diffusion (1/day), R_{wa} and R_{aw} are the diffusion rate from water to air and from air to water (m/day), v_{dry} and v_{wet} are the dry and wet deposition velocity to water (m/day). Based on the previous study (Pennington et al., 2005), the normalized scavenging coefficient and precipitation intensity are used to calculate wet deposition velocity (v_{wet}) in each subarea. A_c is the width of river cross section (m) and A_w is the area of water compartment in subarea i (m^2).

The inter-media mass transfer process from water to soil ($T_{w\text{-}s}$) is estimated through the similar method. The river networks are divided according to the mesh of the soil zone. Then the mass transfer from soil to water via Erosion from soil to water in liquid and solid phase is expressed:

$$T_{s-w} = k_{s-w} M_s = (K_e + K_l) C_s A_s \tag{3-23}$$

where subscript s means soil compartment, K_e and K_l are the runoff rates of dissolved phase and solids in soil (m/d) and the others are described before.

Since the meshes of air compartments have higher spatial resolution based on finite volume

stratification than that of soil zone, the inter-media fluxes from air to soil ($T_{a\text{-}s}$) is estimated based on the related transport processes from the air cells in connection with the soil subarea. Then, the flux from soil to each air cell ($T_{s\text{-}a}$) is estimated from a portion of the total fluxes from the corresponding soil subarea by diffusion. Therefore, the mass transport process between air and soil compartments is described:

$$T_{a-s} = k_{a-s} M_a = (\mathrm{v_{dry}} + \mathrm{v_{wet}}) \mathrm{A_s} \overline{\mathrm{C}}_\mathrm{a} \tag{3-24}$$

$$\mathrm{T}_{s-a} = k_{s-a} M_s = R_{sa} C_s A_s \tag{3-25}$$

where subscript i means the air grid cell i in connection with the soil subarea, $k_{a\text{-}s}$ and $k_{s\text{-}a}$ are the mass transfer rate from air to soil by dry and wet deposition and from soil to air by diffusion (1/day) (Pennington et al., 2005), R_{sa} is the diffusion rate from soil to air (m/day), $\overline{C}_a$ is the average air concentration (g/m^3).

Simulation process

The above-mentioned computational modules are then integrated and executed based on different time steps: [1] the river network modules receive the emission inventory into water compartment and then simulate the spatial distribution of contaminant concentrations in the water and sediment compartments of the entire river network system; [2] the river network system is separated based on the mesh grid of atmosphere. Based on the Equation (3-21), $T_{w\text{-}a}$ is calculated and set as a secondary source for air zone. $T_{w\text{-}s}$ is obtained by the similar method (Pennington et al., 2005). With the source and sink information, the numerical air module runs by a time step (i.e., one day, based on finite volume algorithm); [3] the results of air module are applied to calculate $T_{a\text{-}w}$ and $\mathrm{T_{a\text{-}s}}$ by Equations (3-22) and (3-24). $T_{a\text{-}s}$ and $T_{w\text{-}s}$ are treated as the extra source or sink and inputted into soil module which then runs forward by one day; and [4] based on the results of three modules, $\mathrm{T_{s\text{-}w}}$ and $\mathrm{T_{s\text{-}a}}$ are then calculated by Equations (3-23) and (3-25). The inter-media fluxes to water and air media ($T_{s\text{-}w}$, $T_{a\text{-}s}$ and $T_{s\text{-}a}$) are considered as extra source for these modules at the next time step.

3.3.3 Food Web Module

Under long-term exposure conditions, the intake and removal of organic chemicals by aquatic organisms reach an equilibrium. The steady-state fugacity concept model is used to estimate the contaminant concentration in the aquatic organisms (Campfens & Mackay, 1997; Lim & Lastoskie, 2011):

$$f_W D_W + f_A D_A = f_B (D_W + D_E + D_G + D_M) \tag{3-26}$$

$$C_{B,i} = Z_i f_{B,i} \tag{3-27}$$

where f_A, f_B and f_W represent chemical fugacity (Pa) in the food, tissue and water, the transportation/transformation-relevant parameters D (mol/day Pa) are subscripted W for respiration, A for diet, E for egestion, G for growth dilution and M for metabolism, $C_{B,i}$ is the internal tissue concentration (mol/m^3) in functional group i, and Z is the fugacity capacity (mol/m^3 Pa).

3.4 Sensitivity Analysis

One-step-at-a-time method (OAT)

Sensitivity is a measurement of the effect of change in one factor on another factor. The one-step-at-a-time method (OAT) is one of the most frequently applied approaches (Cho et al., 2016). The sensitivity coefficient is usually defined by computing partial derivatives of the output functions with respect to the parameters. The sensitivity of the input parameter k is calculated by:

$$X_k = \frac{\partial E_k / E_k}{\partial k / k} \approx \frac{E(k + \Delta k) - E(k)}{E_k \times \Delta k / k} \tag{3-28}$$

where E is the output variable after the parameter perturbation. The sensitivity coefficient with respect to any given parameter is in the same unit as the dependent variable. A high value of X_k indicates a parameter has an essential overall influence on the output.

Morris screening method

The Morris screening method could provide a qualitative sensitivity method in which the input vector is scrutinized to obtain their ranking and assess interactions with other parameters (Campolongo et al., 2007). The basic assumption is that the system model is $f(x) = f(x_1, x_2, \ldots, x_n)$, where n is the number of parameters. The values of x_i are standardized with their minimal and maximal values to vary in (0,1). These intervals are then divided into p levels. As the i-th parameter x_i varies by the magnitude of the step Δ which is $1/(p-1)$, the sensitivity of the i-th parameter (SA_i) is described by (Zheng et al., 2012):

$$SA_i = \frac{(f(X^*) - f(X)) / f(X)}{\Delta} \tag{3-29}$$

Campolongo et al (Campolongo et al., 2007) proposed the absolute mean (μ^*) and the standard deviation (σ) of the SAs of each input parameter. Low μ^* and σ indicates little effect, high μ^* suggests a strong influence on the output and high σ value means that the factors are nonlinear to the output or have strong interactions with the others (Shin et al., 2013).

3.5 Uncertainty Analysis and Health Risk Assessment

The Monte Carlo Method (MCM) is used to quantify uncertainties; its outputs are analyzed for the risk assessment (Chen et al., 2010). MCM generates a large number of parameter sets. The resulting distribution can be simulated by the proposed modeling approaches and the results can be applied to characterize 5th and 95th percentile concentrations in different media, which represent system uncertainties.

To account for uncertainties, a probabilistic risk assessment approach is applied. In the case study in Chapter 4, the spatially interpolated values of parameters follow a normal distribution; these values are used in the model. The output distribution describing the probability of various outcomes is applied to calculate the risk levels. The risk can be quantified as follows (Chen et al., 2010):

$$R_s = P(C > C_r) = \int_{Cr}^{\infty} f_L(C)dL \tag{3-30}$$

where R_s is the probability of system failure, f_L is the probability density function and C_r is the environmental criterion (g/m^3).

The risk quotient (*RQ*) that the ratio of measured concentration to benchmark concentration is another useful tool to evaluate the environmental risk of contaminants (Ramírez et al., 2012). The higher the value of *RQ*, the greater the possibility of environmental risk. When *RQ* exceeds 1, adverse effects may be expected. In the case study in Chapter 5, the *RQ* is carried out through *RQ = PEC/KEC*, where *PEC* is the predicted environmental concentration and *KEC* is the known environmental criteria.

Human health risk characterization is based on the assessment of hazard quotients (*HQ*), which is calculated from the ratio of a measured environmental concentration (*MEC*) and a predicted no-effect concentration (*PNEC*) as shown in Equation (3-31) (Leung et al., 2013; Yang et al., 2019). An *HQ* value of more than 1 suggests the possibility of risk related to inadvertent exposure given by:

$$HQ = \frac{MEC}{PNEC} \tag{3-31}$$

PNEC represents the concentration in the surface water at or below which no adverse human health effects are expected. Water is considered to be both a drinking water source and a source of fish for human consumption. Therefore, *PNEC* is estimated for both adults and children using Equation (3-32) (Cunningham et al., 2009):

$$PNEC_{DW+F} = \frac{1000 \times ADI \times BW \times AT}{(IR_{DW} + BCF \times IR_F) \times EF \times ED} \tag{3-32}$$

where *ADI* is the Acceptable Daily Intake (μg/kg day); *BW* is the bodyweight of an adult or child (kg/person); *AT* is the averaging time (day); *BCF* is the bioconcentration factor (L/g); IR_{DW} is the

drinking water ingestion rate (L/day); IR_F is the fish consumption rate (kg/day); *ED* is the exposure duration (year) and *EF* is the exposure frequency (day/year);

The hazard quotient (*HQ*) can be also evaluated by comparing the estimated daily intake (*EDI*) and reference dose (*RfD*) and determined to provide a quantitative evaluation of contaminant hazard to human in Chapter 7 (Fair et al., 2019):

$$HQ = \frac{EDI}{RfD} \tag{3-33}$$

Since the RNEMM contains a food web module, the pollutant concentrations of fish species can be simulated. The *EDI* through fish and drinking water for children and adults are calculated by the Equations (3-34) and (3-35). The fish species selected in the food web model are the major ones in the human diet and their consumption rate are estimated (Ao et al., 2019):

$$EDI_{total} = EDI_{water} + EDI_{fish} \tag{3-34}$$

$$EDI_{water/fish} = \frac{C \times IR \times EF \times ED}{BW \times AT} \tag{3-35}$$

where *C* is the average PFOS concentration in water and fish media of the selected subarea (g/L and g/g). Furthermore, the concentrations in fish are calculated as the mean value of pollutant level in the main fish species mentioned above. The other parameters are introduced above.

3.6 Model Integration and Interface

RNEMM is developed by using the MATLAB 2014b and integrated with the numerical pollutant transport module, the food web module and the health risk assessment module. Besides, the graphical user interface established by using the Python language is developed to run the modules, and manage data inputs, and present results. The required input data of RNEMM are directly entered or imported as excel files through the graphical interface and then stored as files in the binary data container format (.mat). All equations are solved in the MATLAB, and then the

output can be imported to excel as xls format. The simulated results contain the concentration distribution in different media, which requires to be presented as various figure types. Thus, the other software (Origin and ArcGis) are applied to provide the visual graph of the results instead of the interface. The RNEMM has a single graphical interface and a common data storage (Figure 3-6).

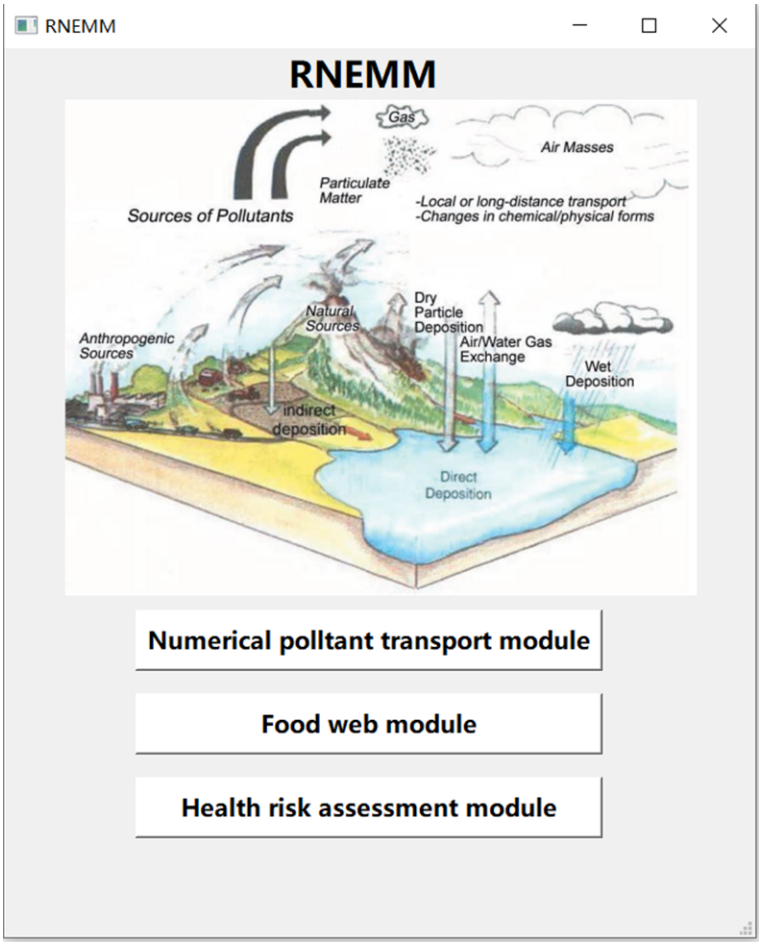

Figure 3-6 Graphical user interface for the RNEMM model

As introduced in Section 3.3, the numerical pollutant transport module consists of three compartments: atmosphere, river network and soil. The interface of this module has a main page that can show different contents by clicking the buttons listed on the left (Figure 3-7). Taking the atmosphere compartment as an example, as shown in Figure 3-7a, it allows the user to directly input the related parameters like the length and height of this compartment and import the

environment properties by the excel file. Then the excel sheet shows the imported information related to the variables. All of the input data are saved in the database by clicking “Save”. After inputting the required data, these data can be linked to the MATLAB and run the simulation processes by clicking the button “Run and validation”. The comparison between simulated and measured data can be seen after the simulation is finished (Figure 3-7b).

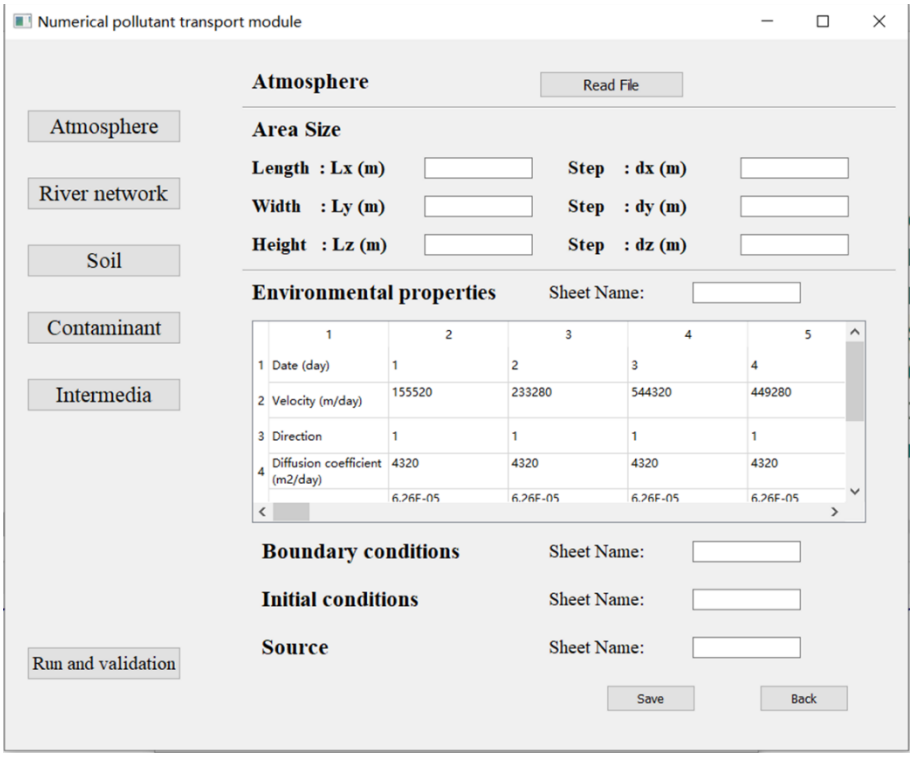

(a)

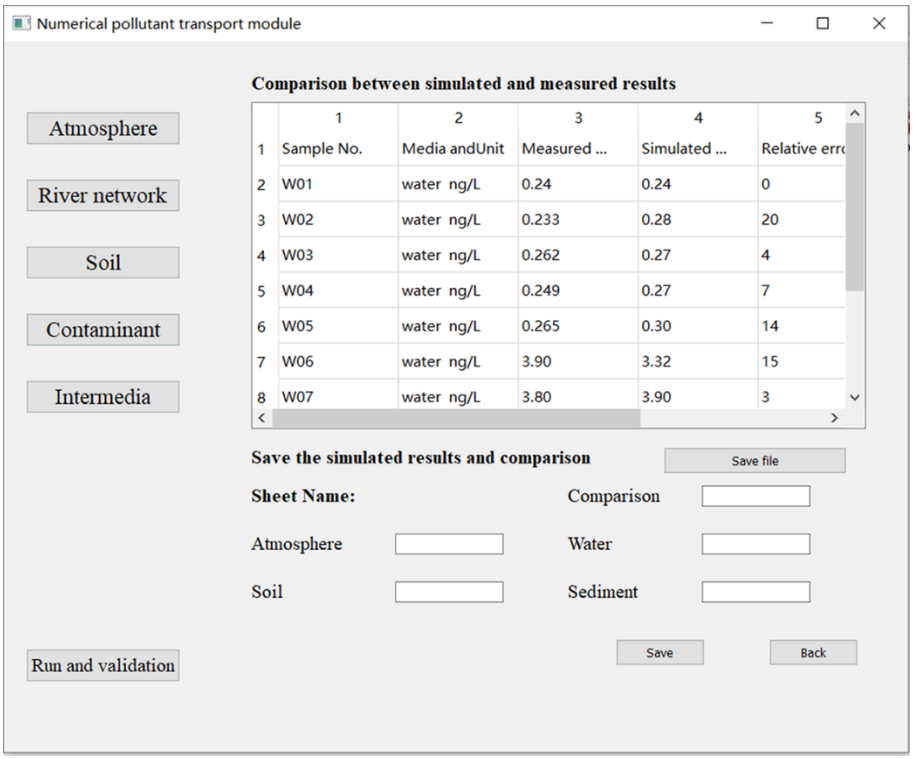

(b)

Figure 3-7 User interface of the numerical pollutant transport module: (a) atmosphere and (b) model validation

Figure 3-8a presents the interface of the food web module, which allows the user to input the contaminant concentrations in water and sediment zone, the organism properties of the food web. The diet matrix can be imported as xls files. By clicking “Run and save (linked to Matlab)”, the concentration levels of the contaminant in each aquatic organism are calculated and the results can be automatically saved as xls files. The health risk assessment module allows the user to input the parameters related to adult and child receptors and the reference dose and import the simulated results in water and fish media as shown in Figure 3-8b. Since the health risk assessment is based on the subarea in the soil compartment, the average contaminant concentrations of water and fish in these subareas are firstly calculated and then input into the related equations for obtaining the *HQs* in each subarea.

The RNEMM integrate different kinds of models to simulate the fate and transport of contaminant in various media and the related health risk assessment. It may be complex and accessible only for experienced people. Therefore, this user-friendly interface is established for making it easy to be executed. The model output is analyzed to provide scientific support for the subsequent management of the resulting environmental impacts.

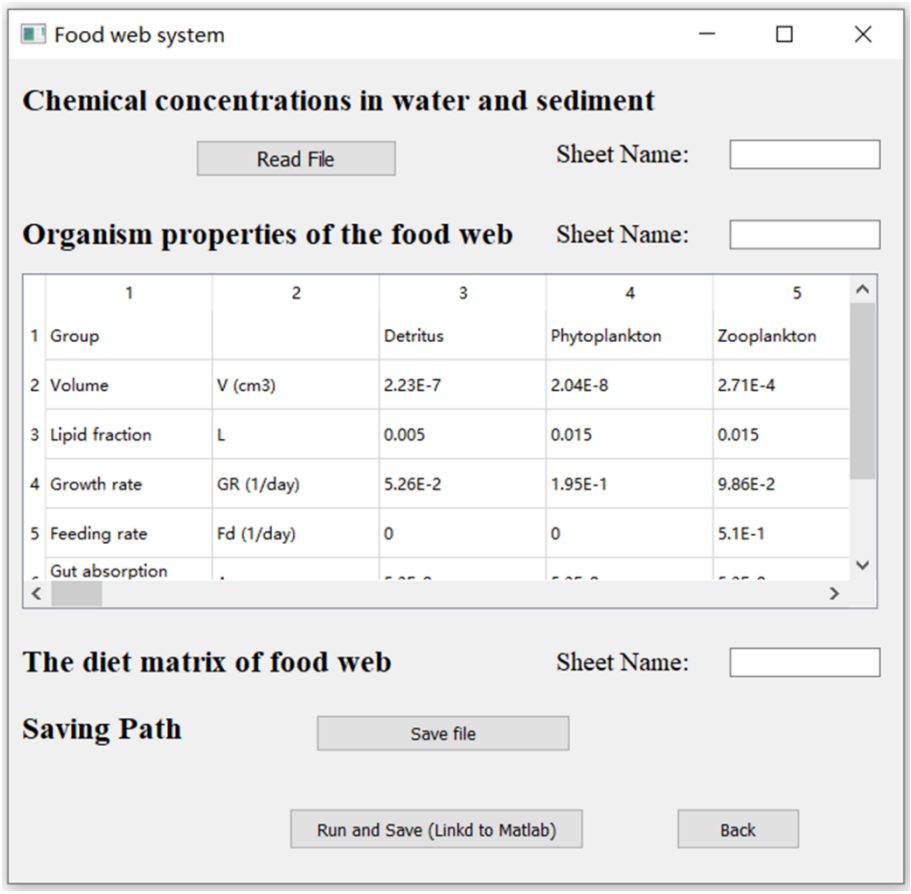

(a)

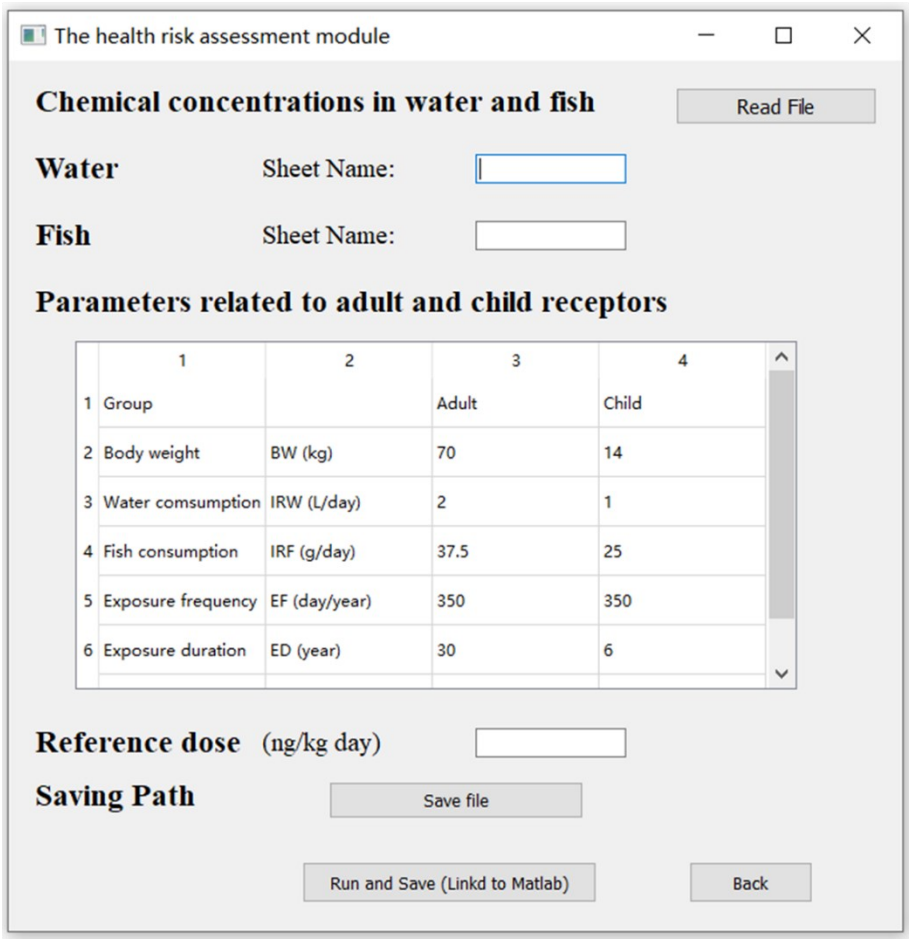

(b)

Figure 3-8 User interface of (a) the food web module and (b) the health risk assessment module

3.7 Summary

In this chapter, a regional-scale numerical environmental multimedia modeling (RNEMM) approach is developed for the multimedia environment. This chapter focuses on integrating different modules with non-uniform boundary conditions and inter-media flux and coupling the modules based on different concepts. After accomplishing these two developments and applying them into the RNEMM, this modeling approach incorporates a water quality simulation module for the river network system, a numerical air contaminant transport module and a mass-balance based calculation module for soil. These modules are integrated based on mass conservation and

mass-flux linkages of modules. A food web module is then coupled to determine the concentration of pollutants in the ecological system of the study region. Different methods (e.g., OAT and Morris screening method) are developed and applied to evaluate the sensitivity of parameters. Considering the uncertainty in the RNEMM, the MCM is selected to assess model uncertainties and the results will serve for the risk assessment. The risk assessment module is presented and incorporated with the RNEMM to evaluate the environmental and health risk based on the results from the environment and ecosystem modules.

Chapter 4 Model Development and Validation for 1D Numerical Environmental Multimedia Model

4.1 Overview of the Study Site

The study area is in east-central Alberta (Figure 4-1) and by neighboring Rocky Mountains, which block moisture-bearing winds from the Pacific Ocean. This results in its sub-humid to semi-arid climate. High winds predominate in the area. Soils in this area have been identified as dark brown chernozemic soils and clay overlaying on a lacustrine deposition. Based on the environmental risk assessment report (Franz Environmental Inc., 2012), an inactive landfill is located approximately 500 m southeast of Drumheller institution in a valley. It covers an area of approximately 150 m × 200 m. This landfill accepted mainly domestic waste and construction waste materials/debris from the institution for more than 20 years (from the middle of 1960s to1988). The topsoil and subsoil layers are not separated to be used as cover material at the time of its closure. According to the investigation (Franz Environmental Inc., 2012), Contaminants in soils in the landfill include heavy metals (e.g., lead and selenium), benzene, and toluene. Moreover, groundwater is encountered at 6.8 to 9.3 m below ground and is inferred to flow east towards the Red Deer River (located to the northeast). Contaminants in groundwater are identified as nitrate and heavy metals (e.g., arsenic and selenium). To evaluate the potential risks, the soil samples are collected in 2005 and 2011, which will be introduced in the next section. In addition, the monitoring wells in the study area are installed in 1999 and 2004. Since the lead (Pb) pollutants are detected in many soil samples, this contaminant is selected as the target chemical in this case study.

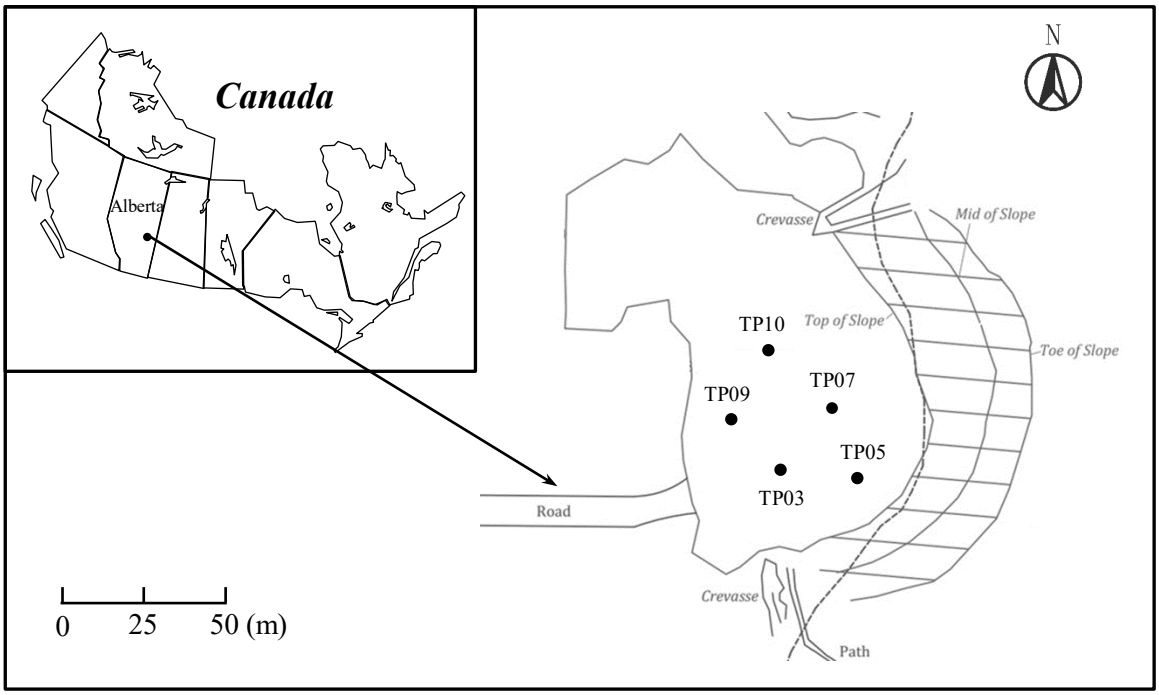

Figure 4-1 Location of the landfill site

4.2 Data Preparation

The site data are obtained from the environmental risk assessment of the landfill (Franz Environmental Inc., 2012). The specific values of the parameters are modified from those of previous studies (Çamur & Yazicigil, 2005; Dokou et al., 2016; Genc & Ulupinar, 2010; Ii, 1995; Lu & Xu, 2009). The distribution coefficient (K_d), hydrodynamic dispersion coefficient (D) and retardation factor (R) of lead are found from the literature to be 220 L/kg, 8.3×10^{-3} cm/s and 936, respectively (Çamur & Yazicigil, 2005). The main parameters of the source zone and unsaturated zone are shown in Table 4-1. The volume of waste in the source zone is about 10-20 % of the total fill volume, while the other material is silty clay. The main material in the vadose zone is also silty clay. The properties of the source zone and unsaturated zone are thus assumed to be similar.

Table 4-1 The parameters of the source, unsaturated and groundwater zones

Parameter	Calculation	Value
Parameters in source zone[a]		
Width	A_y (m)	150
Porosity	φ_{so}	0.4
Pore water velocity	V_L (m/d)	6.7×10^{-3}
Depth	Zso (m)	4.9
Length	A_x (m)	200
Volumetric water content	θ	0.18
Bulk density	ρ_{so} (kg/m^3)	1700
Parameters in unsaturated zone[a,b]		
Average velocity of fluid	V (m/d)	6.7×10^{-3}
Bulk density	ρ_{un} (kg/m^3)	1800
Depth	Z_{un} (m)	3.1
Porosity	φ_{un}	0.4
Volumetric water content	θ	0.18
Parameters in saturated zone[c,d]		
Average velocity of fluid	V (m/d)	4.46×10^{-4}
Bulk density	ρ_{sa} (kg/m^3)	2400
Depth	Z_{sa} (m)	5
Porosity	φ_{sa}	0.3
Longitudinal dispersion coefficient	D_l (m^2/d)	3.28×10^{-4}
Vertical dispersion coefficient	D_t (m^2/d)	1.83×10^{-4}

[a]Based on Franz Environmental Inc. (2012).

[b]Based on Ii (1995).

[c]Based on Genc and Ulupinar (2010).

[d]Based on Dokou et al. (2016).

Five soil samples from 2011 (TP03, TP05, TP07, TP09 and TP10 as shown in Figure 4-1) are taken in locations near the locations of soil samples taken in 2005 (Table 4-2). Since TP08 is collected from the vicinity of TP09, the measured results of TP08 could be estimated to be those of TP09 at a depth of 2-3 m. They could thus be applied to the modeling validation. The groundwater samples are provided only by MW99-3 and MW05-1. The concentration of lead in MW05-1 in 2011 is too low to be detected. In addition, MW99-3 is close to the sampling location of TP09. Therefore, the measured data in MW99-3 is estimated to be the lead concentration of

groundwater at TP09. The lead concentrations of the MW99-3 groundwater samples are 0.6 μg/L in 2005 and 7 μg/L in 2011 at a depth of 9.1 m.

Table 4-2 The lead concentration of soil samples (Franz Environmental Inc., 2012)

Site No.	Depth (m)	Concentration in 2005 (mg/kg)	Concentration in 2011 (mg/kg)
TP03	4-5	13.30	12
TP05	0-1	10.30	10
TP07	3-4	9.90	10
TP10	2-3	10.60	9
TP09	2-3	12.50	12
TP09	5-6	9.25	9

4.3 Results

4.3.1 Field Validation

Figure 4-2 shows a similarity between the one-dimensional results of the numerical methods and those of the analytical solution. It notes that the concentration in the source and unsaturated zones doesn't change greatly because of the high retardation factor of lead, meaning the impact of soil sorption is significant. The measured concentration at a depth of 2-3 m is 12 mg/kg, which is less than the concentration in the simulated results, with a relative error of about 3.7 %. It is assumed that mass entering the saturated zone from the unsaturated soil is mixed in a mixing zone. The analytical solution is applied to assess the concentration at the bottom of the saturated zone. The distributions of lead via different methods in the groundwater zone correspond strongly with the measured results. The concentration of lead (9.1 m) is 6.9 μg/L and the measured concentration is 7.0 μg/L. This is a good agreement with a relative error of 1.4%. According to the results, the transport of lead in the groundwater zone is relatively slow. Compared to FDM, the results from FEM are relatively closer to both the experimental results and the analytical solutions (Figure 4-2a), which indicates that FEM provides better results than FDM. The reason for this may be that FEM methods are able to reduce the numerical dispersion caused by the reduced discretization error.

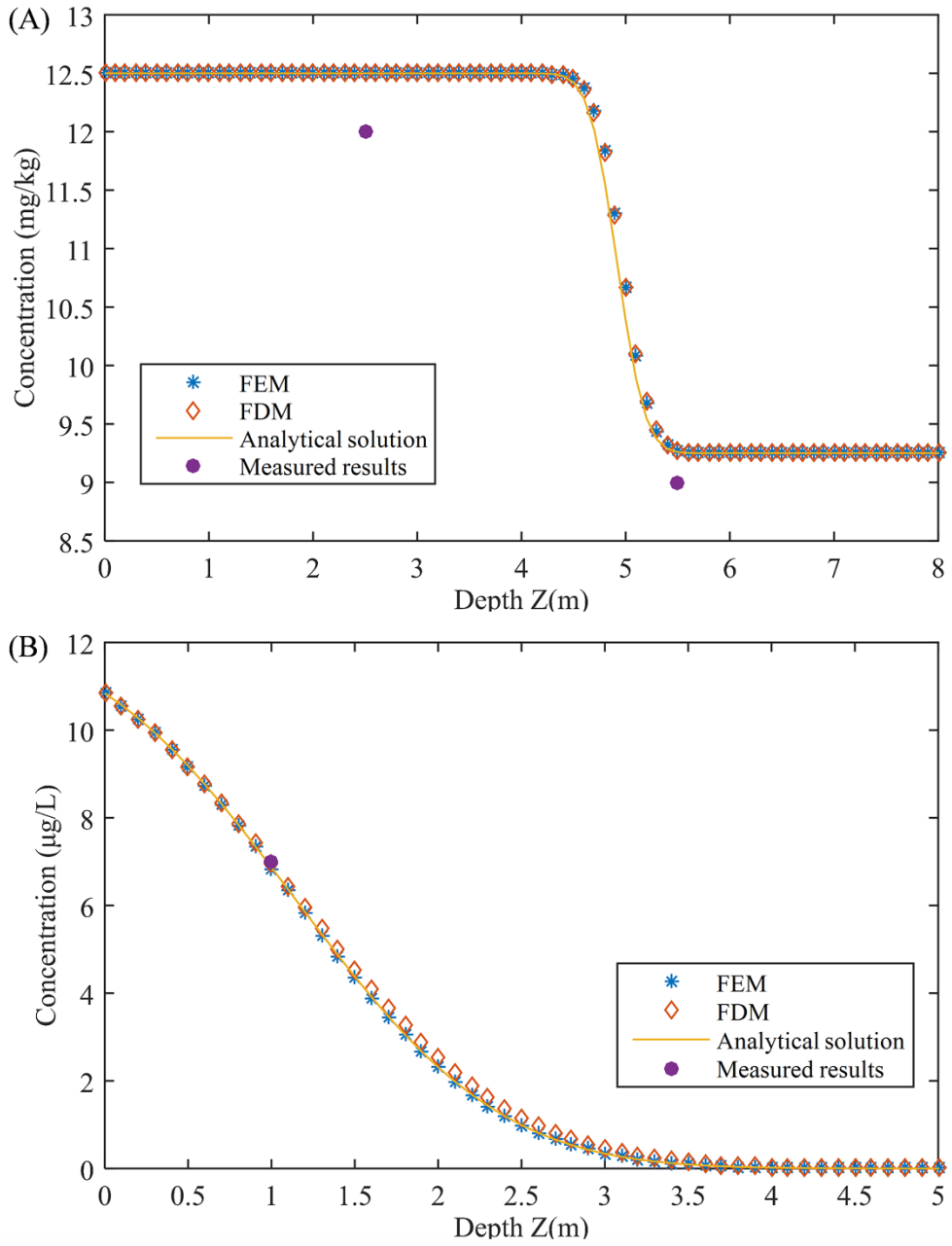

Figure 4-2 Comparison of different methods in (a) soil zone and (b) groundwater zone in 2011. (Sampling location is TP09.)

Detailed modeling results of the lead contaminant in the soil zone are given in Table 4-3. Each sample was measured at different locations and at various ranges of depth (e.g. the depth of TP03

was 4-5 m). The modeling results are the average concentration of the range. The simulated results correspond strongly to the measured ones. For most results, the relative error is less than 10 %.

Table 4-3 Comparison between modeling and measured results in soil zone (mg/kg)

Site No.	Depth (m)	Simulated results (mg/kg)	Measured results (mg/kg)	Relative error (%)
TP03	4-5	12.76	12.00	6.3
TP05	0-1	10.30	10.00	2.5
TP07	3-4	10.00	9.90	0.8
TP10	2-3	10.60	9.00	13.3

The comparison between the numerical, analytical and measured results is shown in Figure 4-3. It can be seen that the lead concentration profiles along the vertical direction are accurately calculated by both methods. As mentioned above, the measured concentration in the source zone represents the value of samples taken near TP09 which may not be exactly the same as the values of TP09. The other values are similar to those found in the simulated results. In conclusion, the numerical method provides satisfactory predicts lead transport in a multimedia system.

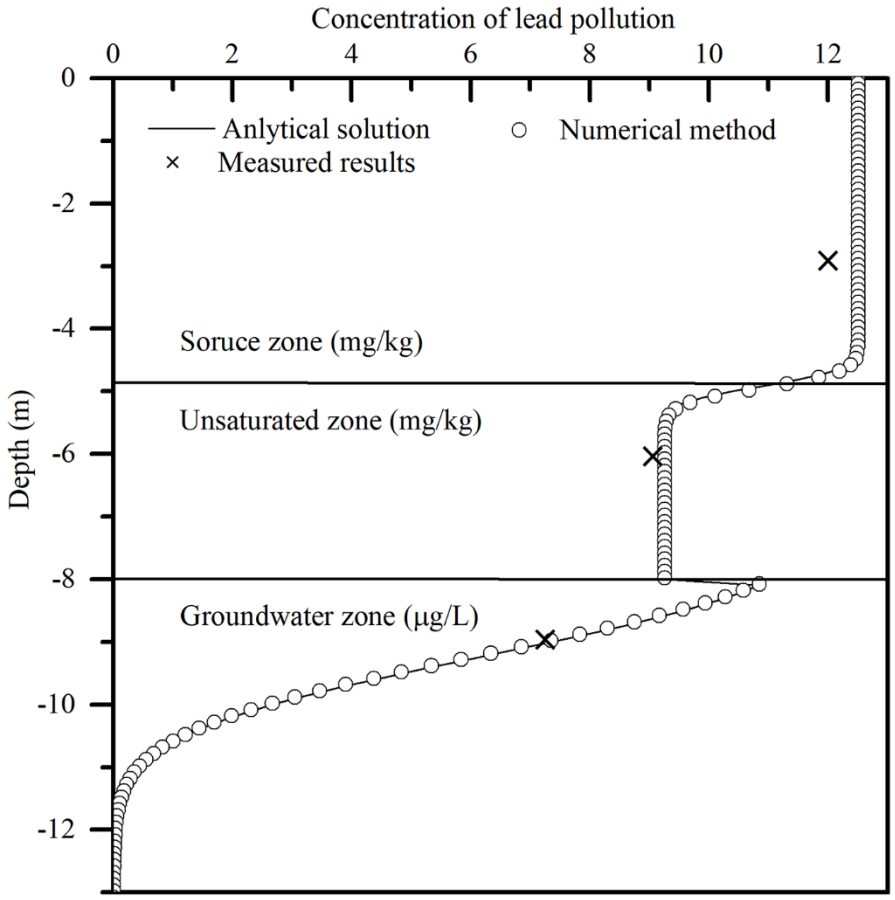

Figure 4-3 Concentration of contaminants based on the proposed approach in 2011. (Sampling location is TP09.)

4.3.2 Sensitivity Analysis

The fate of lead simulated by the modeling approach is highly reliant on the environmental properties including retardation factor, dispersion coefficient, hydraulic conductivity, effective porosity, and water content. These parameters are associated with highly uncertain information and estimation of them is difficult (e.g., Lu & Xu, 2009). In this case study, the detailed hydrogeology and contaminant transport data are provided in Table 4-1. Sensitivity analysis is conducted to explain the relationship between those properties and to examine the related uncertainties.

The chosen parameters in the soil zone were the retardation factor, dispersion coefficient and hydraulic conductivity, which are fundamental parameters in contaminant transport and fate. The retardation factor affects the pollutant's transfer time and peak. The dispersion coefficient and hydraulic conductivity have essential impact on the dispersion and advection process (Bou-Zeid & El-Fadel, 2004). These parameters were adjusted by factors of 25%, 50%, 200% and 400%. Figure 4-4a shows that the results from OAT. The sensitivity coefficient of the retardation factor changes from -0.03 % to -4.8 %, meaning that altering the retardation factor has the most significant impact on the model output. The negative value means that the concentration decreases as the retardation factor increases. The other parameters are less sensitive than the retardation factor. The results indicate that the dispersion coefficient and hydraulic conductivity have a positive influence on the transport of lead pollution. The variance of the model output due to changes in hydraulic conductivity was tiny (from 0.025% to 0.039%).

The sensitivity analysis of hydraulic conductivity, vertical dispersity and effective porosity for the groundwater zone is presented in Figure 4-4b. Vertical dispersity has little influence on the lead concentration. The most sensitive parameter is hydraulic conductivity. The sensitivity coefficients of the hydraulic conductivity range from 10 % to 24 %. The concentration of lead contaminants in the groundwater zone decreases considerably as the hydraulic conductivity is reduced to 25%. The sensitivity coefficient declines as the hydraulic conductivity rises. The tendency of effective porosity is adverse. The reason for this is that both factors contribute to the process of advection. When hydraulic conductivity is larger or effective porosity is smaller, the advection process becomes faster.

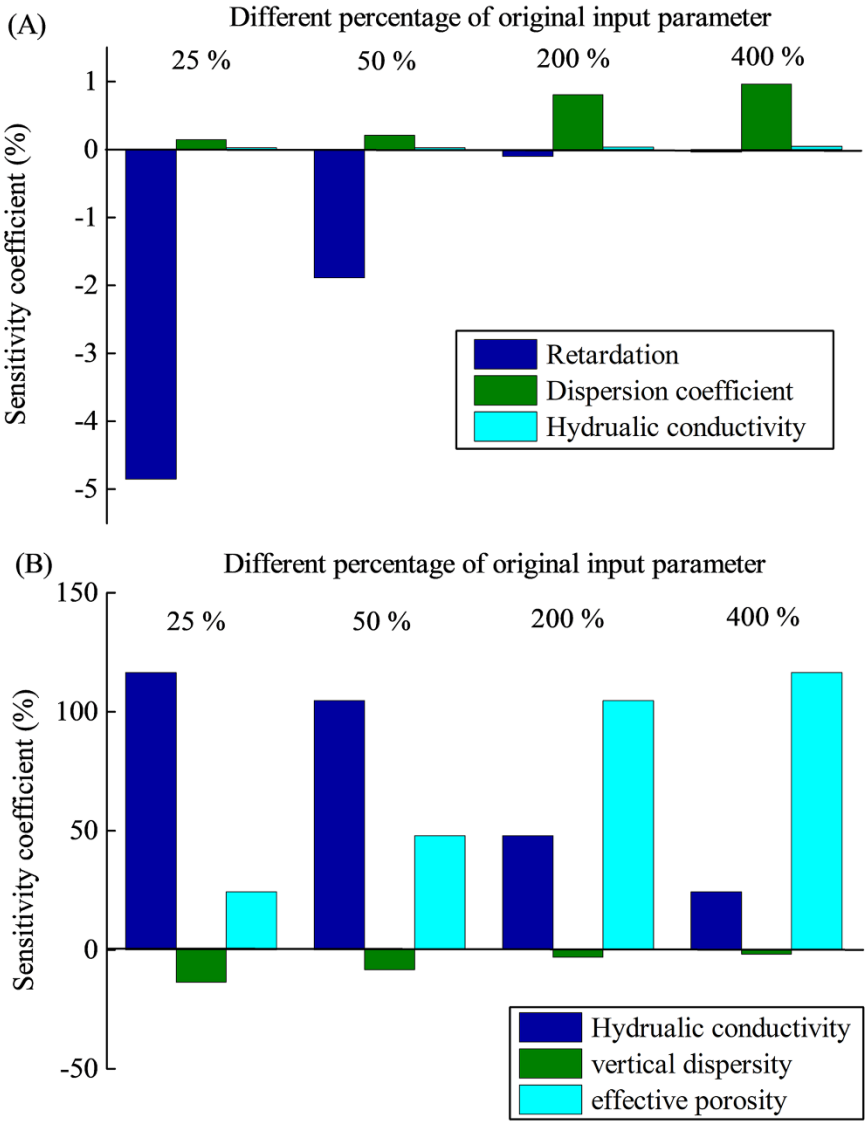

Figure 4-4 Sensitivity analysis for parameters in (a) soil zone; and (b) groundwater zone.

According to the results mentioned above, the most sensitive parameters in the soil and groundwater zones are respectively the retardation factor and the hydraulic conductivity. Once the input data are entered using the MCM, the parameters' probability density functions (PDFs) are generated and the simulated results are provided in a MCM output. In the following section,

EMMS uses the entire range of simulated values for each randomly selected parameter variant for the fate and transport simulation. The normal distribution is chosen to represent each uncertainty.

4.3.3 Uncertainty Analysis

The retardation factor (R) was assigned a normal distribution with mean and standard deviations of 936 and 100, respectively. Soil samples (e.g., TP05) collected for the surface of the source zone indicates that the Pb concentrations in 2005 and 2011 are stable (Franz Environmental Inc., 2012). Therefore, the upper boundary conditions of the study area were considered to be stable during the period from 2011 to 2021. The intervals of lead concentration in the MW99-3 soil zone from 2011 to 2021 were conducted (Figure 4-5a). The depth of the soil sample is 5.5 m in the unsaturated zone. Figure 4-5a indicates that the average concentration of lead increases slowly from 9.26 to 9.4 mg/kg during this period. The 5th and 95th percentile concentrations also gradually increase. The reason for this tendency is that the absorption of soil leads to pollutant stability. The MCM results can be presented in the form of probability distribution.

When evaluating the uncertainty of the output attributed to retardation factor, the standard deviation was applied to identify the locations where the output was most uncertain. Simulating the spatial distribution of uncertainty is significantly useful in establishing the model verification plane. Areas of high uncertainty can be supplemented with samples. Figure 4-5b shows the uncertainty analysis for the retardation factor at various depth and probability density function at the sampling location. It indicates that standard deviations in the area near the bottom of the source zone (4.9 m) are significantly higher than those of the other areas. The standard deviations drop at the bottom of the source zone. The peak value is 0.054 mg/kg at a depth of 5.2 m. A similar tendency is shown in the area close to the upper boundary of the unsaturated zone (Figure 4-5b). This may be traceable to the fact that these locations are the most uncertain points and the areas near the interface between two zones have high variance in concentration.

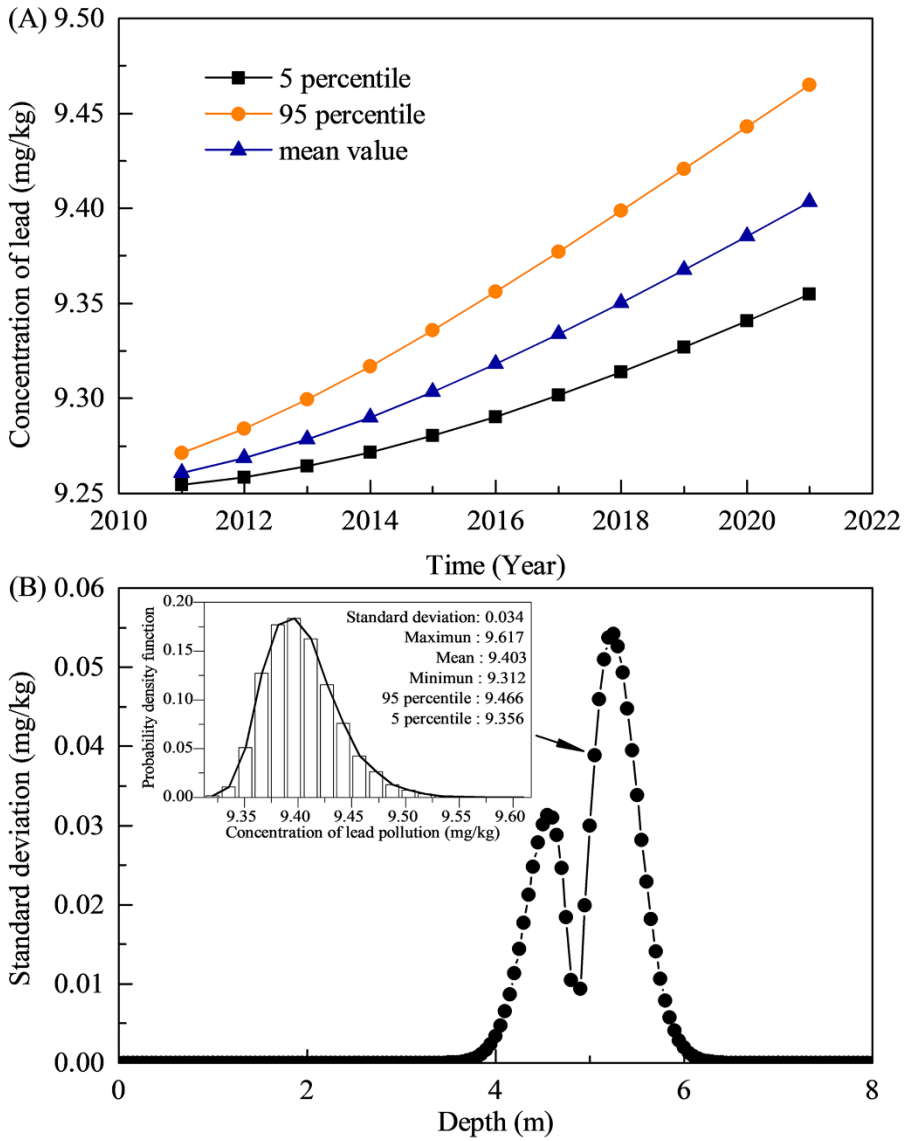

Figure 4-5 Uncertainty analysis for retardation factor in soil zone of TP09: (a) 5th-percentile, mean value, and 95th-percentile concentrations from 2011 and 2021; and (b) uncertainty analysis for retardation factor at various depths in 2021 and probability density function at the sampling location.

As illustrated in Figure 4-6a, the interval of lead concentration at the bottom of the groundwater zone increases from 2011 to 2021. In the first three years, there is no pollutant at the

bottom. The quantity then increases rapidly due to the flux from the unsaturated zone moving slowly toward the groundwater zone. Figure 4-6b indicates the probability plot for the model output in the groundwater zone. The minimum and maximum values are 0.87 and 1.70 μg/L. The 50th percentile concentration also matches the simulated value. In brief, the MCM can be accepted as an accurate method of estimating model uncertainties. The uncertainty analysis for hydraulic conductivity with different depths in 2021 is provided in Figure 4-6. The standard deviations reach a peak when the depth is 3.1 m. The peak point is, therefore, the most uncertain.

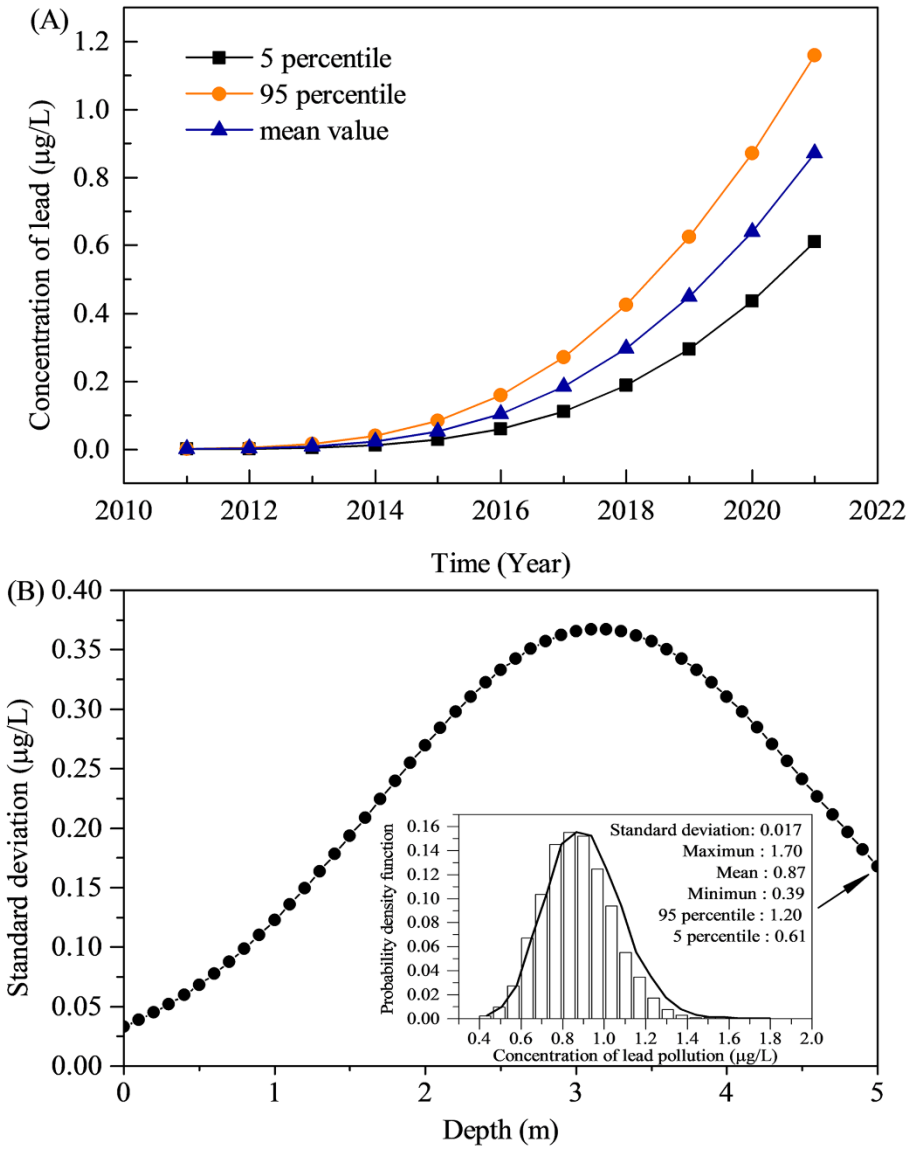

Figure 4-6 Uncertainty analysis for hydraulic conductivity in groundwater zone of TP09: (a) 5th-percentile, mean value, and 95th-percentile concentrations from 2011 and 2021; and (b) uncertainty analysis for hydraulic conductivity at various depths in 2021 and probability density function at the bottom of saturated zone.

4.3.4 Risk Assessment

The model validation, as shown in Figure 4-3, indicates that the developed modeling tool provides reasonable results. A prediction was therefore made regarding the lead concentration at the bottom of the groundwater zone in 2011 and 2021. There are five samples (TP02, TP03, TP06, TP09 and TP16) in the unsaturated zone, which are applied as the source for the groundwater zone. These samples are chosen because they are distributed evenly throughout the entire landfill site and can be utilized to establish a contour map. The concentrations of lead at the bottom of the groundwater zone were calculated. Based on these results, contour maps of the whole landfill area were presented in Figure 4-7. The highest lead concentration in 2011 is 4.03 ng/L, even in the worst-case scenario (95th percentile distribution of lead concentration). In the 95th percentile lead concentration plot in 2021 (Figure 4-7c), the order of lead concentration is 0.8 to 3.3 μg/L. The 5th percentile concentrations (Figure 4-7d) are generally low, being 0.45 to 1.7 μg/L. In the worst-case prediction, the areas where the lead concentration is beyond 1 μg /L make up more than 90% of the bottom of the groundwater zone.

According to the Canadian Environmental Quality Guidelines (Canadian Council of Ministers of the Environment, 2004), the recommendations concerning lead pollutants vary depending on water pH, hardness, etc. The range of the guidelines for risk assessment is 1 to 7 μg/L. These five previously applied sites were chosen to investigate risk-assessment scenarios for these criteria (Table 4-4). Probabilistic risk levels were generated using a stochastic risk-assessment approach (Equation 3-30). For the worst site, the probabilistic risk level is 0.99 for the 1 μg/L Pb criterion, representing a 99 % probability that the criterion will be violated. For the 2 μg/L criterion, the risk level is 0.83. For the 7 μg/L criterion, the probability is zero, meaning the concentration of pollutants will never surpass the standard. According to the risk assessment results, most sites at the bottom of the groundwater zone have a high probability of violating the regulated value (1 μg/L).

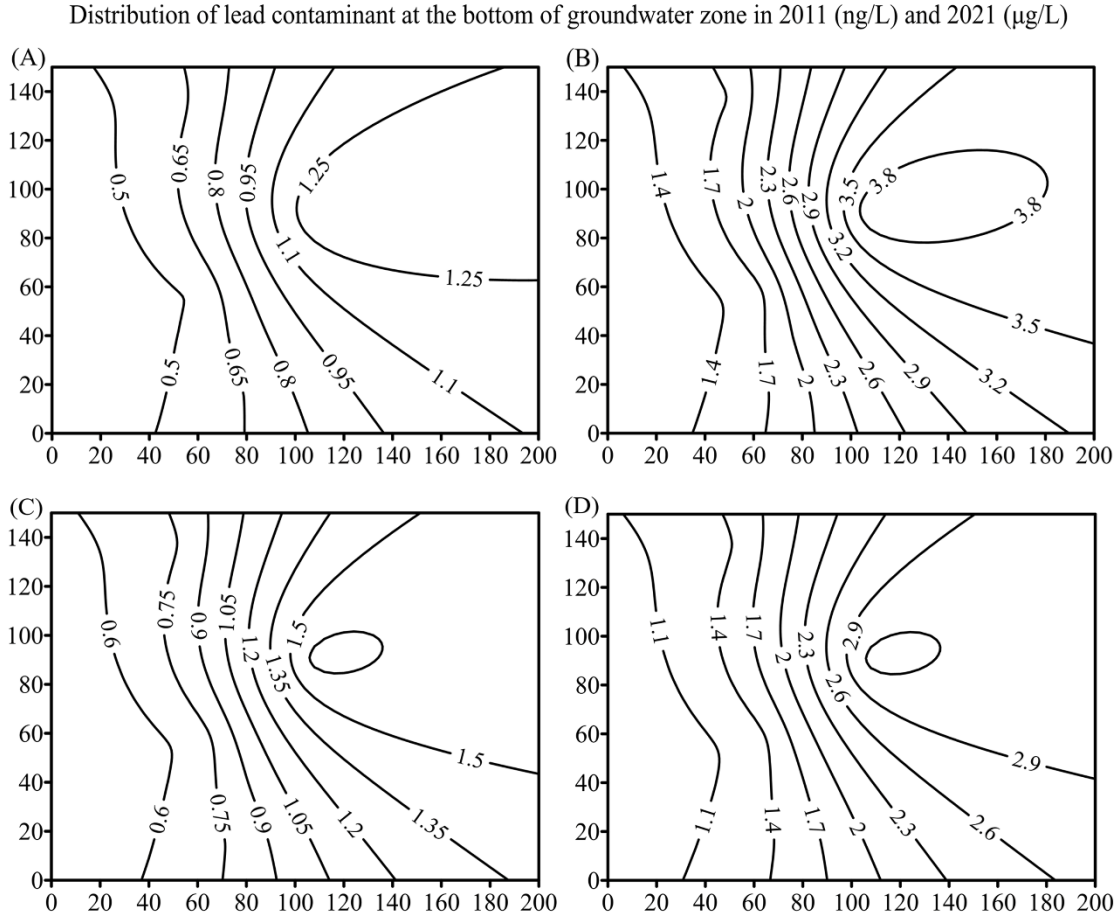

Figure 4-7 5th-percentile and 95th-percentile lead concentration contour maps in (a and b) 2011; and (c and d) 2021 at the bottom of groundwater zone.

Table 4-4 Risk-assessment results of lead concentrations in 2021

Regulated value (μg/L)	Stochastic risk				
	TP2	TP3	TP6	TP9	TP16
1.0	0.68	0.80	0.99	0.31	0.47
2.0	0.01	0.01	0.83	0	0
4.0	0	0	0.01	0	0
7.0	0	0	0	0	0

4.4 Discussion

The case study shows that both the numerical and analytical methods provide results that match well with the observed data. Under the same conditions, FEM offers relatively better results

than the other approaches since it reduces the numerical dispersion. Sensitivity analysis is conducted by performing OAT to evaluate the applicability and performance of the numerical environmental multimedia model. The most sensitive parameters in the soil and groundwater zone were found respectively as the retardation factor and the hydraulic conductivity. The uncertainty analysis further predicted the risks of the study site. The risk assessment based on this modeling approach reflects not only the uncertainties of the entire environmental multimedia system but also those of the model parameters.

4.4 Summary

In this chapter, the new model in 1D with non-uniform boundary conditions and inter-media flux has been examined to simulate the fate and transport of Pb in a landfill case. The validation results show that this model enables a systematic examination of the fate and transport of contaminants in a case site with complex conditions. It can also be used to examine the fate, transport, and risk of other heavy metal contaminants to support decisions in the cleanup of contaminant sites.

Chapter 5 Model Development and Validation for 2D Numerical Environmental Multimedia Model

5.1 Overview of the Study Site

The study area is a landfill located in Victoria city (Figure 5-1), in which the source zone covers approximately 500 m × 700 m. The site is divided into two distinct areas referred to as Phase 1 and Phase 2. Phase 1 has reached its capacity and capped in 1997. Phase 2 is currently receiving waste. Furthermore, the leachate generating in the landfill is collected by the collecting system and then discharged to the leachate lagoon. As shown in Figure 5-1, some monitoring wells are installed in the study area. The measured data from some monitoring wells (Figure 5-1) are used for estimating the environmental properties of the study area and model validation. The chromium (Cr) contaminants are detected in the groundwater samples from 2010 to 2015. Thus, this heavy metal contaminant is selected as the target contaminant in this case study.

Groundwater elevations measured in monitoring wells in refuse and bedrock are shown in Figure 5-2 (AECOM, 2016a). The height of the source zone is about 20 m. Besides, the lower portions of the Phase 1 landfill are in hydraulic connection with the regional groundwater flow system in the bedrock beneath the landfill. There are two series of purge wells located at the south and north boundary of source zone.

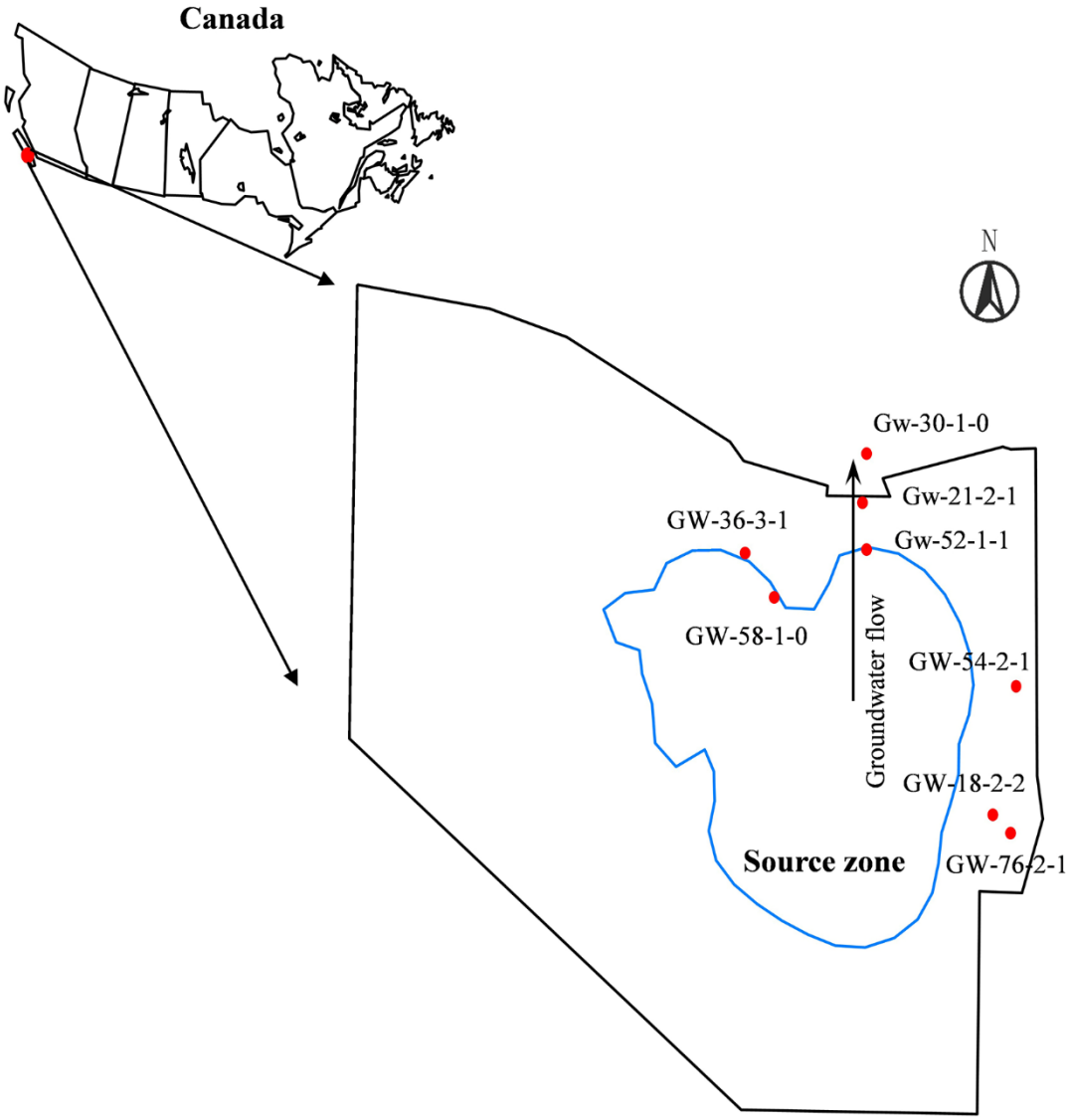

Figure 5-1 Location of the study area and monitoring wells

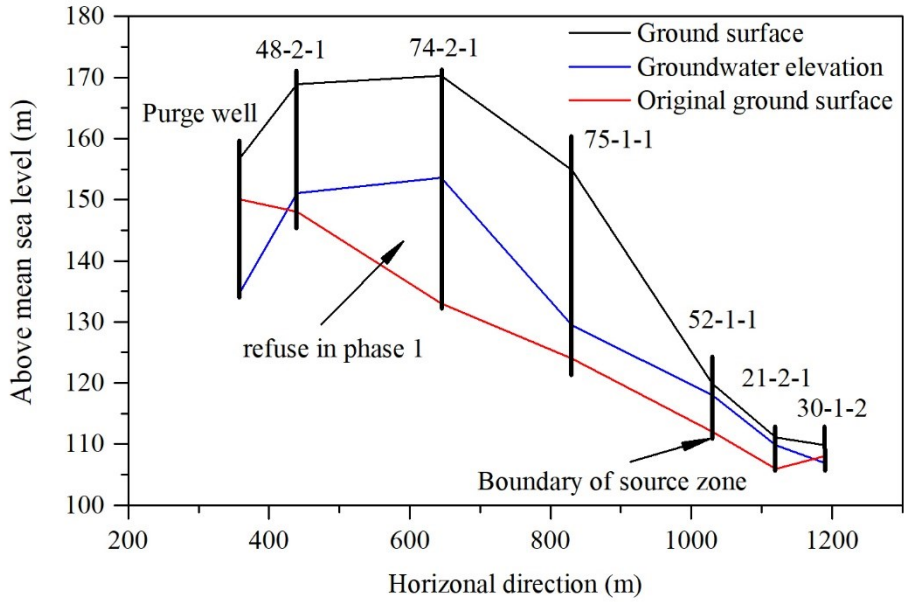

Figure 5-2 Details of the landfill in vertical direction

5.2 Data Collection

5.2.1 Environmental Properties

The operating landfill footprint is approximately 33 hectares with an estimated municipal solid waste of 6,800,000 tonnes at the end of 2016 (AECOM, 2016b). Assuming the amount of refuse in the next years equals to that in 2016, the annual weight and bulk density of disposal are estimated as 146,700 tonnes/year and 800 kg/m^3, respectively.

The environment monitoring annual report of this landfill (AECOM, 2016a) provides the site data including the scale and the description of each zone. The specific values of parameters in these zones are collected based on previous studies as shown in Table 5-1 (Abdelaziz et al., 2013; Harrar et al., 2007; Lu et al., 2011; Nilsson et al., 2001; Staub et al., 2018). The properties of Chromium (Cr) estimated that the diffusion coefficient is 4.64 $\times 10^{-8}$ m^2/s in 90 % clay and 10 % lime (Lu et al., 2011) and the distribution coefficient as 5.5 L/kg (Buczko et al., 2004).

Table 5-1 The parameters of source, unsaturated and groundwater zone (Abdelaziz et al., 2013; Harrar et al., 2007; Lu et al., 2011; Nilsson et al., 2001; Staub et al., 2018)

Parameters in source zone (Staub et al., 2018 and Lu et al., 2011)					
Length	A_x (m)	700	Width	A_y (m)	500
Volumetric air content	φ_a	0.3	Volumetric water content	φ_w	0.2
Pore water velocity	V (m/d)	1.07	Bulk density	ρ_{so} (kg/m^3)	800
Depth	Z_{so} (m)	20			
Parameters in unsaturated zone (Nilsson et al., 2001)					
Average velocity of fluid	V_{un} (m/d)	0.33	Porosity	φ_{un}	0.2
Bulk density	ρ_{un} (kg/m^3)	1460	Depth	Z_{un} (m)	3
Longitudinal dispersion coefficient	D_l (m^2/d)	8.9×10^{-4}	Transverse dispersion coeffcient	D_t (m^2/d)	8.9×10^{-5}
Parameters in groundwater zone (Harrar et al., 2007, Abdelaziz et al., 2013)					
Darcy velocity	V_d (m/d)	0.54	Porosity	φ_{gw}	0.08
Bulk density	P_{gw} (kg/m^3)	2800	longitudinal dispersion coefficient	D_x (m^2/d)	1.64×10^{-4}
Depth	Z_{wt} (m)	10	vertical dispersion coefficient	D_z (m^2/d)	9.10×10^{-5}

5.2.2 Initial and Boundary Conditions

The entire system including consisting of source, unsaturated and groundwater zones is illustrated in Figure 5-3. As the source of contaminant is simplified as the constant flow from source zone and the refuse is only disposed in Phase 2, the location of contaminant flux is in the range of 400 m to 600 m from the top of source zone in *x*-direction. The leachate is collected by the leachate collection system located at the bottom of source zone; the average leachate flow rate and Cr concentration from 2010 to 2015 is 1071 m^3/d and 45 μg/L (AECOM 2016a). Leachate mainly generates by the infiltration of rainwater through the waste and degradation of waste (VanGulck et al., 2003). The average daily rainfall height is 4.3 mm (AECOM 2016a), which

means the volume of rainfall in the study area is estimated as about 1400 m^3/d. Therefore, considering some of the rainfall may not infiltrate into the waste, the emission of Cr contaminant to Phase 2 is estimated as 1.2 times of Cr contaminant collected by this system. Two series of wells are settled in the south and north boundary of source zone. Since the well locations of each series are parallel in *y*-direction, they are simplified as two wells situated in the south (20 m in *x*-direction) and north (690 m in *x*-direction) of source zone, respectively. The amount of discharge is estimated as 25 m^3/day as no data was recorded.

According to the monitoring program annual report in 2009 (AECOM 2009), the average Cr concentration of leachate in Phase 2 is 30.65 µg/L and that of leachate collected from Phase 1 is 10 µg/L in 2009. Therefore, the Cr concentration in Phase 2 of source zone is taken as 30.65 mg/m^3 and that of other areas is taken as 10 mg/m^3. The Cr concentration in Gw-52-1-1, GW-21-2-1, and Gw-30-1-2 are 1.3, 0.3, and 0.20 µg/L (AECOM 2009). The interpolation method is applied to assess the Cr concentrations in groundwater zone. The initial concentrations in *z*-direction are estimated as identical; the upper and lower boundaries are estimated as zero mass flux boundary.

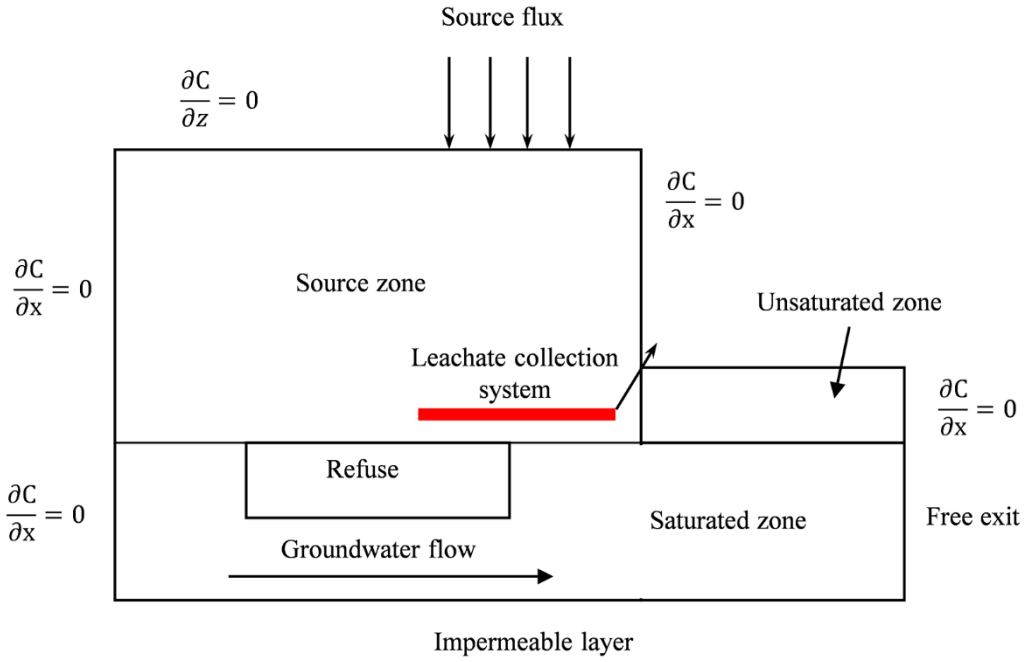

Figure 5-3 Boundary conditions in the study area

5.3 Results

5.3.1 Field Validation

The spatial distribution of Cr in the source zone from 2010 to 2015 is provided in Figure 5-4. It indicates that Cr contaminant transport downwards gradually and only a small amount moves through *x*-direction. This could be ascribed to the fact that the main transport processes in the source zone are advection and dispersion in *z*-direction. Most contaminants stay in phase 2, where they are released into the landfill. The peak concentrations reach 125 mg/m^3. It is worth noting that a part of contaminants is discharged and collected by the existing leachate system so that the concentrations at the bottom of Phase 2 changed a modicum at about 75 mg/m^3 in 2014 and 2015.

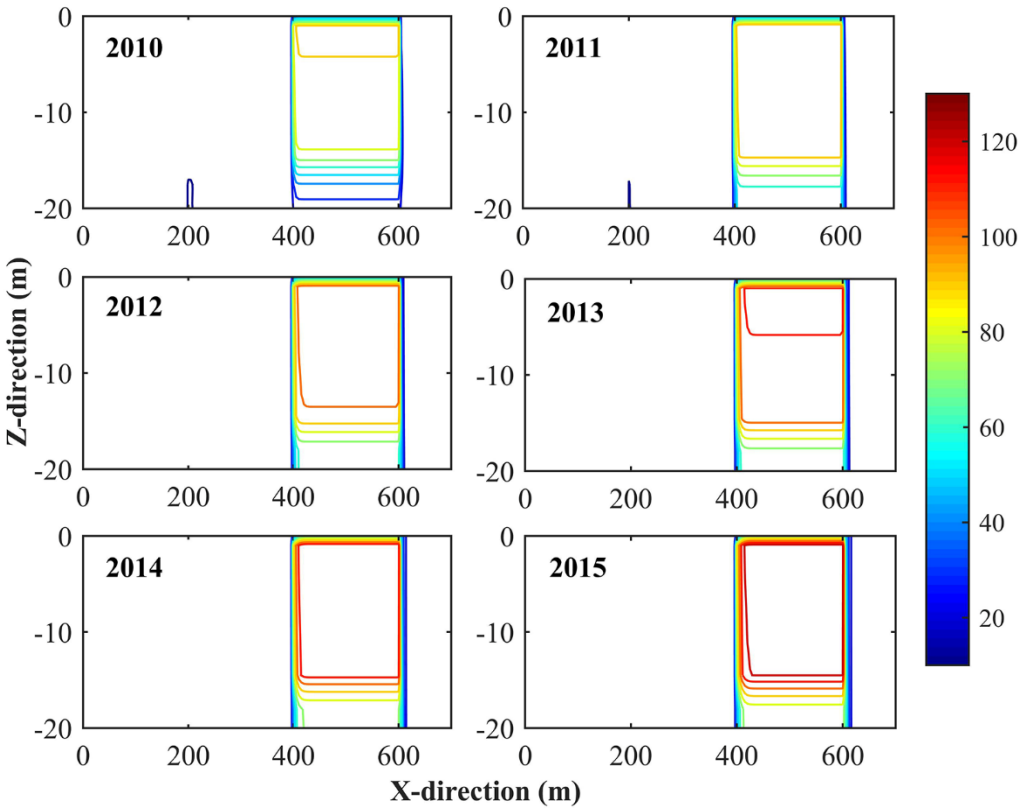

Figure 5-4 Spatial distribution of Cr contaminant in source zone (mg/m^3)

Figure 5-5 presents the spatial distribution of Cr contaminants in groundwater zone from 2010 to 2015. Part of flux transport with a higher rate in the area of refuse due to the lower retardation factor than the others. The concentrations at the bottom of groundwater remain stable over 6 years. With two series of wells discharging the groundwater, the concentrations around are lower than the others. Additionally, because of these purged wells, the concentrations surrounding three monitoring wells are stable. The contaminant migrates into the unsaturated zone tardily in a small amount.

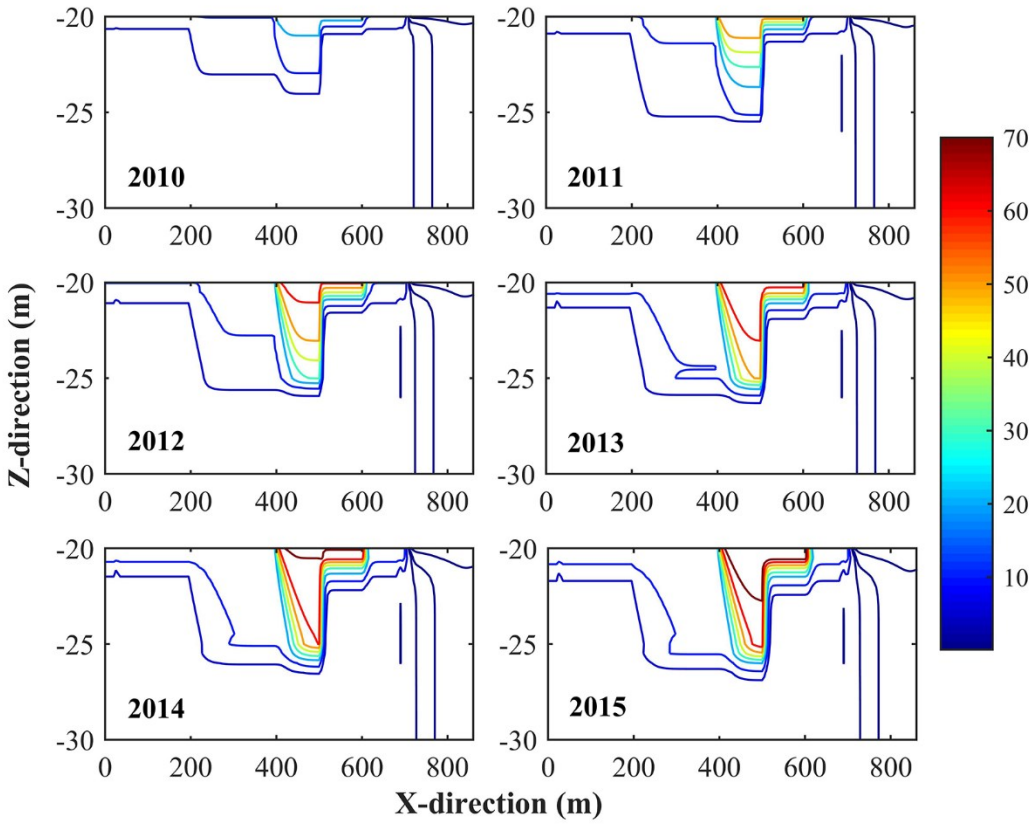

Figure 5-5 contaminant distribution in groundwater zone (mg/m^3)

Figure 5-6 depicts the distribution in the whole system at the end of 2015. As mentioned above, a small percentage of contaminants move into groundwater. The main cause can be that the leachate system collects the majority of Cr contaminant and the rest of leachate transport slowly

due to the high retardation factor in the groundwater system. After 6 years, the highest concentration in the groundwater zone reached 70 mg/m^3 and the concentrations in monitoring wells are stable.

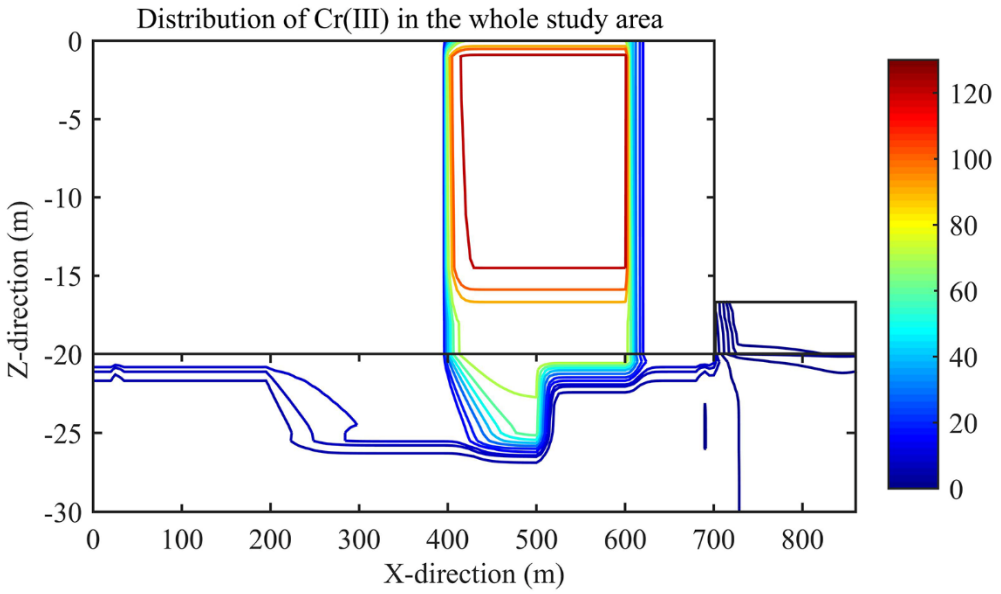

Figure 5-6 Distribution of Cr contaminant in the whole area in 2015 (mg/m^3)

The comparison with simulated and measured results is displayed in Table 5-2. The leachate in Phase 2 cleanout is collected from the leachate collection system in the source zone. Each well (Gw-52-1-1, GW-21-2-1, and Gw-30-1-2) has its own depth and screen elevation. Because of this, the average simulated results in their own screen elevation are compared with the measured data. The measured results show a similar tendency with simulated results. Most of the relative errors are below 30%.

The difference between simulated and measured results of GW-30-1-2 in 2012 is more obvious as shown in Table 5-2. This is probably due to the fact that the samples from these wells are collected each September. In fact, the precipitation rate of September 2012 was relatively low and didn't exceed 0.5 mm, which is extremely lower than in previous years (average value is 60 mm)

(AECOM, 2016a). A high level of contaminant remained in the soil and thus its concentration in groundwater is below the simulated value. According to the result of GW-21-2-1 in 2012, the error is 37.5 % higher than the average level which also supports this assumption. It seems probable that the diverse geological conditions in the groundwater zone cause this difference. Additionally, the relative errors of GW-21-2-1 in 2013 and 2014 are also higher than 40 %. The possible reason is that: (1) The water elevation of the nearby purge well GW-21-2-1 in 2013 is lower than the other years (AECOM, 2013). This is possibly associated with a discharge rate of this well higher than the other years of this well, which makes the amount of contaminants transporting to GW-21-2-1 less. This is not considered in the model; (2) this study only considers two dimensional which might neglect the contaminants' transport from the y-direction. Overall, the simulated and measured results and the application of this 2D model in the multimedia environmental system lead to credible results for a field-scale study.

Table 5-2 Comparison between simulated and measured data (AECOM, 2010; 2011; 2012; 2013; 2014; 2015)

Sites	Years	Measured results (µg/L)	Simulated results (µg/L)	Relative error (%)
Phase 2 cleanout (Source zone)	2010	n/a	77.1	n/a
	2011	107.0	92.6	13.4
	2012	n/a	99.5	n/a
	2013	137.7	106.4	22.7
	2014	120.4	113.2	6.0
	2015	100.7	120.2	19.4
Gw-52-1-1 (groundwater zone)	2010	1.90	1.52	20.0
	2011	n/a	1.67	n/a
	2012	1.38	1.76	27.5
	2013	1.60	1.81	13.1
	2014	1.68	1.83	8.9
	2015	1.40	1.83	30.7
GW-21-2-1 (groundwater zone)	2010	0.30	0.31	3.3
	2011	n/a	0.32	n/a
	2012	0.24	0.33	37.5

Sites	Years	Measured results (μg/L)	Simulated results (μg/L)	Relative error (%)
GW-21-2-1 (groundwater zone)	2013	0.21	0.34	61.9
	2014	0.25	0.35	40.0
	2015	0.30	0.35	16.7
Gw-30-1-2 (groundwater zone)	2010	n/a	0.20	n/a
	2011	0.20	0.19	5.0
	2012	0.11	0.19	72.7
	2013	0.16	0.19	18.7
	2014	0.16	0.18	12.5
	2015	n/a	0.18	n/a

5.3.2 Sensitivity Analysis

The fate of Cr simulated by this system highly relies on the environmental properties. The relative influence of input parameters to model output is defined qualitatively by the Morris screening method. The required simulation number to compute R replicates of the sensitivities for n parameters is $N=R\times(n+1)$ (Cho et al., 2016). The R and n are set as 20 and 4 respectively, thereby 100 simulations are required for sensitivity analysis in source and groundwater zone. The absolute means (μ^*) and the standard deviation (σ) of the input parameters in the source zone and groundwater zone are presented in Figure 5-7. In the source zone, the input parameters include vertical hydraulic conductivity (K_z), vertical diffusion coefficient (D_z), water content (φ_w) and bulk density in source zone (ρ_{so}). The input parameters in the groundwater zone contain longitudinal hydraulic conductivity (K_x), longitudinal diffusion coefficient (D_x), effective porosity (φ_{gw}) and density in groundwater zone (ρ_{gw}). Specifically, K_z is a crucial parameter in the source zone. Its standard deviation value is below other parameters, which indicates that K_z has less interaction with them. By contrast, the most sensitive factor in groundwater zone is K_x that has strong interaction. The relevance of hydraulic conductivity on the contaminant transport in porous media can be easily illustrated. Hydraulic conductivity can impact the velocity of fluid, which directly contributes to contaminant transport.

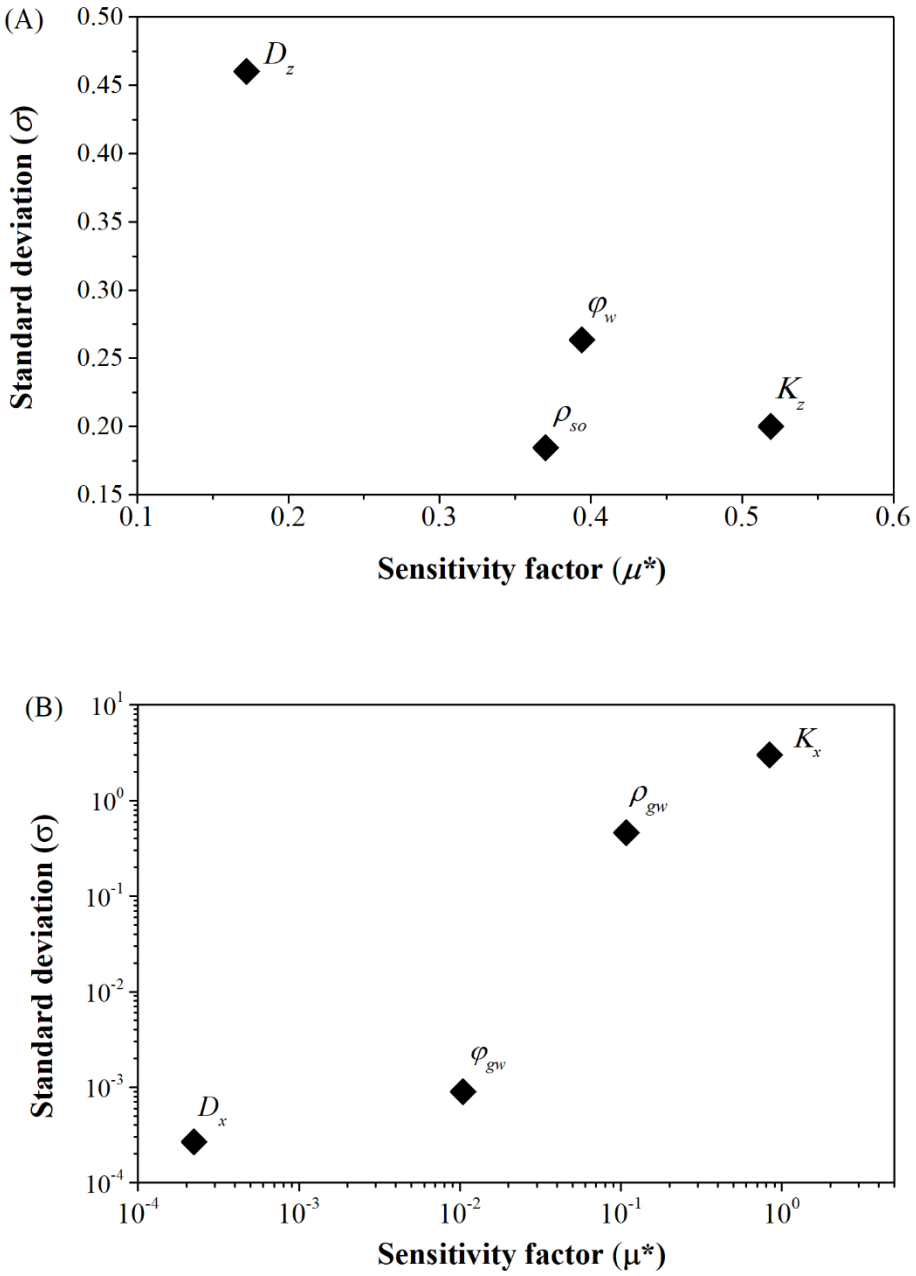

Figure 5-7 Morris screening ranking results for (a) source zone and (b)groundwater zone.

This 2D model is a spatio-temporal environmental fate model, which allows the parameters variation on a spatial scale. Thus, to gain additional insights, it is desirable to assess the spatial variability in the sensitivity analysis. The most sensitive parameters (K_z in source zone and K_x in the groundwater zone) are selected. Figure 5-8 shows the spatial maps of sensitivity indices of

these factors, which reveals some interesting spatial patterns of sensitivity. Firstly, Phase 2 (400-600 m in *x*-direction) is the most sensitive area because this area continually receives refuse which is the major source of contaminant. Sensitivities of the area in the downstream of Phase 2 (*x*-direction) are small, which reveals that Phase 2 has an insignificant impact on the horizontal direction. Sensitivities in the vertical direction of Phase 2 are stable, while values get lower downwardly due to the leachate collection system. The amount of contaminants discharged from this system relies on the concentration of upper flux. The level of contamination increases with the increase in upper flux density. Thus, this system mitigates the variance of contaminant concentrations in Phase 2 bottom. In groundwater zone, Longitudinal hydraulic conductivity is the most sensitive in the downstream of the refuse area which accumulates a large amount of contaminant. Moreover, the sensitivity indices in purged wells are higher than in the nearby area. On the account of the inter-media flux between the unsaturated and groundwater zones, the interface has the highest sensitive indices.

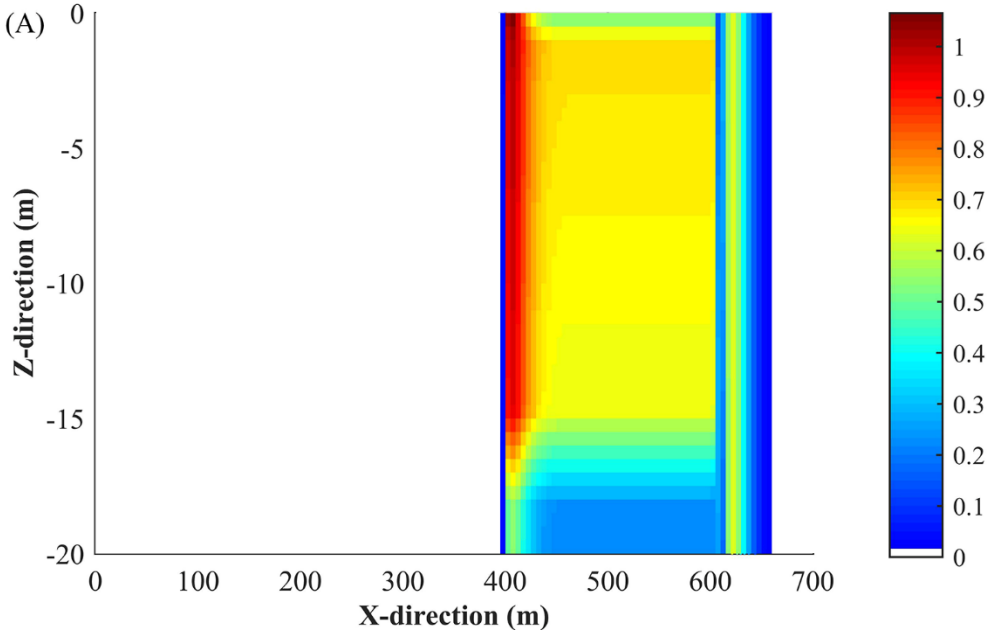

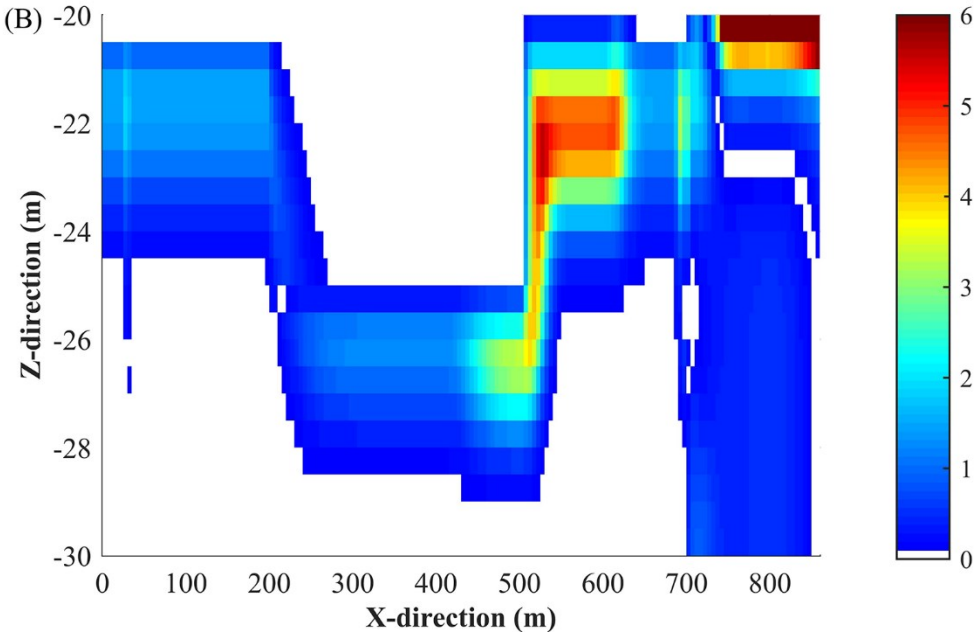

Figure 5-8 Maps of the sensitivity indices for the most sensitive parameters of source and groundwater zone in each grid cell

5.3.3 Risk Assessment

Since this landfill is still receiving the disposal, future risks are assessed. Based on the results mentioned above, two key parameters (K_z and K_x) are selected and a normal distribution is followed. According to the generated Monte Carlo results for the whole system, 95 and 5 percentile contour maps are conducted. Based on the Canadian Environmental Quality Guidelines, the criteria of Cr is 8.90 µg/L. The 95 percentile concentration distribution (Figure 5-9b) may represent a "worst-case" prediction. The *RQs* in source zone as many as 80 represents a high risk. However, that in the other areas, especially monitoring wells, are stable. *RQs* in monitoring wells are from 0.05 to 0.20 which represents a relatively low risk. Compared to *RQs* for 95 percentiles, results of 5 percentile prediction (Figure 5-9a) are generally lower. But *RQs* in source zone still exceeding 1, which is considered as high risk. For the risks in monitoring wells, results of 5 and 95 percentiles provide a similar tendency because of the leachate collection system and purge wells. *RQs* are

more likely to raise without these mitigations. Therefore, although there is no high risk in monitoring wells, attention should be paid when estimating the long-time impact of heavy metal contaminants on the environment and human health. This is a simple and effective method to visually rank the risk zones for the heavy metal contaminant. However, this model system is unable to estimate the risk zone in three dimensions. Moreover, this model is only applied for a small scale case covering 45 hectares. Based on these results, future work will focus on 3D mesh generation and model improvement for large scale applications.

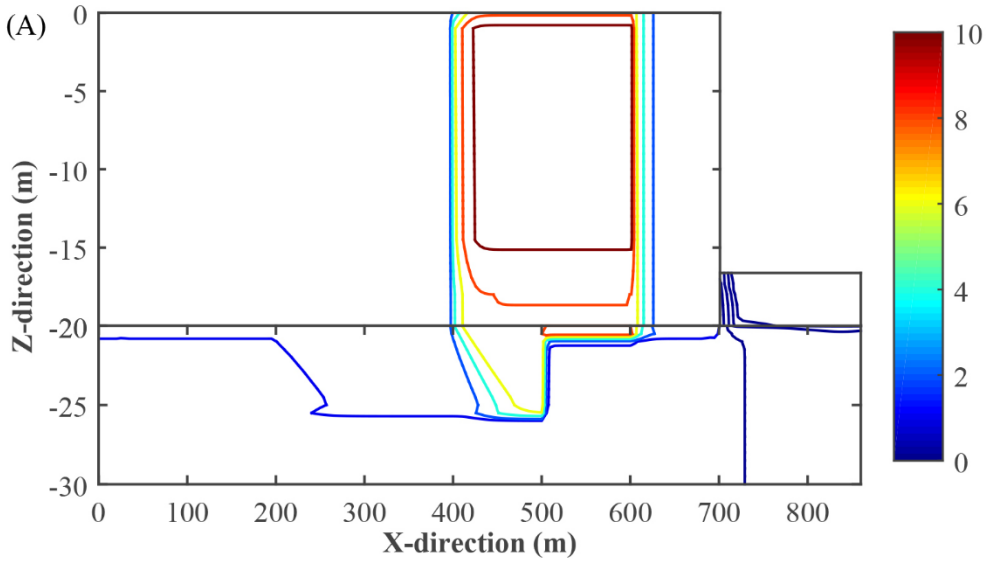

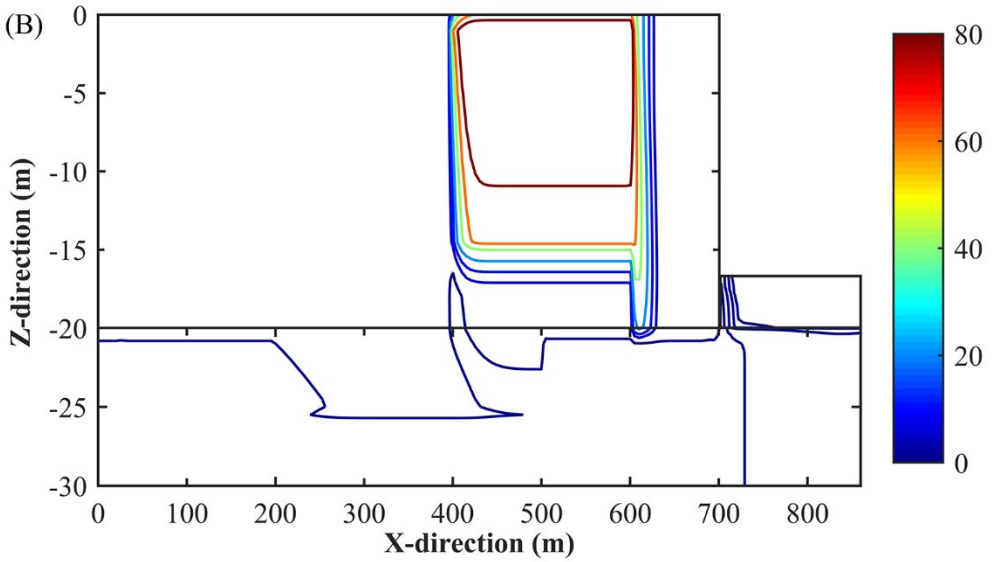

Figure 5-9 Uncertainty predictions showing (a) 5 and (b) 95 percentile *RQs* in the whole area at 2020 (mg/m^3)

5.4 Summary

This proposed modeling approach in 2D version is applied to simulate the environmental fate of Cr in a landfill area, which includes source, unsaturated and groundwater zone modules and integrates these different modules within an entire framework through considering uniform and unsteady flow impacts of leachate emissions. Applying the alternating direction implicit method, it addresses two-dimensional environmental multimedia contaminant problems for temporal and spatial consideration.

The comparison between simulated results and monitoring data shows that almost differences are under 30%. This reveals the efficiency of this model in providing satisfactory results. By applying the Morris screening method, vertical hydraulic conductivity and longitudinal hydraulic conductivity are the most sensitive parameters in soil and groundwater zones. The risk assessment for the landfill site is also investigated through the MCM which predicts a negligible and low risk

in the landfill site in 2020. Considering the leachate collection system and purged wells, the concentration at the boundary of the groundwater zone might remain unchangeable. However, *RQs* in source zone could exceed 10, which are regarded as high risk. These results imply a possibility that without mitigation efforts, a large amount of contamination with Cr from the source zone may have long term adverse impacts on the ecosystems and human health.

To put in a nutshell, besides modeling the spatial distribution of pollutant concentrations, the proposed modeling approach also contributes to environmental risk assessments on regional spatial scales. Additionally, spatial sensitivity analysis provided by this model is useful to identify where to have the most sensitive factors and where the change in sensitivity is high, which is crucial for contaminant mitigation and control decisions.

Chapter 6 First Development and Validation of RNEMM for Assessing the Risk of Antibiotics in Multimedia River Basin System

6.1 Overview of the Study Site

Figure 6-1 shows the study area, which is part of Tianjin city. It includes six main rivers: the Yongding River, the Yongdingxin River, the Beiyun River, the Nanyun River, the Xihe River and the Haihe River. Some of them consist of only part of a river. The whole study area is divided into eight subareas of 380 km^2. The monitoring data and locations of the sampling sites are collected from literatures (Gao et al., 2012; Luo et al., 2011; Zou et al., 2011). The properties of these six rivers are estimated based on the available hydrological data as shown in Table 6-1 (Han et al., 2014; Hong, 1995; Lu & Que, 2007; Ministry of Water Resources the People's Republic of China, 2009; Zhang et al., 2014). The rivers are separated into several sections based on the locations of tributaries and the flow rate is changed due to the inflow from these tributaries. According to the land use of Tianjin city (Tianjin Municipal Bureau of Statistics, 2010), the area of the soil compartment in each subarea is provided in Table 6-2.

Table 6-1 Properties of six rivers

River No.	Section	Flow rate (m^3/h)	Average width (m)	Depth (m)	Velocity (m/h)
1	Yongding	5.49×10^5	200	4	6.86×10^2
2	Yongdinxin-1	3.65×10^5	200	4	4.57×10^2
3	Yongdinxin-2	1.05×10^6	200	4	1.32×10^3
4	Beiyun-1	1.84×10^5	100	4	4.59×10^2
5	Xihe	1.60×10^4	100	2	8.00×10^1
6	Nanyun	1.14×10^5	100	4	2.85×10^2
7	Beiyun-2	2.00×10^5	100	4	4.99×10^2
8	Beiyun-3	2.57×10^5	100	4	6.43×10^2
9	Haihe-1	3.71×10^5	150	4	6.19×10^2
10	Haihe-2	5.55×10^5	150	4	9.26×10^2
11	Haihe-3	6.49×10^5	100	4	1.62×10^3
12	Haihe-4	6.90×10^5	100	4	1.73×10^3
13	Haihe-5	7.66×10^5	150	4	1.28×10^3

Table 6-2 Soil compartment area in each subarea

Subarea	1	2	3	4	5	6	7	8
Soil area (10^7 m^2)	19	7.6	23	7.6	23	15	23	19

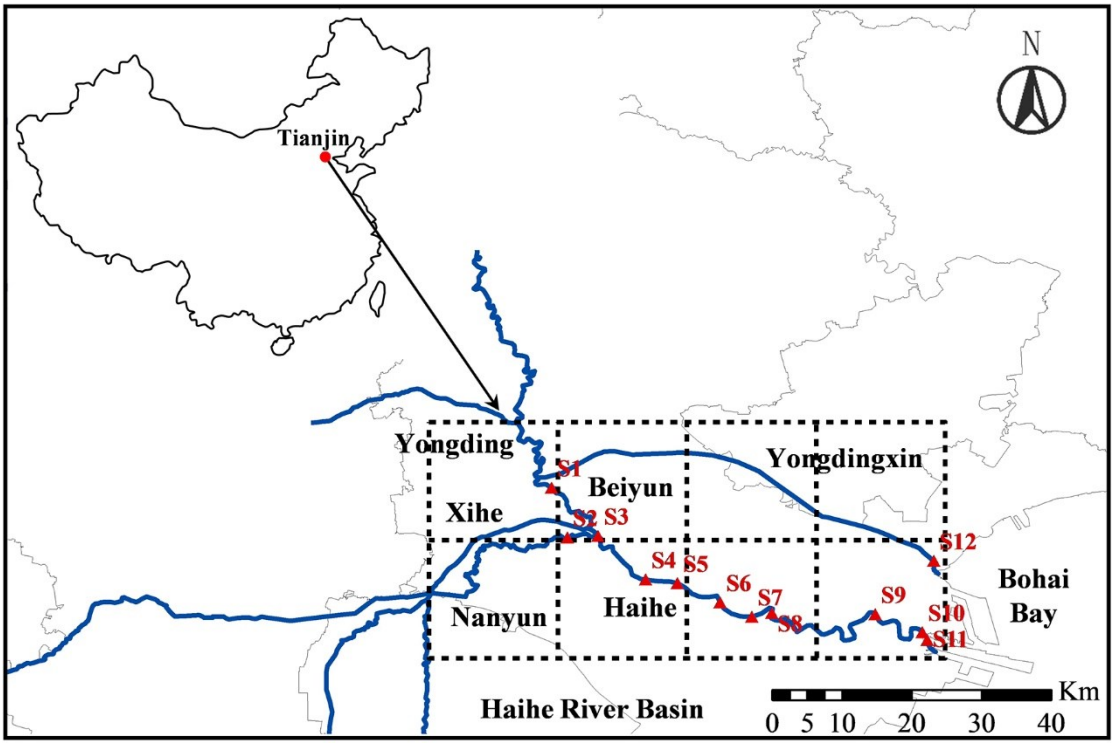

Figure 6-1 Study area and sampling sites

6.2 Data Preparation

6.2.1 Emission Inventory

Sulfadiazine (SDZ) is selected as the target chemical, which is used as an antibiotic for livestock including pigs, chickens and other animals. The data of SDZ use and excretion rates in the study area are collected and examined (Zhang et al., 2015), and other data including the populations of these animals in each subarea are taken from the Tianjin statistical yearbook for this study (Tianjin Municipal Bureau of Statistics, 2010). In terms of antibiotic emissions from animal sources, chicken excretions are assumed to enter the soil compartment. For pigs and other animals, 100% of the urine and about 20% of the total feces are discharged into the water

compartment (Wu, 2005). The source details are given in Table 6-3.

Table 6-3 Source data in subareas

Emission (mol/h)	1	2	3	4	5	6	7	8
Pig	0.200	0.121	0.299	0.048	0.206	0.167	0.156	0.269
Chicken	0.027	0.015	0.041	0.001	0.016	0.012	0.008	0.012
Other	0.008	0.002	0.009	0.001	0.027	0.024	0.006	0.004

The antibiotic pollutants emitted from the human population are mainly found in the discharge from WWTPs. As shown in Figure 6-1, sampling sites S6-S8 are located in the vicinity of numerous animal husbandry and aquaculture industry operations, including approximately 177 CAFOs (concentrated animal feeding operations) and 66.7 km^2 of aquaculture farms (Luo et al., 2011). Therefore, the SDZ discharges from pigs and other animals in subarea 3 are estimated to be emitted evenly into this section. The location, river flow rate and SDZ concentrations of five tributaries in which SDZ is detected are provided in Table 6-4.

Table 6-4 Details of five river tributaries

Tributaries	River	Location (m)	Flow rate (m^3/h)	water (ng/L)
T1	Haihe	11,900	1.84×10^5	430
T2	Haihe	16,400	9.36×10^4	290
T3	Haihe	33,800	7.56×10^4	270
T4	Beiyun	16,100	5.76×10^4	71
T5	Yongdingxin	57,600	6.89×10^5	20

6.2.2 Boundary and Initial Conditions

The upper boundary conditions of the Yongding River are based on the pollutant concentrations of Beijing City, since the water pollutants are discharged from Beijing City to Yongding River. The upper boundary condition is estimated to be 37 ng/L (X. Liu et al., 2019). Those of the Xihe and Nanyun Rivers are estimated to be the same as that of the contaminant from Baiyangdian Lake, namely 118 ng/L (Li et al., 2012). The initial conditions in the system are set to be zero in 2006.

6.3 Results

6.3.1 Model Validation

The RSEMM is regarded as a preliminary version of RNEMM, which incorporates a water quality model for the river network and a fugacity model. This model is applied to simulate the fate and transport of SDZ in the study area. The spatial distribution of SDZ in the soil compartment (Figure 6-2) shows that higher contaminant concentrations are found in the subarea near the urban area of Tianjin City. The highest value is in subarea 2, although the emissions into subarea 2 are not the highest. The reason for this may be that subarea 2 includes the urban area of Tianjin City, and thus its soil compartment area is the lowest. For soil zone, although there is no measured data in the study area, the presence of SDZ and other sulfonamide antibiotics in agricultural soil is detected in the other provinces of China (J. Sun et al., 2017). For instance, the concentrations of SDZ in the agricultural soil samples in the Yangtze River Delta in China range from 0 to 0.91 ng/g (J. Sun et al., 2017). The concentrations of SDZ in the vegetable farm soil of four provinces in China vary from 0 to 0.67 ng/g (Yi et al., 2019). Thus, the simulated results in the study area have the same magnitude as the values reported in the literature. The concentrations in the air compartment are negligible (1.05- 2.99×10^{-11} ng/L), as shown in Table 6-5, which aligns well with the results from the literature (Zhang et al., 2015). The reason for this is possible that little SDZ evaporates from the soil and water compartments to the atmosphere due to the properties of SDZ.

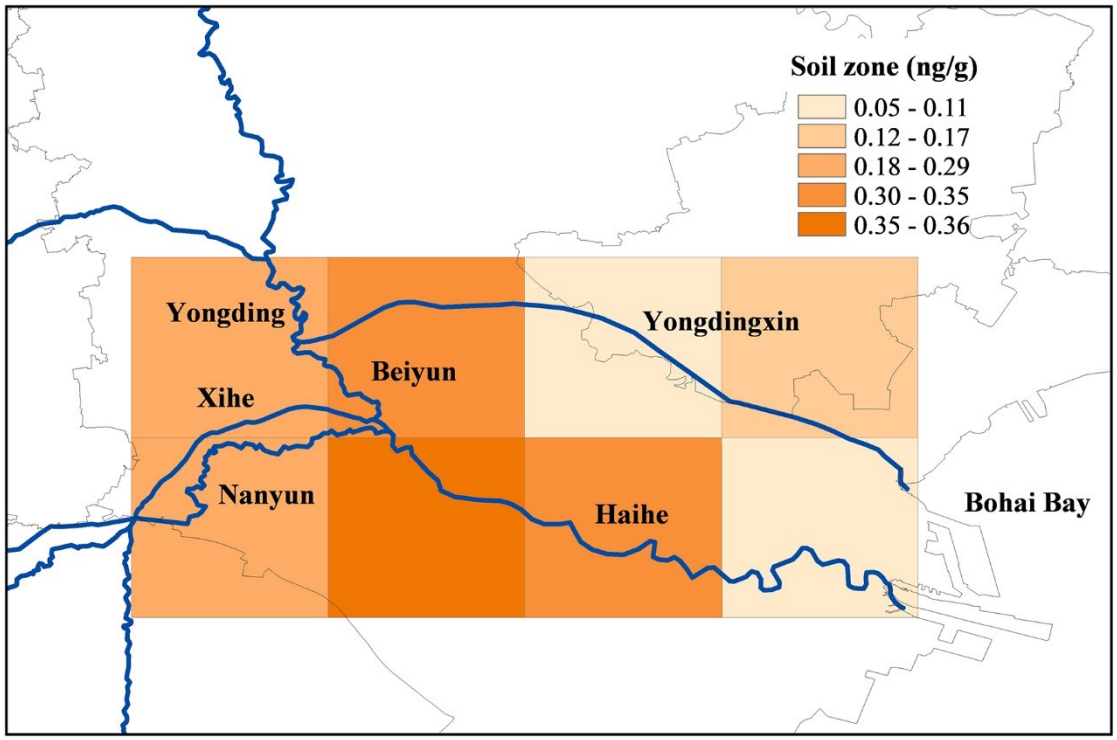

Figure 6-2 Spatial distribution of SDZ concentrations for soil compartments

Table 6-5 Concentrations of antibiotics in soil and air zones

Subarea	1	2	3	4	5	6	7	8
Air (10^{-11} ng/L)	1.88	2.99	2.61	1.30	1.83	2.54	1.05	1.26
Soil (ng/g)	0.29	0.36	0.34	0.05	0.28	0.35	0.11	0.17

Figure 6-3 provides the distribution of SDZ concentrations in the Beiyun and Haihe Rivers. The results are compared with the measured data (Gao et al., 2012; Luo et al., 2011; Zou et al., 2011). The comparison indicates that the simulated results align with the monitoring values. In the part of Haihe River (30-50 km) that includes numerous animal husbandry and aquaculture industry operations, the model underestimates the concentration of SDZ. Possible reasons for this include, firstly, that the emissions may be underestimated since the use of SDZ is estimated based on the average value in China. Secondly, the estimated emission is postulated to be discharging evenly, so in some specific sites, it is lower than the real value. According to the comparison between the numerical results and the measured data (Table 6-6), the majority of the relative differences are lower than 40 % for river water systems in this study. The results prove that the developed river

scale multimedia model can analyze the spatial distribution of antibiotic contaminants in multiple environmental media compartments.

Table 6-6 Comparison between modeling results and measured data (Gao et al., 2012; Luo et al., 2011; Zou et al., 2011)

Sampling No	River	Measured results		Simulated results		Relative error	
		Water (ng/L)	Sediment (ng/g)	Water (ng/L)	Sediment (ng/g)	Water (%)	Sediment (%)
S01	Beiyun	5.9	-	4	0.6	32.2	-
S02	Nanyun	2.5	-	2.8	0.4	12.0	-
S03	Beiyun	31.9	-	18.8	2.6	41.1	-
S04	Haihe	100	5.4	145.2	7.9	45.2	46.3
S05	Haihe	150	26	126.5	13.7	15.8	47.3
S06	Haihe	78	16	86.2	12.3	10.5	23.1
S07	Haihe	180	20	149.6	20.9	16.9	4.5
S08	Haihe	270	30	277.3	34.3	2.7	14.3
S09	Haihe	-	8.1	58.6	8.3	-	2.5
S10	Haihe	18.7	-	27.2	3.9	45.5	-
S11	Haihe	-	3.4	25.4	3.6	-	5.9
S12	Yongdingxin	21	-	17.4	1.8	17.1	-

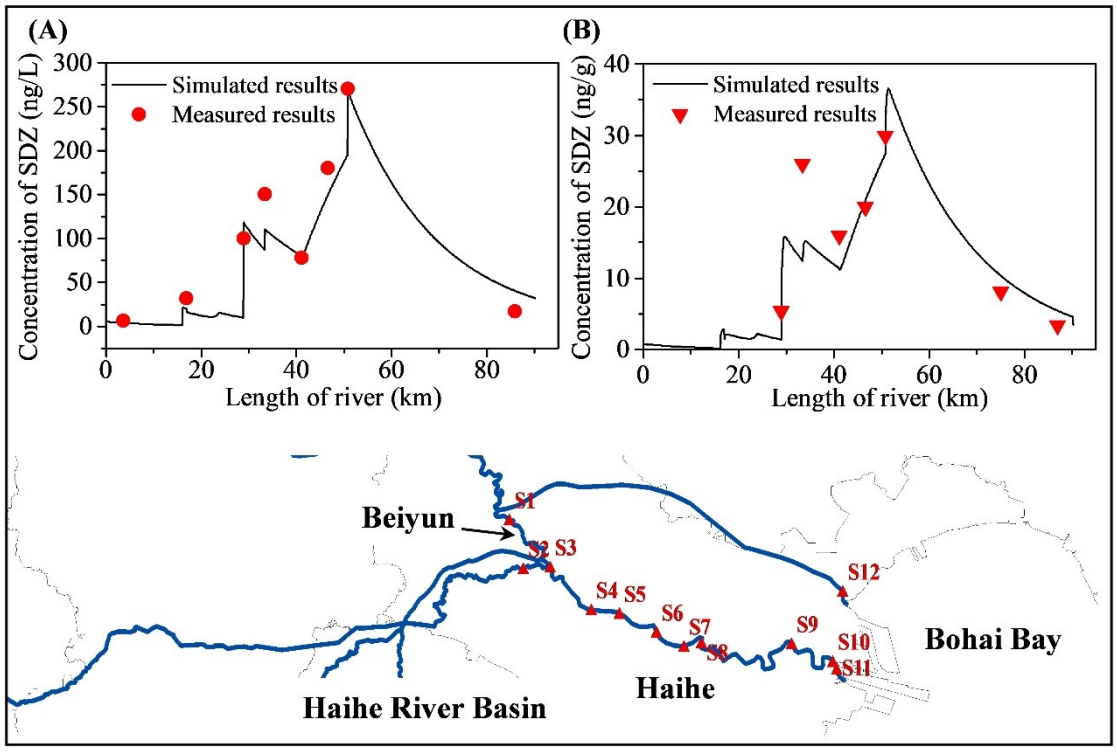

Figure 6-3 Distribution of SDZ in (a) water and (b) sediment zones in the Beiyun & Haihe Rivers

The results from the multi-compartment EMM in most locations for soil and sediment zone are generally lower than the measured results due to the above-mentioned reasons. Especially the simulated concentrations in the sediment show considerable differences in magnitude from the measured data. This is because the multi-compartment EMM only represents the screening level or average results. It confirms that the multi-compartment EMM needs to be further improved in terms of spatial resolution for better accuracy.

6.3.2 Sensitivity Analysis

The Morris screening method is used to identify qualitatively important factors for the regional spatial multimedia model in this study. Four model input parameters are selected for the water and sediment compartments. The p and the number of elementary effects (R) are set as 4 and 5 respectively. The number of simulations is 50.

The Morris screening ranking results are shown graphically in Figure 6-4. K_{se} and K_w are the degradation rates in the sediment and water zones; h_{se} and h_w are the depths of the sediment and water compartments; u_{ss} is the sedimentation velocity; ρ_{ss} is the concentration of suspended particulates; D_x is the dispersion coefficient; Q_w is the flow rate. Each factor is represented by a point with the coordinate (μ^*, σ). A large magnitude of μ^* indicates the importance of its associated parameter. Figs. 6-4a and 6-4b indicate that active depths in the sediment zone (h_{se}) and flow rate (Q_w) are the most sensitive factors in the sediment and water compartments. This aligns with the conclusions of previous research (e.g., (Giri et al., 2001)). The scatter plots also aid in identifying anomalies as well as separating nonlinearities from the interaction. The σ values of h_{se} and Q_w are also the strongest interacting parameters.

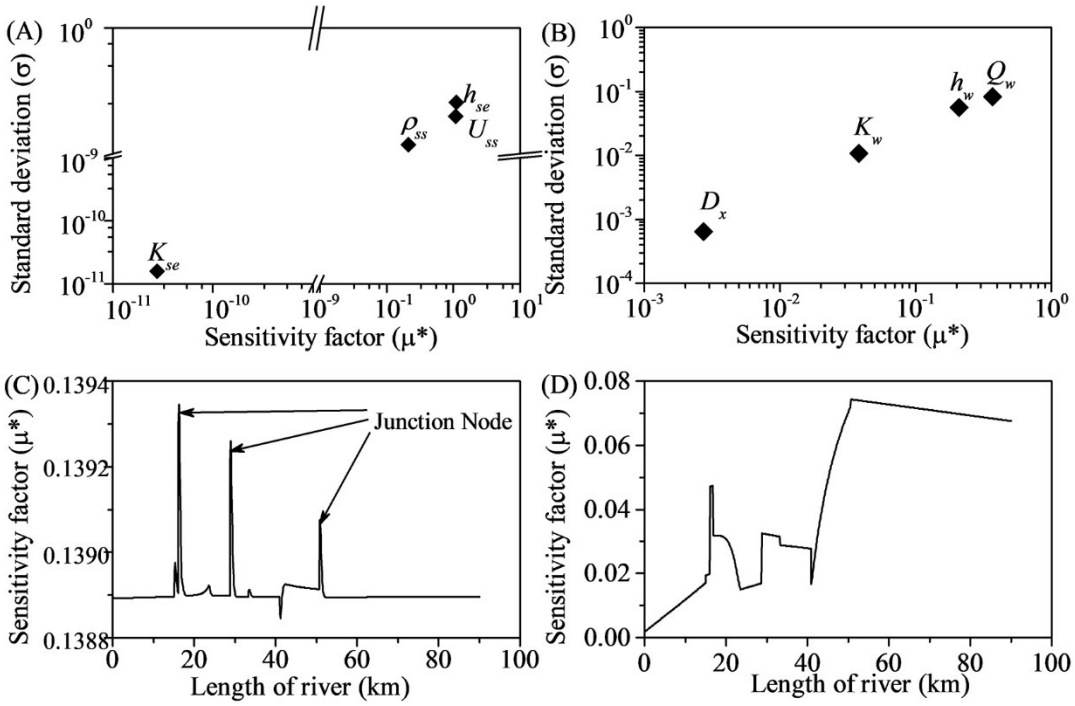

Figure 6-4 Morris screening ranking results for (a) sediment concentration and (b) water concentration; the plot of sensitivity indices of (c) active sediment depth and (d) flow rate within Beiyun and Haihe Rivers.

For the sake of performing a spatial sensitivity analysis, the plots of the sensitivity indices of the active sediment depth and flow rate within the Beiyun and Haihe Rivers are presented in Figs. 6-4c and 6-4d. Figure 6-4c indicates that the values of μ^* at the majority of sites are stable and that in the junction nodes and source points have relatively higher values, which means the locations have little influence on the model output in the sediment compartment. A possible reason for this is that the only source of pollutants is sedimentation from suspended particulates. Figure 6-4d shows that the factors with the highest effects varied throughout the rivers depending on the locations. In the junction nodes and source points, the plot displays larger sensitivity indices. Unlike the tendency seen in the sediment compartment, the junction nodes and source points also have a great impact on the sensitivity indices downstream. It is essential to understand which locations have the most sensitive factors and where the change in sensitivity is high. Generating a

spatial distribution of the sensitivity factors is useful while planning sampling for model validation and regulatory compliance.

6.3.3 Health Risk Assessment

According to the recent national action plan for inhibiting the growing threat of antimicrobial resistance (Xiao, 2017), the percentage of veterinary antibiotics sold based on prescription will be increased to 50% in 2020, which means the overuse of antibiotics will be managed. Therefore, two scenarios (A and B) are studied using the developed RSEMM to see the possible health risks in the future with and without the control of antibiotics, respectively. Scenario A assumes that the use of human antibiotics in the study area will be reduced by 50%. Considering the increasing livestock population, the amount of veterinary antibiotics will be reduced by 40%. Scenario B, the use of antibiotics is estimated to increase at a constant rate from 2007 to 2020 (Zhiyan Consulting Group, 2015). The amount of antibiotics consumed in 2020 will be about three times more than in 2009 if there is no antibiotics control action.

Water is both a source of drinking water and a pollutant source for fish. The spatial distributions of SDZ concentrations are calculated using RSEMM and the hazard quotients (*HQs*) are then estimated with consideration to the acceptable daily antibiotic intake data for adults and children. *HQ* is a commonly used ranking criterion in environmental risk assessment (Zhang et al., 2018) and also used in human health risk assessment (Leung et al., 2013). In general, $HQ > 1$ means the contamination in that area is of high risk, $HQ < 1$ means it is of medium risk and $0.01 < HQ < 0.1$ indicates low health risk. Figure 6-5 presents the spatial distribution of *HQs* for two scenarios in 2020. Since there are no sources in the Yongding and Xihe Rivers, the results of the two scenarios are the same for these two rivers. This indicates that the health risks in the study area could be reduced in correspondence with possible mitigation actions. However, they will increase dramatically without control of the use of antibiotics. The *HQs* in the Jinnan district, located about 40-60 km from the Haihe River, are the highest as this area features a large amount of animal husbandry and aquaculture industry operations. The *HQs* of each subarea (Table 6-7)

also align with the results. The highest *HQ* value is 6.82×10^{-3} in subarea 3, and all the values are lower than 0.01, suggesting that they are less likely to cause serious adverse toxic effects in humans. The results in other areas in China provide similar results, wherein most of the *HQ* values of SDZ are lower than 0.01 (Hu et al., 2018; Lu et al., 2018). However, the results should be treated carefully since single contaminant exposure scenarios are unrealistic due to the hybrid effect of multiple contaminants in the real environment (Yan et al., 2013). Therefore, special attention should be paid when estimating the presence of antibiotics in the environment for the health of humans and ecosystems.

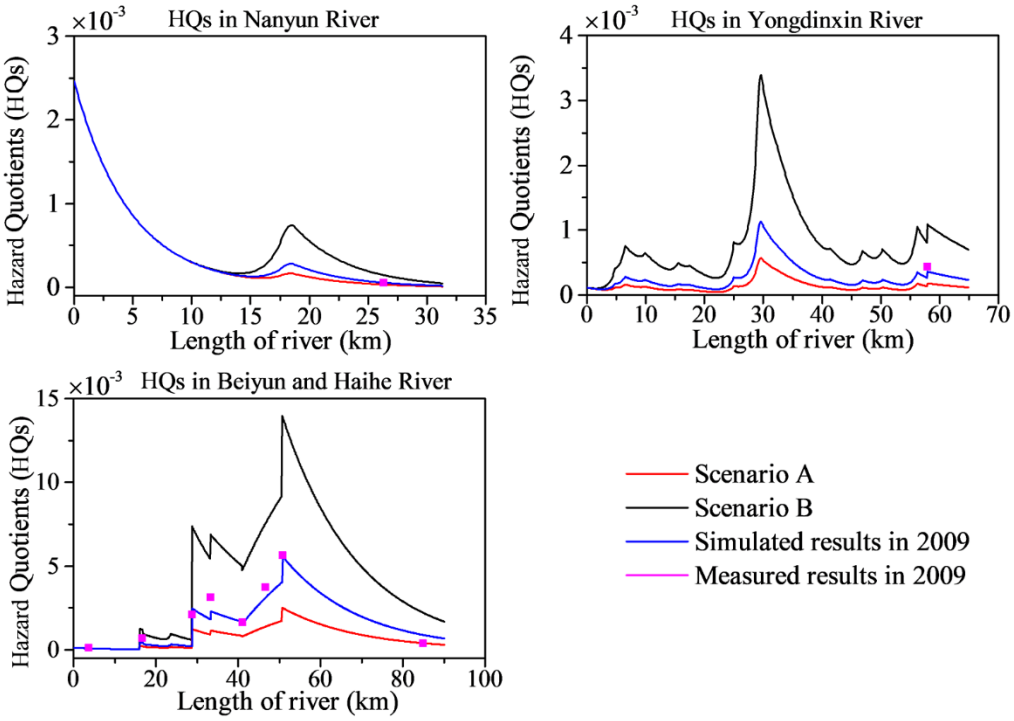

Figure 6-5 Spatial distribution of *HQs* (children) in rivers for two scenarios in 2020

Table 6-7 *HQs* of each subarea in 2020

Scenario	*HQs* (10^{-3})	1	2	3	4	5	6	7	8
A	Adults	0.27	0.22	0.63	0.31	0.11	0.04	0.11	0.05
	Children	0.53	0.42	1.22	0.60	0.22	0.07	0.22	0.10
B	Adults	0.32	1.26	3.51	1.72	0.12	0.17	0.67	0.30
	Children	0.62	2.45	6.82	3.34	0.22	0.32	1.31	0.58

6.4 Summary

The developed RSEMM model integrating a water quality model and a multi-compartment EMM is tested and applied to the Beijing-Tianjin area in China with SDZ being selected as the target pollutant. The overall comparison between the simulated and monitored data indicates a good alignment between the SDZ concentrations in the water and sediment compartments. Most of the average relative errors for the SDZ concentrations are lower than 40%. This approach is a modeling tool that could be extended to apply to other emerging contaminants such as tetracyclines and fluoroquinolones.

The Morris screening method is used to evaluate the sensitivity of the model parameters. The active sediment depth and flow rates are the most sensitive factors and have the most interaction with the other parameters in the sediment and water compartments, respectively. Two modeling scenarios are performed for predicting health risks and for examining antibiotic contaminants' control policies. It can be concluded that the *HQs* could shrink considerably if antibiotic use is more tightly controlled. However, if antibiotic use thrives at the current rate, the *HQ* values in 2020 will be three times than they were in 2009. The first application of RSEMM for SDZ in the Haihe River Basin demonstrates the usefulness of this model in describing the spatial and temporal distributions of the emerging contaminant in a multimedia environment.

7. Validation of RNEMM through Assessing Spatial Eco-environmental exposure risk of Perfluorooctane Sulfonate (PFOS) in the Pearl River Basin

7.1 Overview of the Study Site

The study area is in the Pearl River Basin, which is located in Southern China as shown in Figure 7-1. The Pearl River Basin includes several main river tributaries: Beijiang River, Dongjiang River, Pearl River and Xijiang River, which are the drinking water supply for millions of people in this region (Liu et al., 2015). However, the anthropogenic activities including manufacture, application and disposal of PFASs have caused serious PFOS contamination in the Pearl River Basin. Figure 7-1 shows the case study area over the Pearl River Basin including urban zones of Foshan, Guangzhou and Dongguan Cities, which is divided into eight segments that each of them covers around 510 km^2.

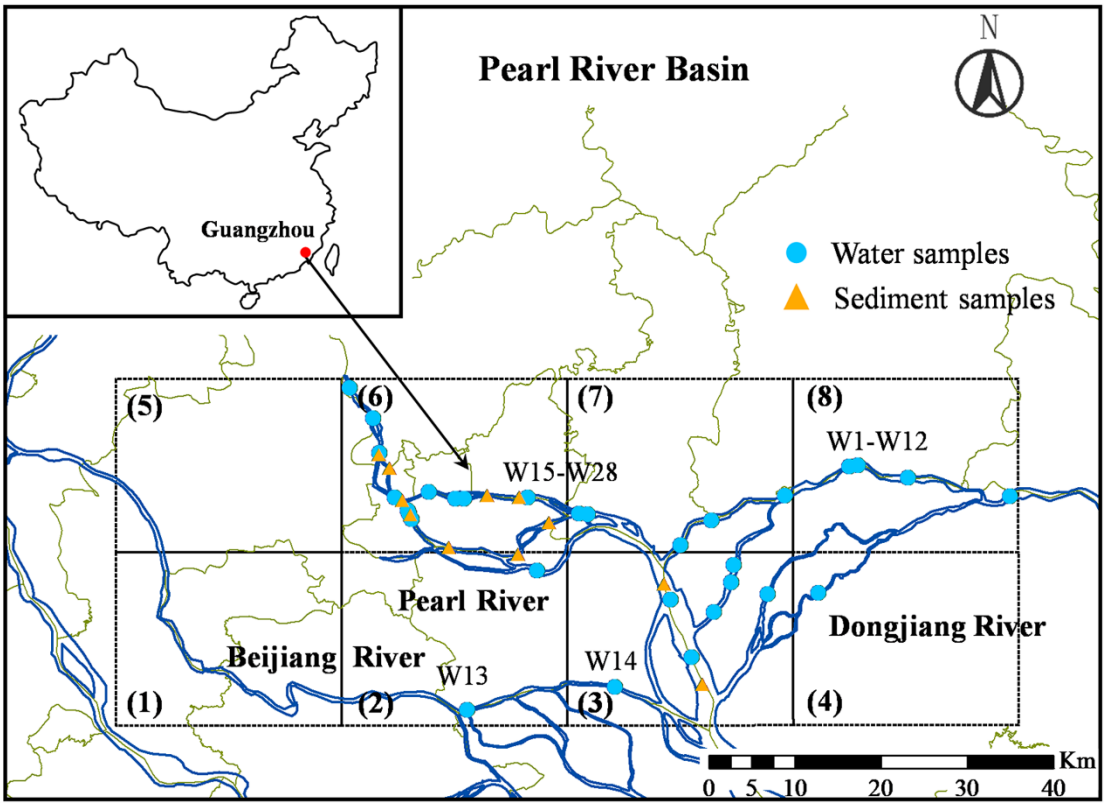

Figure 7-1 Study area and the conceptual model

7.2 Data Collection

7.2.1 Environmental Properties

The chemical and physical properties of PFOS are listed in Table B-1. Table B-2 provides the characteristics of these rivers based on the available hydrological data. The content of suspended particulates in Dongjiang, Beijiang and Pearl River is taken as 0.103, 0.130 and 0.120 kg/m^3 (Hydrologic Bureau of the Ministry of Water Resources, China, 2013). Table B-3 provides the area (km^2) of each soil cell in each subarea according to the land use (Resource and Environment Data Cloud Platform, 2015). Besides, the parameters and data of soil and atmosphere are shown in Table B-4. The average wind speed in x- and y-direction are analyzed based on the meteorological data of Guangzhou in 2013 (National Meteorological Information Center, 2012).As introduced in section 2.1.4, the transfer rates for intermedia transport are mainly estimated based on the specific

processes. According to the related equations and the values of required parameters provided by Kong et al. (2018) and Zhang et al. (2015), the R_{wa} and R_{aw} are estimated as 2.43×10^{-5} and 0.51 m/day, respectively. Moreover, the R_{sa} is estimated as 0.48 m/day (Mackay et al., 1996).

7.2.2 Emission Inventory

The direct sources of PFOS in soil are the application of aqueous fire-fighting foams (AFFFs), use of sulfluramid, stacking of solid waste and disposal of sludge (Meng et al., 2018). The number of fire accidents with the application of AFFF containing PFOS, usage of pesticide, the amount of wastewater discharge and solid waste generation in the study area are collected to estimate these four emission sources (Statistics Bureau of Guangdong Province, 2013). Xie, Wang, et al. (2013) investigated different source categories of PFOS and established the equations for estimating the amount of PFOS emission from these sources. For instance, the number of fire accidents in the study area is considered to estimate the emission from the usage of AFFFs (Xie, Wang, et al., 2013). The emissions of PFOS into the soil subareas in the study region from the usage of AFFFs are estimated in Table 7-1 based on the distribution of fire accidents in three major urban areas of the study region (Statistics Bureau of Guangdong Province, 2013). Table 7-1 provides the PFOS emission inventories to soil zone in each subarea.

Table 7-1 PFOS emission inventories to soil zone in each subarea

Subarea	Application of AFFFs (g/d)	Use of sulfluramid (g/d)	Disposal of sludge (g/d)	Stacking of solid waste (g/d)
1	14.30	14.89	15.93	6.66
2	6.40	11.11	7.62	2.54
3	13.11	21.53	18.14	10.30
4	18.37	27.00	10.83	4.63
5	6.27	22.32	7.56	4.04
6	29.74	14.53	107.11	12.56
7	8.59	15.83	27.19	1.71
8	11.83	32.65	21.72	2.61

The PFOS emission to surface water classified by two different type: domestic emission and industrial emission. As domestic emission is mainly discharged from WWTPs, the domestic

emission density (*ED*, g/km^2 day) of PFOS in the service area of a WWTP is estimated based on population density (*PD*, capita/km^2) and per capita disposable income (*PCDI*, RMB) (Xie, Lu, et al., 2013):

$$f(PD, PCDI)_{PFOS} = 1.254 \times 10^{-11} \times PD^{1.317} \times PCDI^{1.664} \quad (7\text{-}1)$$

According to locations and discharge rate of WWTPs in the study area, the domestic emission amount of PFOS from WWTPs are estimated.). (Xie, Wang, et al., 2013) classified the industrial sources of PFOS as direct and indirect sources. The former ones are the discharges during manufacture and application, and the latter ones are the discharge as impurities during fabrication of POSF-derivatives and by breakdown from PFOS-precursors. This study also investigated the amount of PFOS in Guangdong Province and suggests that textile treatment and metal plating are the major sources of PFOS industrial emission in Guangdong Province (Xie, Wang, et al., 2013), which emits to the environment through WWTPs to water or direct release to the atmosphere and soil. The locations of these industries are obtained from the China Client Platform (China Client Platform, 2019), which provides the marketing information database in China, and the emissions of PFOS into the river system from each industrial location are then determined. The direct emission to atmosphere is mainly from the metal plating and PFOS production processes, and the point air emission sources are determined based on the locations of these industries. The total emission amount for the study region is then estimated based on the average emission density (g/km^2 year) of Guangdong Province (Xie, Wang, et al., 2013).

7.2.3 Food Web System Analysis

Table 7-2 classifies the species in aquatic ecosystem into different guilds and their diet matrix. Based on the previous study (Wang, 2016), this diet matrix is simplified and some fish species mainly consumed by human are selected. The biocommunity of the study river network comprises of 11 functional groups, which include detritus (G1), phytoplankton (G2), zooplankton (G3), macrophyte (G4), herbivorous feeders (G5), crucian carp (G6), mud carp (G7), tilapia (G8), grass

carp (G9), common carp (G10) and leather catfish (G11) as shown in Table 7-2. The other related information for the local food web system is provided in Table B-5.

Table 7-2 The diet matrix of the aquatic ecosystem in the study area (Wang, 2016)

		Predator										
	Prey	1	2	3	4	5	6	7	8	9	10	11
1	Detritus	0	0	0.84	0.40	0.55	0.31	0.80	0.77	0.79	0.23	0
2	Phytoplankton	0	0	0.15	0.20	0.30	0.02	0.03	0.03	0	0.01	0
3	Zooplankton	0	0	0.01	0.40	0.15	0.04	0.04	0.04	0	0.01	0
4	Macrophyte	0	0	0	0	0	0	0	0.06	0.13	0	0
5	Herbiorous feeders	0	0	0	0	0	0.55	0.12	0.10	0.08	0.69	0.19
6	Crucian carp	0	0	0	0	0	0	0	0	0	0	0
7	Mud carp	0	0	0	0	0	0	0	0	0	0	0.37
8	Tilapia	0	0	0	0	0	0	0	0	0	0	0.06
9	Grass carp	0	0	0	0	0	0	0	0	0	0	0
10	Common carp	0	0	0	0	0	0	0	0	0	0	0.33
11	Leather catfish	0	0	0	0	0	0	0	0	0	0	0

7.2.4 Parameters of Health Risk Assessment

Based on section 3.5, the hazard quotient (*HQ*) can be evaluated by comparing the estimated daily intake (*EDI*) and reference dose (*RfD*). The value of *RfD* for PFOS is estimated with 25 ng/kg day (Pan, Zhao, et al., 2014). The daily freshwater fish intake rate of children and adults in the coastal area of Guangdong Province is 25.0 and 37.5 g/day, respectively (Li et al., 2013). Furthermore, the required parameters in equation 3-35 are shown in Table 7-3.

Table 7-3 Parameters related to adult and child receptors (Dong et al., 2019; Li et al., 2013)

Parameters	Symbol	Units	Adult	Child
Body weight	BW	kg	70	14
Water consumption	IR_{DW}	L/day	2	1
Fish consumption	IR_F	g/day	37.5	25
Exposure frequency	EF	day/year	350	350
Exposure duration	ED	year	30	6
Averaging time	AT	day	10950	2190

7.3 Results

As aforementioned, the emission inventory and main environmental properties of the study area in 2013 are collected. Concentrations of PFOS in all environmental media are then calculated by the RNEMM. The obtained spatial distribution of PFOS situation in 2013 are compared with the measured data.

7.3.1 Spatial Distribution of PFOS in Water and Sediment Zone

Figure 7-2 provides the spatial distribution of PFOS in the middle-downstream of Pearl River including Qianhaidao (QHD) and Zhujiangzhudao (ZJZG) and two tributaries of Dongjiang River (Dongjiangbei, DJB, and Dongjiangnan, DJN). The simulated results are then compared with measured data as shown in Table 7-4. The measured data of water zone are collected in 2012 and 2013, and that of sediment zone are collected in 2009 (Bao et al., 2010; Gao et al., 2015; Liu et al., 2015; Zhang et al., 2013). The results indicate that most of the simulated results agree well with the measured values and the majority of relative errors are less than 40 %. It indicates a high relative error in the end of ZJZD, where is the estuary of Pearl River with fresh water and sea water exchanges. More results of model evaluation statistics include the ratio of the root mean square error to the standard deviation of measured data (RSR), Nash-Sutcliffe efficiency (NSE) and Percent bias (PBIAS), which are the most widely used estimators (Setegn et al., 2010). When the values of RSR$<$ 0.7, NSE$>$ 0.5 and PBIAS ϵ [−70 %, +70 %], the model prediction can be regarded as agreeable (Kundu et al., 2017). When comparing the simulated results and measured data of water zone collected in 2013 in this study, the values of RSR, NSE and PBIAS are 0.53, 0.72 and -4.42 %, respectively.

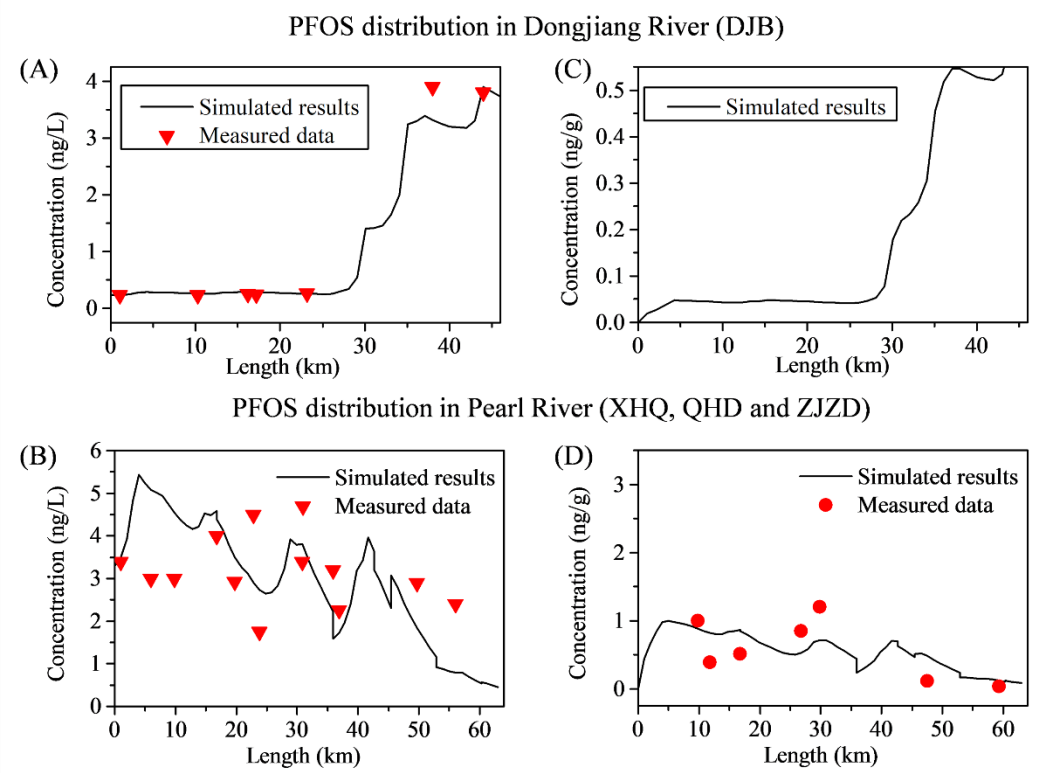

Figure 7-2 Comparison between simulated and measured results of PFOS distribution in water (a and b) and sediment (c and d) compartments in 2013 (Bao et al., 2010; Gao et al., 2015; Liu et al., 2015; Zhang et al., 2013)

Table 7-4 Comparison between simulated and measured results in water and sediment zones (Bao et al., 2010; Gao et al., 2015; Liu et al., 2015; Zhang et al., 2013)

Water Sample No.	Measured results (ng/L)	Simulated results (ng/L)	Relative error (%)	Sediment Sample No.	Measured results (ng/g)	Simulated results (ng/g)	Relative error (%)
W1	0.24	0.24	0	S1	1	0.88	12
W2	0.233	0.28	20	S2	0.39	0.82	110
W3	0.262	0.27	4	S3	0.51	0.85	66
W4	0.249	0.27	7	S4	0.85	0.52	38
W5	0.265	0.30	14	S5	1.2	0.71	41
W6	3.9	3.32	15	S6	2	0.74	63
W7	3.8	3.90	3	S7	1.1	0.63	42
W8	4.1	1.25	70	S8	0.58	0.68	17
W9	2.778	1.13	59	S9	0.43	0.24	45

Water Sample No.	Measured results (ng/L)	Simulated results (ng/L)	Relative error (%)	Sediment Sample No.	Measured results (ng/g)	Simulated results (ng/g)	Relative error (%)
W10	3.9	0.91	77	S10	0.11	0.39	255
W11	0.392	0.50	27	S11	0.03	0.10	225
W12	0.433	0.40	8				
W13	1.6	1.58	1				
W14	1	1.68	68				
W15	3.4	3.49	3				
W16	3	5.08	69				
W17	3	4.55	52				
W18	4	4.59	15				
W19	2.928	3.50	19				
W20	4.5	2.90	36				
W21	1.748	2.74	57				
W22	3.4	3.80	12				
W23	10.608	4.14	61				
W24	4.178	3.79	9				
W25	3.038	4.14	36				
W26	3.2	1.96	39				
W27	2.268	1.73	24				
W28	2.228	2.91	30				
W29	2.9	1.84	37				
W30	2.4	0.78	67				

The PFOS distribution of water and sediment zone in the study area is presented in Figure 7-3. The PFOS concentrations in the upstream of Pearl River are quite higher than the other areas since the area is located in the urban zone of Guangzhou City where there are more than 2 million people and many industries (Statistics Bureau of Guangdong Province, 2013). The PFOS concentrations in Beijiang and Dongjiang Rivers vary from 0.4-2.3 and 0.24-3.3 ng/L, respectively, where the downstream concentrations are relatively higher than upstream in these two rivers due to more industries located in the downstream. With the flow entering the estuary of Pearl River, the PFOS concentration decreases due to less industrial emission sources.

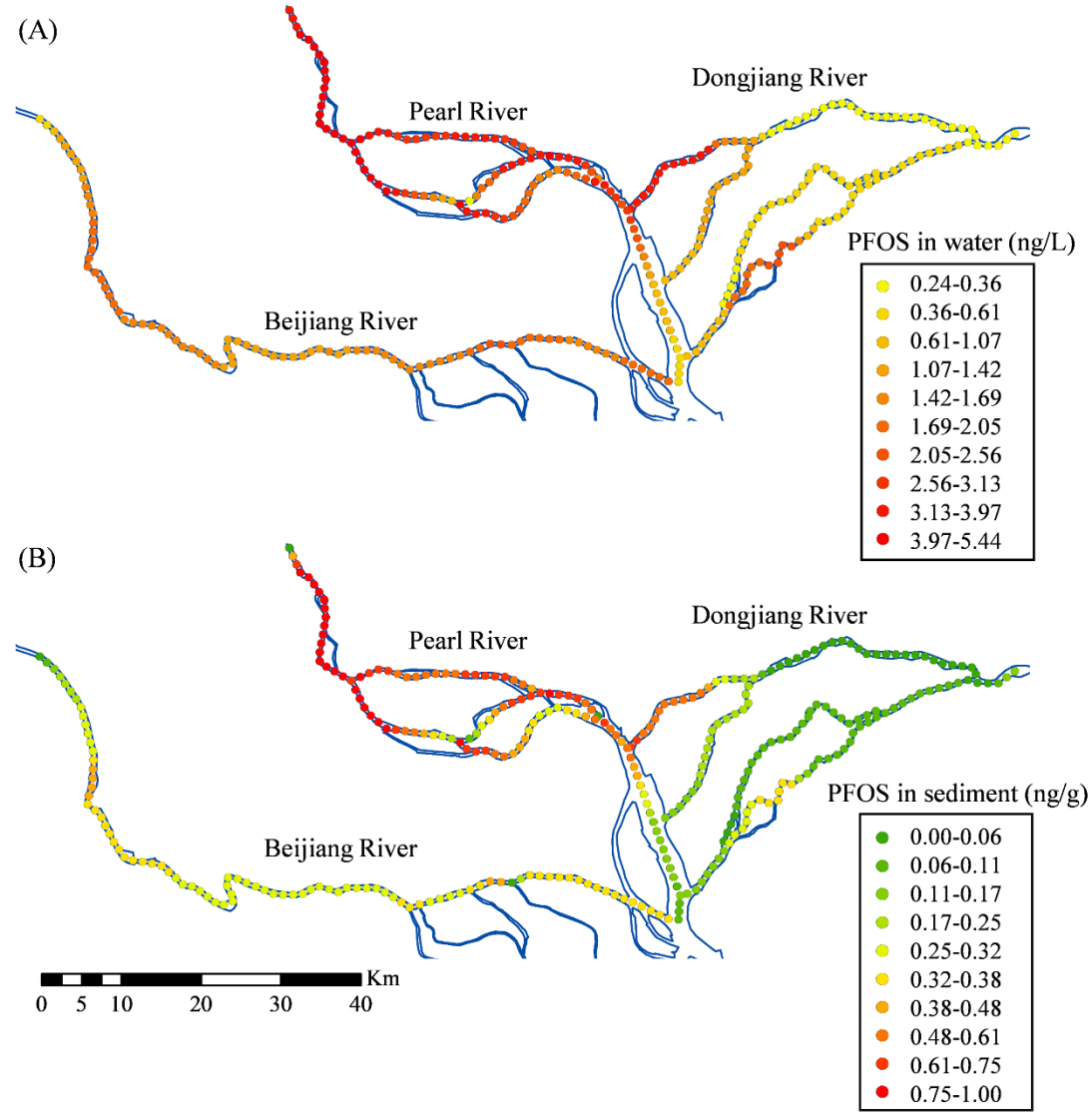

Figure 7-3 Simulated PFOS distribution in (a) water and (b) sediment compartments of the study area in 2013

7.3.2 Spatial Distribution of PFOS in Soil Zone

The spatial distribution of PFOS in soil compartments (Figure 7-4a) indicates that the concentrations in subareas close to the urban area are higher than the other subareas. The highest value is found in the subarea #6, which shows the same tendency in the water and sediment compartments in this populated region with higher amounts of PFOS emissions from local

WWTPs in this subarea. Table 7-5 shows the comparison between simulated results and measured data. It indicates that the ranges of PFOS concentration in Foshan, Guangzhou and Dongguan City are 0.15-1.24, 0.05-0.83 and 0.12-1.48 ng/g, respectively. The simulated soil concentrations in Subarea #6 located in Guangzhou City was found to be higher than the range of measured results. The possible reason may be: 1) as shown in Table 1, more PFOS are discharged through the disposal of WWTPs sludge in this area, which is considered as a major source input in the RNEMM, and 2) however, the PFOS source from WWTPs sludge may not be fully counted in the monitoring data during the regular soil sampling in local urban and rural areas (Hu et al., 2013; Sun, 2017), which may cause lower monitoring values compared to RNEMM results.

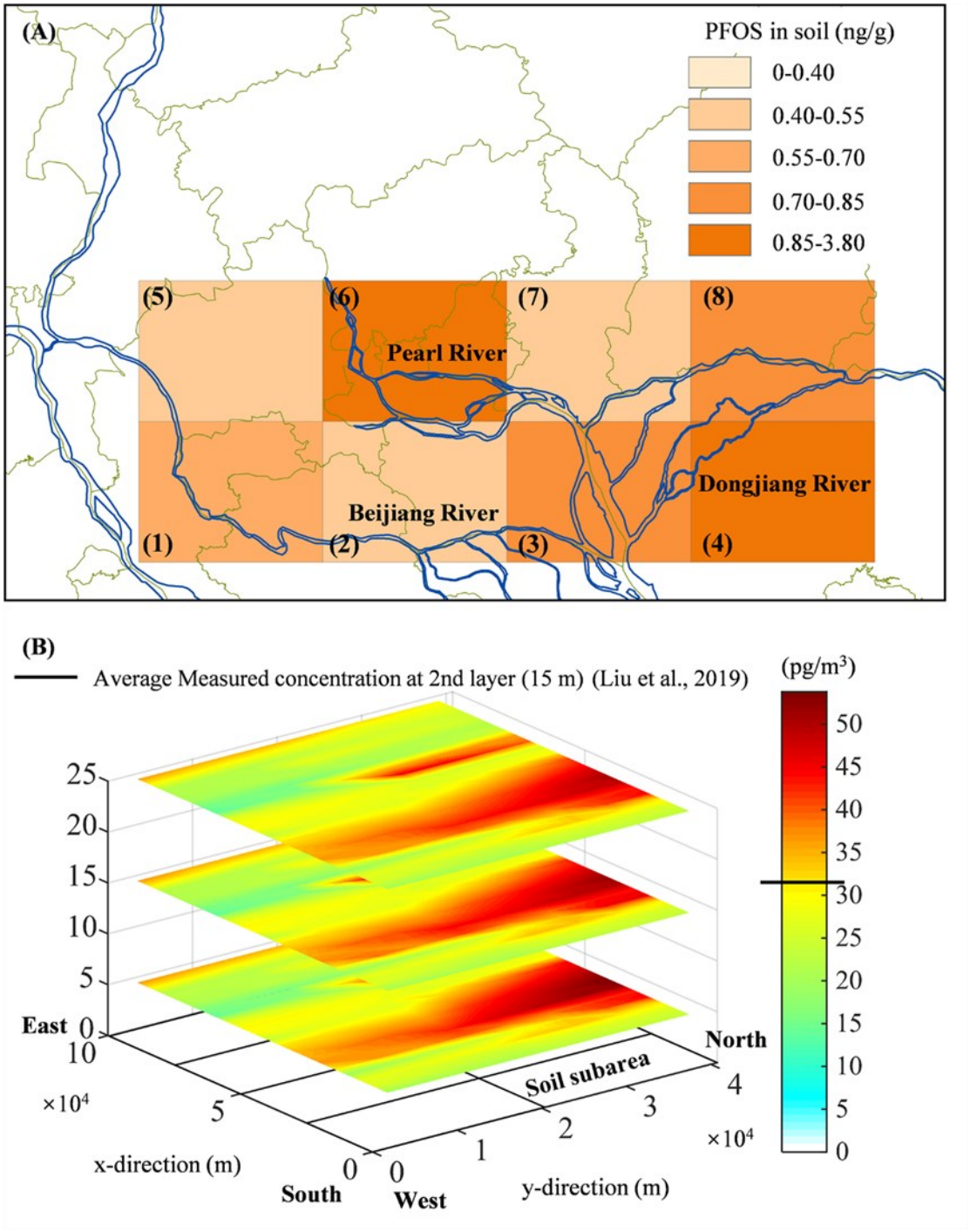

Figure 7-4 Simulated spatial distribution of PFOS concentrations in (a) soil zone and (b) air zone in 2013

Table 7-5 Comparison between RNEMM simulated results and measured results (Hu et al., 2013; Sun, 2017)

Subarea	1	2	3	4	5	6	7	8
Simulated results (ng/g)	0.70	0.40	0.70	0.82	0.57	3.76	0.55	0.67
Measured results (ng/g)	0.15-1.24	0.05-0.83	0.12-1.48	0.12-1.48	-	0.05-0.83	-	0.05-0.83

7.3.3 Spatial Distribution of PFOS in Air Zone

Modeling results for PFOS distribution in the atmosphere at different heights (5m, 15m and 25m) are provided in Figure 7-4b. This atmosphere zone is above the soil compartment and is stratified with a higher spatial resolution. *x* is set from west to east and *y* is from south to north. The distribution pattern will be affected by instant changes of wind directions and speeds. Therefore, to represent the exposure scenario in the atmosphere at 2013, the modeling results contours are generated after 365 days of model run using the average wind direction and speed in 2013. The air samples are collected at 15-20 m above the ground from the urban areas of Guangzhou, Foshan and Dongguan Cities in the end of 2013, and the average range of monitored PFOS concentrations in the urban areas is 31.9 ± 21.7 pg/m^3 (B. Liu et al., 2019). Since only average PFOS concentration is available, the modeling results in the urban area of these three cities are compared with the monitored average values. As shown in Figure 7-4b, they have a good agreement and the average simulated concentration is 30.9 pg/m^3, which means the relative error is less than 5%.

7.3.4 PFOS Concentrations in the Biota

In this section, RNEMM extends multimedia exposure assessment to consider the aquatic ecosystem with a focus on the local food web system. Aquatic organisms take up organic pollutants by respiration and diet, both of which are related to the water environment. Quantitatively, outputs from water module of RNEMM or observed PFOS concentrations in the water can be used as inputs to the ecosystem module of RNEMM, to estimate the PFOS concentrations in the food web

system. As described in Section 3.3, the typical aquatic organisms and fishes in the study region include detritus (G1), phytoplankton (G2), zooplankton (G3), macrophyte (G4), herbivorous feeders (G5), crucian carp (G6), mud carp (G7), tilapia (G8), grass carp (G9), common carp (G10) and leather catfish (G11). In the meantime, observed concentrations in the fish species (G6 - G11) of the food web system (Pan, Ying, et al., 2014; Pan, Zhao, et al., 2014) are collected to compare with the simulated results. The simulated and observed PFOS concentrations in the food web system are given in Figure 7-5. The solid horizontal line in a box represents the median and the square represents the mean. The box denotes the 25 % and 75 % percentiles. The whiskers represent the minimum and maximum and the small squares are the simulation average values. The blue color represents that the measured PFOS concentrations in water zone are applied to simulate the PFOS level in tilapia (G8) and leather catfish (G11). The results show a general agreement between the observed and calculated PFOS concentrations in the food web fish species. Specifically, the measured PFOS concentrations in the water, where tilapia (G8) and leather catfish (G11) are collected, are from 15.7 to 290 ng/L (Pan, Zhao, et al., 2014), which are considerably larger than the computed PFOS level in the water of the study area. Therefore, this study uses the measured concentrations in these two water locations to calculate the PFOS level in tilapia (G8) and leather catfish (G11). Table B-6 gives the monitored PFOS levels in aquatic species (Pan, Zhao, et al., 2014). As shown in Figure 7-5, the median values of calculated PFOS level in the fish species are used to compare to observed data, which indicates a good agreement between them.

There are several possible reasons for the discrepancies: (1) a real food web system is subject to dynamic changes, but the ecosystem module can only represent a simplification for a specific period (Hu et al., 2014); (2) the physicochemical properties of PFOS like the Partition coefficients varies with environmental factors like pH and temperature (Banks et al., 2020). For instance, as most solid phases in natural water contain alumina, Wang and Shih (2011) (Wang & Shih, 2011) investigated the PFOS adsorption behavior on alumina, which indicates that an increase in pH leads to a decrease in PFOS adsorption on alumina due to the reduction in electrostatic interaction. When pH increases from 4 to 7, the adsorption capacity of PFOS decreases to 40%. Additionally,

the fish weight and lipid fraction can also affect the bioaccumulation process and then contribute to the variance of PFOS level in the fish body (Sun et al. 2017); and (3) the PFOS levels in water of the locations, where the fish species including crucian carp (G6), mud carp (G7), grass carp (G9) and common carp (G10), are from 0.17 to 37 ng/L (Pan, Zhao, et al., 2014), which are generally higher than the computed PFOS levels. These high PFOS levels in the aquatic environment cause the difference between the measured data and simulated PFOS levels in fishes.

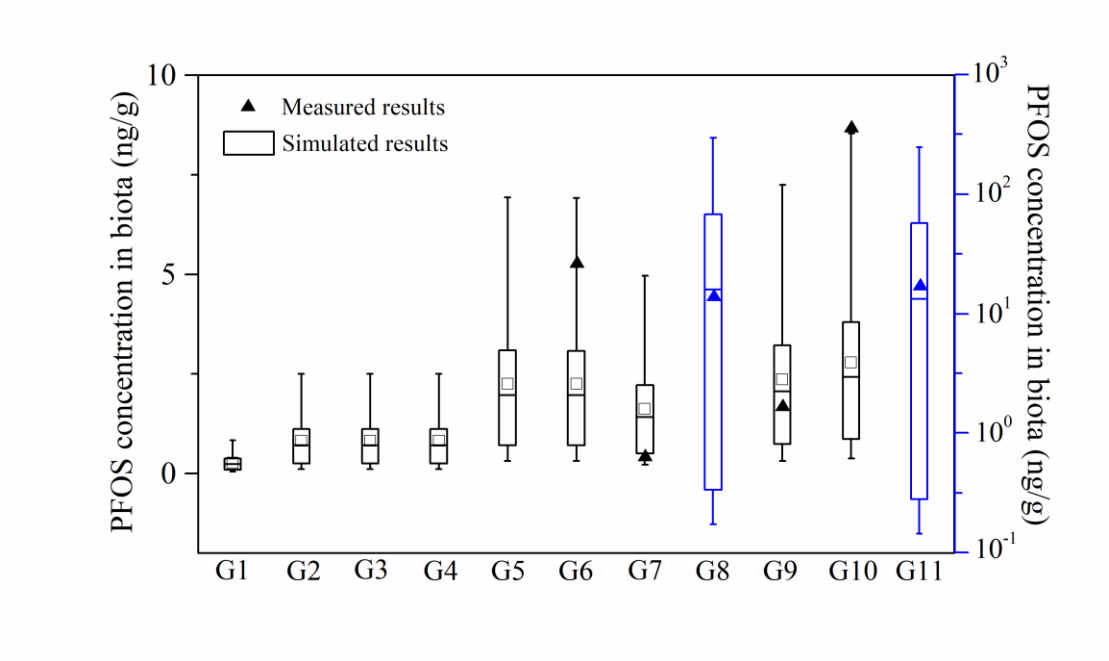

Figure 7-5 Box-and-whisker plots of concentrations in biota.

7.3.5 Health Risk Assessment

In general, hazard quotient (*HQ*) > 1 means the contaminant is of high risk, 0.1 < *HQ* < 1 represents medium risk and 0.01 < *HQ* < 0.1 indicates low health risk (Lu et al., 2018). To evaluate the health risk of PFOS for humans in this study area, *HQ* is calculated for children and adults as shown in Table 7-6. It is found that the *HQ* for children in most of the eight subareas are higher than 0.1, which suggests a medium level hazard for children and possibly increase their risk, for example, to get asthma and allergy (Timmermann et al., 2017). In line with other RNEMM results, the *HQ* in subarea #6 shows the highest exposure risk with a *HQ* value of 0.33 similarly due to

more industrial emissions and a high population in this zone. This finding agrees with previous studies in the Pearl River Basin, which shows low or medium exposure risks of PFOS (Pan, Zhao, et al., 2014; Zhao et al., 2011). Although the results do not show high risks and mainly freshwater fish consumption is considered in this study, attention should be paid to control industrial emission sources in the region.

Table 7-6 The *HQ* of PFOS to children and adults

Subarea	1	2	3	4	5	6	7	8
Children	0.15	0.19	0.13	0.08	0.10	0.33	0.20	0.03
Adults	0.05	0.06	0.04	0.03	0.03	0.10	0.06	0.01

7.4 Summary

A regional numerical environmental multimedia modeling system (RNEMM) has been developed and validated by studying the spatial distribution of PFOS in multiple environmental media and freshwater fish species in the Guangzhou-Foshan-Dongguan area of the Pearl river basin. The model validation results have shown a good agreement for PFOS. In the surface water and sediment zone, most of the relative errors are less than 40 %. When only comparing the simulated results and the measured data collected in 2013, the value of RSR, NSE and PBIAS are 0.53, 0.72 and -4.42 %, which is good or very good on the rating scale. The agreement between measured data and simulated results in the other media like soil, atmosphere and fish are also acceptable. The health risk assessment for children and adults is further conducted based on the simulated results in surface water and fish. It indicates that the *HQ* values in most subareas are higher than 0.1, which suggests medium risk. The application of RNEMM proves the capacity of this modeling system to examine the spatial exposure patterns of emerging contaminants in a multimedia environment with complicated conditions.

8. Conclusions and Future Work

8.1 Conclusions

In this thesis study, a novel regional numerical multimedia environmental modeling (RNEMM) approach has been developed for assessing the environmental fate transport and its related eco-environmental risk of contaminants in regional scale study areas. RNEMM is intended to address a wide range of contamination problems, which have adverse effects on the multimedia environment involving local atmosphere, soil, water, and ecosystem. The main modules in RNEMM include a water quality simulation module for river network system, a numerical air contaminant transport module, a mass-balance based calculation module for soil, a food web module and a health risk assessment. Particularly, two developments have been made to integrate these modules into the RNEMM: (1) numerically integrating different modules with non-uniform boundary conditions and inter-media flux and (2) coupling the modules based on available computational schemes (e.g., ADE and fugacity concept). The sensitivity analysis techniques (OAT and Morris screening method) are embedded in these novel models to rank the parameter sensitivities.

The environmental multimedia model involves a wide range of parameters and also uncertainties. The probability distributions of parameters are defined by performing uncertainty analysis using MCM. Subsequently, based on the MCM-assisted modeling outputs, an integrated risk assessment module is developed to quantify the exposure risk levels including risk quotient (*RQ*) and hazard quotient (*HQ*) factors. This is useful to map the possible eco-environmental exposure risk severities in a temporal and spatial scheme.

The developed 1D and 2D RNEMM approaches have been applied to four regional scale real cases. First, the RNEMM approach to integrate different modules with non-uniform boundary conditions and inter-media flux is applied to two real landfills in Canada, one in 1D and another one in 2D, to assess the exposure risks of heavy metals in landfill emissions in the surrounding

environment. Modeling and validation results show that the developed new EMM method is capable of numerically coupling environmental multimedia modules to generate acceptable modeling results to assess complex multimedia exposure risk problems. Secondly, the RNEMM approach integrates the modules based on computational schemes including ADE and fugacity concept, which is capable of selecting the appropriate models for different media based on specific situations and then integrating them into an entire system. This extends the new EMM method to a regional spatial environmental multimedia model (RSEMM). The RSEMM has been applied to examine emerging contaminants, i.e., antibiotics in a river basin region in urban area. The results show that the RSEMM approach performs well based on field data validation and has provided quantified concentration profiles of emerging contaminants and related health risk assessment for the regional scale urban area. Thirdly, the RNEMM approach is further extended with better numerical solution algorithms for air and water modules for assessing the environmental fate and exposure risk of emerging water contaminant (i.e., PFOS) at higher temporal-spatial resolution in regional river basin area. The field case study results further confirm that the RNEMM approach can help the understanding of pollutant fate and transfer processes and the potential exposure pathway for complex environmental systems with potential risks to public health and ecosystem. The validation and application results from four case studies indicate that the RNEMM could provide a realistic and complex assessment of the contaminant transport activities and address the long-term environmental risks associated with the contaminants.

8.2 Contributions

The main contribution of this study is the development of the novel RNEMM approach. In addition to the conclusion section, specific contributions are summarized below:

1. The developed numerical environmental multimedia model in 1D and 2D is the main contribution compared to previous analytical and uniform-compartment EMM methods. In the computational scheme, the initial and boundary conditions can be represented in the non uniform multimedia conditions, and the latest different solving methods (i.e., FDM, FEM and

analytical solutions) are utilized in the RSEMM.

2. The RSEMM incorporating a numerical water quality model for the river network multimedia system is another contribution not reported in previous EMM studies. It is capable of predicting concentration profiles of contaminants at a regional scale for vulnerable river basin area. For the river network module, the numerical solution is used to solve the ADE and the concentration distribution in surface water and sediment compartments are estimated with high spatial resolution. For air and soil modules, the fugacity model is applied to calculate the concentrations and inter-media fluxes of pollutant. These modules are then integrated by considering the mass fluxes between them. The integration method employed in the RSEMM is useful to integrate various methods for different media for a complex environmental system.

3. The sensitivity analysis techniques (OAT and Morris screening method) are embedded in these novel models to examine the parameter sensitivities. Further uncertainty analysis is incorporated using MCM based on the probability distribution of parameters. An integrated risk assessment model is then developed to apply the risk quotient (*RQ*) and hazard quotient (*HQ*) factors for quantifying the risk levels. The exposure risk assessment for children and adults is further conducted based on the integrated risk assessment model. This model is useful to map the possible health risk severities in a temporal and spatial scheme.

In summary, the RNEMM approach is developed based on numerical integration of a river network simulation module, a gaseous phase simulation module, a mass balance analysis module for soil compartment, and a food web analysis module. The RNEMM is a useful management tool to assess the exposure risks associated with emerging contaminants on regional water, soil, and ecosystem at an adequate spatial-temporal resolution. Additionally, it can be anticipated that the RNEMM can be extended to examine other emerging contaminants at regional scale and applied to the cases in North America and the other regions.

8.3 Recommendations for Future Work

In spite of the results presented in the previous chapters, the novel RNEMM still have some limitations. Future work recommended are as the following:

1. In the RNEMM, the river network, soil and atmosphere are considered. However, groundwater is also an essential medium for assessing the fate and transport of contaminants. It is recommended to further extend the soil module to better include the groundwater compartment and consider the transport processes between soil, surface water and groundwater.

2. For future work, it is recommended to extend the RNEMM to more complicated considerations. The temporal variance of physical processes like temperature and streamflow could be taken into account.

3. The present studies only evaluate the health risk impact of one target chemicals, while humans are usually exposed to many chemicals with the same or similar categories. To quantify the comprehensive risk level, health risks from multiple pollutants should be considered.

4. It is recommended to improve the present user interface system to provide more kinds of analysis and the visual graph for the results.

References

Abdelaziz, R., Pearson, A. J., & Merkel, B. J. (2013). Lattice Boltzmann modeling for tracer test analysis in a fractured Gneiss aquifer. *Natural Science*, *5*(03), 368. DOI:10.4236/ns.2013.53050

AECOM. (2009). *Hartland landfill groundwater, surface water and leachate monitoring program annual report 2009. Capital Regional District*. Retrieved May 12, 2018 from www.crd.bc.ca/service/waste-recycling/hartland-landfill-facility/environmental-monitoring/hartland -landfill-reports

AECOM. (2010). *Hartland landfill groundwater, surface water and leachate monitoring program annual report 2010. Capital Regional District.* Retrieved May 12, 2018 from www.crd.bc.ca/service/waste-recycling/hartland-landfill-facility/environmental-monitoring/ hartland -landfill-reports

AECOM. (2011). *Hartland landfill groundwater, surface water and leachate monitoring program annual report 2011. Capital Regional District.* Retrieved May 12, 2018 from www.crd.bc.ca/service/waste-recycling/hartland-landfill-facility/environmental-monitoring/ hartland -landfill-reports

AECOM. (2012). *Hartland landfill groundwater, surface water and leachate monitoring program annual report 2012. Capital Regional District.* Retrieved May 12, 2018 from www.crd.bc.ca/service/waste-recycling/hartland-landfill-facility/environmental-monitoring/ hartland -landfill-reports

AECOM. (2013). *Hartland landfill groundwater, surface water and leachate monitoring program annual report 2013. Capital Regional District.* Retrieved May 12, 2018 from www.crd.bc.ca/service/waste-recycling/hartland-landfill-facility/environmental-monitoring/ hartland -landfill-reports

AECOM. (2014). *Hartland landfill groundwater, surface water and leachate monitoring program annual report 2014.* Capital Regional District. Retrieved May 12, 2018 from

www.crd.bc.ca/service/waste-recycling/hartland-landfill-facility/environmental-monitoring/ hartland -landfill-reports

AECOM. (2015). *Hartland landfill groundwater, surface water and leachate monitoring program annual report 2015. Capital Regional District.* Retrieved May 12, 2018 from. www.crd.bc.ca/service/waste-recycling/hartland-landfill-facility/environmental-monitoring/ hartland -landfill-reports

AECOM. (2016a). *Hartland landfill groundwater, surface water and leachate monitoring program annual report 2016. Capital Regional District.* Retrieved May 12, 2018 from www.crd.bc.ca/service/waste-recycling/hartland-landfill-facility/environmental monitoring/ hartland -landfill-reports

AECOM (2016b). *Hartland landfill – landfill gas monitoring annual report 2016. Capital Regional District.* Retrieved May 12, 2018 from www.crd.bc.ca/service/waste-recycling/hartland-landfill-facility/environmental-monitoring/ hartland -landfill-reports

Albani, R. A. S., & Albani, V. V. L. (2019). Tikhonov-type regularization and the finite element method applied to point source estimation in the atmosphere. *Atmospheric Environment*, *211*, 69-78. https://doi.org/10.1016/j.atmosenv.2019.04.063

Ao, J., Yuan, T., Xia, H., Ma, Y., Shen, Z., Shi, R., Tian, Y., Zhang, J., Ding, W., Gao, L., Zhao, X., & Yu, X. (2019). Characteristic and human exposure risk assessment of per- and polyfluoroalkyl substances: A study based on indoor dust and drinking water in China. *Environmental Pollution*, *254*, 112873. https://doi.org/10.1016/j.envpol.2019.07.041

Bailey, R. T., Morway, E. D., Niswonger, R. G., & Gates, T. K. (2013). Modeling variably saturated multispecies reactive groundwater solute transport with MODFLOW-UZF and RT3D. *Groundwater*, *51*(5), 752-761. https://doi.org/10.1111/j.1745-6584.2012.01009.x

Bajpai, R., Mishra, G. K., Mohabe, S., Upreti, D. K., & Nayaka, S. (2011). Determination of atmospheric heavy metals using two lichen species in Katni and Rewa cities, India. *Journal of Environmental Biology*, *32*(2), 195-199. http://europepmc.org/abstract/MED/21882655

Banks, D., Jun, B. M., Heo, J., Her, N., Park, C. M., & Yoon, Y. (2020). Selected advanced water

treatment technologies for perfluoroalkyl and polyfluoroalkyl substances: A review. *Separation and Purification Technology*, *231*, 115929. https://doi.org/10.1016/j.seppur.2019.115929

Bao, J., Liu, W., Liu, L., Jin, Y., Ran, X., & Zhang, Z. (2010). Perfluorinated compounds in urban river sediments from Guangzhou and Shanghai of China. *Chemosphere*, *80*(2), 123-130. https://doi.org/10.1016/j.chemosphere.2010.04.008

Berk, M., Williams, L. J., Andreazza, A. C., Pasco, J. A., Dodd, S., Jacka, F. N., Moylan, S., Reiner, E. J., & Magalhaes, P. V. S. (2014). Pop, heavy metal and the blues: secondary analysis of persistent organic pollutants (POP), heavy metals and depressive symptoms in the NHANES National Epidemiological Survey. *BMJ Open*, *4*(7), e005142. https://doi.org/10.1136/bmjopen-2014-005142

Bernard, A. (2008). Cadmium & its adverse effects on human health. *Indian Journal of Medical Research*, *128*(4), 557. http://hdl.handle.net/2078.1/35901

Borgonovo, E., & Plischke, E. (2016). Sensitivity analysis: A review of recent advances. *European Journal of Operational Research*, *248*(3), 869-887. https://doi.org/10.1016/j.ejor.2015.06.032

Bou-Zeid, E., & El-Fadel, M. (2004). Parametric sensitivity analysis of leachate transport simulations at landfills. *Waste Management*, *24*(7), 681-689. https://doi.org/10.1016/j.wasman.2004.03.004

Buczko, U., Hopp, L., Berger, W., Durner, W., Peiffer, S., & Scheithauer, M. (2004). Simulation of chromium transport in the unsaturated zone for predicting contaminant entries into the groundwater. *Journal of Plant Nutrition and Soil Science*, *167*(3), 284-292. https://doi.org/10.1002/jpln.200421371

Campfens, J., & Mackay, D. (1997). Fugacity-based model of PCB bioaccumulation in complex aquatic food webs. *Environmental Science & Technology*, *31*(2), 577-583. https://doi.org/10.1021/es960478w

Campolongo, F., Cariboni, J., & Saltelli, A. (2007). An effective screening design for sensitivity

analysis of large models. *Environmental Modelling & Software*, *22*(10), 1509-1518. https://doi.org/10.1016/j.envsoft.2006.10.004

Çamur, M. Z., & Yazicigil, H. (2005). Laboratory determination of multicomponent effective diffusion coefficients for heavy metals in a compacted clay. *Turkish Journal of Earth Sciences*, *14*(1), 91-103.

Canadian Council of Ministers of the Environment (CCME). (1999). *Canadian environmental quality guidelines*. Accessed June 20, 2018 from http://ceqg-rcqe.ccme.ca/en/index.html#void

Cariboni, J., Gatelli, D., Liska, R., & Saltelli, A. (2007). The role of sensitivity analysis in ecological modelling. *Ecological Modelling*, *203*(1-2), 167-182. https://doi.org/10.1016/j.ecolmodel.2005.10.045

Chaparro-Ortega, A., Betancourt, M., Rosas, P., Vázquez-Cuevas, F. G., Chavira, R., Bonilla, E., Casas, E., & Ducolomb, Y. (2018). Endocrine disruptor effect of perfluorooctane sulfonic acid (PFOS) and perfluorooctanoic acid (PFOA) on porcine ovarian cell steroidogenesis. *Toxicology in Vitro*, *46*, 86-93. https://doi.org/10.1016/j.tiv.2017.09.030

Chen, H., Jing, L., Teng, Y., & Wang, J. (2018). Multimedia fate modeling and risk assessment of antibiotics in a water-scarce megacity. *Journal of Hazardous Materials*, *348*, 75-83. https://doi.org/10.1016/j.jhazmat.2018.01.033

Chen, Z., & Yuan, J. (2009). An extended environmental multimedia modeling system (EEMMS) for landfill case studies. *Environmental Forensics*, *10*(4), 336-346. https://doi.org/10.1080/15275920903347396

Chen, Z., Zhao, L., & Lee, K. (2010). Environmental risk assessment of offshore produced water discharges using a hybrid fuzzy-stochastic modeling approach. *Environmental Modelling & Software*, *25*(6), 782-792. https://doi.org/10.1016/j.envsoft.2010.01.001

China Client Platform. (2019). *Directories of wastewater treatment plants in Guangdong Province*. Retrieved June 10, 2019 from http://www.ltmic.com/index.php?m=data

Cho, E., Arhonditsis, G. B., Khim, J., Chung, S., & Heo, T. Y. (2016). Modeling metal-sediment

interaction processes: Parameter sensitivity assessment and uncertainty analysis. *Environmental Modelling & Software*, *80*, 159-174. https://doi.org/10.1016/j.envsoft.2016.02.026

Christensen, E. R., Zhang, R., Codling, G., Giesy, J. P., & Li, A. (2019). Poly- and per-fluoroalkyl compounds in sediments of the Laurentian Great Lakes: Loadings, temporal trends, and sources determined by positive matrix factorization. *Environmental Pollution*, *255*, 113166. https://doi.org/10.1016/j.envpol.2019.113166

Codling, G., Sturchio, N. C., Rockne, K. J., Li, A., Peng, H., Tse, T. J., Jones, P. D., & Giesy, J. P. (2018). Spatial and temporal trends in poly- and per-fluorinated compounds in the Laurentian Great Lakes Erie, Ontario and St. Clair. *Environmental Pollution*, *237*, 396-405. https://doi.org/10.1016/j.envpol.2018.02.013

Cote, I., Vandenberg, J. J., Druwe, I. L., & Angrish, M. M. (2019). Incorporating epigenetics into a risk assessment framework. In S. D. McCullough & D. C. Dolinoy (Eds.), *Toxicoepigenetics* (pp. 289-310). Academic Press. https://doi.org/10.1016/B978-0-12-812433-8.00013-7

Csiszar, S. A., Daggupaty, S. M., Verkoeyen, S., Giang, A., & Diamond, M. L. (2013). SO-MUM: A coupled atmospheric transport and multimedia model used to predict intraurban-scale PCB and PBDE emissions and fate. *Environmental Science & Technology, 47*(1), 436-445. https://doi.org/10.1021/es3033023

Csiszar, S. A., Diamond, M. L., & Daggupaty, S. M. (2014). The magnitude and spatial range of current-use urban PCB and PBDE emissions estimated using a coupled multimedia and air transport model. *Environmental Science & Technology*, *48*(2), 1075-1083. https://doi.org/10.1021/es403080t

Cunningham, V. L., Binks, S. P., & Olson, M. J. (2009). Human health risk assessment from the presence of human pharmaceuticals in the aquatic environment. *Regulatory Toxicology and Pharmacology*, *53*(1), 39-45. https://doi.org/10.1016/j.yrtph.2008.10.006

Daggupaty, S. M., Banic, C. M., Cheung, P., & Ma, J. (2006). Numerical simulation of air

concentration and deposition of particulate metals around a copper smelter in northern Quebec, Canada. *Geochemistry: Exploration, Environment, Analysis*, *6*(2-3), 139-146. https://doi.org/10.1144/1467-7873/05-094

Dahmardeh Behrooz, R., Kaskaoutis, D. G., Grivas, G., & Mihalopoulos, N. (2021). Human health risk assessment for toxic elements in the extreme ambient dust conditions observed in Sistan, Iran. *Chemosphere*, *262*, 127835. https://doi.org/10.1016/j.chemosphere.2020.127835

De Silva, A. O., Spencer, C., Scott, B. F., Backus, S., & Muir, D. C. G. (2011). Detection of a cyclic perfluorinated acid, perfluoroethylcyclohexane sulfonate, in the Great Lakes of North America. *Environmental Science & Technology*, *45*(19), 8060-8066. https://doi.org/10.1021/es200135c

Diamond, M. L., Gingrich, S. E., Fertuck, K., McCarry, B. E., Stern, G. A., Billeck, B., Grift, B., Brooker, D., & Yager, T. D. (2000). Evidence for organic film on an impervious urban surface: Characterization and potential teratogenic effects. *Environmental Science & Technology*, *34*(14), 2900-2908. https://doi.org/10.1021/es9906406

Diamond, M. L., Priemer, D. A., & Law, N. L. (2001). Developing a multimedia model of chemical dynamics in an urban area. *Chemosphere*, *44*(7), 1655-1667. https://doi.org/10.1016/S0045-6535(00)00509-9

Dile, Y. T., Daggupati, P., George, C., Srinivasan, R., & Arnold, J. (2016). Introducing a new open source GIS user interface for the SWAT model. *Environmental Modelling & Software*, *85*, 129-138. https://doi.org/10.1016/j.envsoft.2016.08.004

Dokou, Z., Karagiorgi, V., Karatzas, G. P., Nikolaidis, N. P., & Kalogerakis, N. (2016). Large scale groundwater flow and hexavalent chromium transport modeling under current and future climatic conditions: The case of Asopos River Basin. *Environmental Science and Pollution Research*, *23*(6), 5307-5321. https://doi.org/10.1007/s11356-015-5771-1

Domínguez-Morueco, N., Diamond, M. L., Sierra, J., Schuhmacher, M., Domingo, J. L., & Nadal, M. (2016). Application of the multimedia urban model to estimate the emissions and

environmental fate of PAHs in Tarragona County, Catalonia, Spain. *Science of The Total Environment*, *573*, 1622-1629. https://doi.org/10.1016/j.scitotenv.2016.09.163

Dong, J., Chen, Z., Wang, Q., Guo, J., Pu, Y., Han, Y., Xia, J., & Haghighat, F. (2019). A regional spatial environmental multimedia modeling (RSEMM) approach for assessing the risk of antibiotics in river basin system – a China case study. *Sustainable Cities and Society*, *50*, 101624. https://doi.org/10.1016/j.scs.2019.101624

Duan, J., & Tan, J. (2013). Atmospheric heavy metals and arsenic in China: Situation, sources and control policies. *Atmospheric Environment*, *74*, 93-101. https://doi.org/10.1016/j.atmosenv.2013.03.031

Fair, P. A., Wolf, B., White, N. D., Arnott, S. A., Kannan, K., Karthikraj, R., & Vena, J. E. (2019). Perfluoroalkyl substances (PFASs) in edible fish species from Charleston Harbor and tributaries, South Carolina, United States: Exposure and risk assessment. *Environmental Research*, *171*, 266-277. https://doi.org/10.1016/j.envres.2019.01.021

Fang, S., Gertner, G. Z., Shinkareva, S., Wang, G., & Anderson, A. (2003). Improved generalized Fourier amplitude sensitivity test (FAST) for model assessment. *Statistics and Computing*, *13*(3), 221-226. https://doi.org/10.1023/A:1024266632666

Fantke, P., Bijster, M., Guignard, C., Hauschild, M. Z., Huijbregts, M., Jolliet, O., Kounina, A., Magaud, V., Margni, M., & McKone, T. E. (2017). *USEtox® 2.0 documentation (version 1.00)*. Retrieved October 12, 2019 from https://usetox.org/model/documentation

Feng, L., Sun, X., & Zhu, X. (2016). Impact of floodgates operation on water environment using one-dimensional modelling system in river network of Wuxi City, China. *Ecological Engineering*, *91*, 173-182. https://doi.org/10.1016/j.ecoleng.2016.02.042

Ferretti, F., Saltelli, A., & Tarantola, S. (2016). Trends in sensitivity analysis practice in the last decade. *Science of The Total Environment*, *568*, 666-670. https://doi.org/10.1016/j.scitotenv.2016.02.133

Font, C., Bregoli, F., Acuña, V., Sabater, S., & Marcé, R. (2019). GLOBAL-FATE (version 1.0.0): A geographical information system (GIS)-based model for assessing contaminants fate in

the global river network. *Geoscientific Model Development,* 1-30. https://doi.org/10.5194/gmd-2019-8

Fraga, I., Charters, F. J., O'Sullivan, A. D., & Cochrane, T. A. (2016). A novel modelling framework to prioritize estimation of non-point source pollution parameters for quantifying pollutant origin and discharge in urban catchments. *Journal of Environmental Management*, *167*, 75-84. https://doi.org/10.1016/j.jenvman.2015.11.003

Franco, A., Price, O. R., Marshall, S., Jolliet, O., Van den Brink, P. J., Rico, A., Focks, A., De Laender, F., & Ashauer, R. (2017). Toward refined environmental scenarios for ecological risk assessment of down-the-drain chemicals in freshwater environments. *Integrated Environmental Assessment and Management*, *13*(2), 233-248. https://doi.org/10.1002/ieam.1801

Franz Environmental Inc. (2012). *Correctional Services Canada (CSC) – Drumheller institution No. 530 landfill remediation: Environmental assessment report.* Retrieved December 28, 2017 from https://buyandsell.gc.ca/procurement-data/tender-notice/PW-PWZ-102-8195?order=php&sort=asc

Gao, L., Shi, Y., Li, W., Liu, J., & Cai, Y. (2012). Occurrence, distribution and bioaccumulation of antibiotics in the Haihe River in China. *Journal of Environmental Monitoring*, *14*(4), 1247-1254. https://doi.org/10.1039/C2EM10916F

Gao, Y., Fu, J., Meng, M., Wang, Y., Chen, B., & Jiang, G. (2015). Spatial distribution and fate of perfluoroalkyl substances in sediments from the Pearl River Estuary, South China. *Marine Pollution Bulletin*, *96*(1), 226-234. https://doi.org/10.1016/j.marpolbul.2015.05.022

Gavrilescu, M., Demnerová, K., Aamand, J., Agathos, S., & Fava, F. (2015). Emerging pollutants in the environment: Present and future challenges in biomonitoring, ecological risks and bioremediation. *New Biotechnology*, *32*(1), 147-156. https://doi.org/10.1016/j.nbt.2014.01.001

Genc, A., & Ulupinar, E. (2010). Transport of lead (Pb^{2+}) ions through silty-clayey soils under acidic conditions. *Transport in Porous Media*, *84*(3), 699-709.

https://doi.org/10.1007/s11242-010-9535-6

Gewurtz, S. B., Bradley, L. E., Backus, S., Dove, A., McGoldrick, D., Hung, H., & Dryfhout-Clark, H. (2019). Perfluoroalkyl acids in Great Lakes precipitation and surface water (2006–2018) indicate response to phase-outs, regulatory action, and variability in fate and transport processes. *Environmental Science & Technology*, *53*(15), 8543-8552. https://doi.org/10.1021/acs.est.9b01337

Giri, B. S., Karimi, I. A., & Ray, M. B. (2001). Modeling and Monte Carlo simulation of TCDD transport in a river. *Water Research*, *35*(5), 1263-1279. https://doi.org/10.1016/S0043-1354(00)00379-1

Gusev, A., Mantseva, E., Shatalov, V., and Strukov, B. (2005). *Regional multicompartment model MSCE-POP*. Retrieved April 10, 2018 from http://en.msceast.org/index.php/j-stuff/msce-pop

Han, Y., Wang, F., Zhao, R., & Yang Y. (2014). Sectioning method of ecological water requirement for North Canal. *Journal of North China Institute of Water Conservancy and Hydroelectric Power, China. 35*(2), 25-29.

Hansen, K., Christensen, J., Brandt, J., Frohn, L., & Geels, C. (2004). Modelling atmospheric transport of α-hexachlorocyclohexane in the Northern Hemisphere with a 3-D dynamical model: DEHM-POP. *Atmospheric Chemistry and Physics*, *4*(4), 1125-1137.

Harrar, W. G., Murdoch, L. C., Nilsson, B., & Klint, K. E. S. (2007). Field characterization of vertical bromide transport in a fractured glacial till. *Hydrogeology Journal*, *15*(8), 1473-1488. https://doi.org/10.1007/s10040-007-0198-5

Hodges, J. E. N., Vamshi, R., Holmes, C., Rowson, M., Miah, T., & Price, O. R. (2014). Combining high-resolution gross domestic product data with home and personal care product market research data to generate a subnational emission inventory for Asia. *Integrated Environmental Assessment and Management, 10*(2), 237-246. https://doi.org/10.1002/ieam.1476

Hollander, A., Schoorl, M., & van de Meent, D. (2016). SimpleBox 4.0: Improving the model

while keeping it simple…. *Chemosphere*, *148*, 99-107. https://doi.org/10.1016/j.chemosphere.2016.01.006

Hong, W. (1995). Investigation and evaluation of entry sewage in Nanyun River. *South-to-North Water Transfers and Water Science & Technology, China, 2*, 70-71.

Hou, Z. W., Qin, C. Z., Zhu, A., Liang, P., Wang, Y. J., & Zhu, Y. Q. (2019). From manual to intelligent: A review of input data preparation methods for geographic modeling. *International Journal of Geo-Information*, *8*(9), 376. https://doi.org/10.3390/ijgi8090376

Hu, G. C., Zheng, H., Zhang, L. J., Xu, Z. C., Chen, L. G., He, D. C., & Li, H. S. (2013). Contamination characteristics of perfluorinated compounds in soil from Pearl River Delta, South China. *China Environmental Science. 33*, 37-42.

Hu, J., & Li, S. (2009). Modeling the mass fluxes and transformations of nutrients in the Pearl River Delta, China. *Journal of Marine Systems*, *78*(1), 146-167. https://doi.org/10.1016/j.jmarsys.2009.05.001

Hu, Y., Gong, X., Xu, Y., Song, X., Liu, H., Deng, X., & Ru, S. (2014). Risk assessment of butyltins based on a fugacity-based food web bioaccumulation model in the Jincheng Bay mariculture area: I. model development. *Environmental Science: Processes & Impacts*, *16*(8), 1994-2001. DOI: 10.1039/C4EM00219A

Hu, Y., Yan, X., Shen, Y., Di, M., & Wang, J. (2018). Antibiotics in surface water and sediments from Hanjiang River, Central China: Occurrence, behavior and risk assessment. *Ecotoxicology and Environmental Safety*, *157*, 150-158. https://doi.org/10.1016/j.ecoenv.2018.03.083

Huang, L., Zhang, C., & Bi, J. (2017). Development of land use regression models for $PM_{2.5}$, SO_2, NO_2 and O_3 in Nanjing, China. *Environmental Research*, *158*, 542-552. https://doi.org/10.1016/j.envres.2017.07.010

Huang, Y., Sun, X., Liu, M., Zhu, J., Yang, J., Du, W., Zhang, X., Gao, D., Qadeer, A., Xie, Y., & Nie, N. (2019). A multimedia fugacity model to estimate the fate and transport of polycyclic aromatic hydrocarbons (PAHs) in a largely urbanized area, Shanghai, China. *Chemosphere*,

217, 298-307. https://doi.org/10.1016/j.chemosphere.2018.10.172

Hydrologic Bureau of the Ministry of Water Resources, China (2013). *Annual Hydrological Report, P.R. China*. Hydrologic Bureau of the Ministry of Water Resources, China.

Ii, H. (1995). Effective porosity and longitudinal dispersivity of sedimentary rocks determined by laboratory and field tracer tests. *Environmental Geology*, *25*(2), 71-85. https://doi.org/10.1007/BF00767863

Jolliet, O., Wannaz, C., Kilgallon, J., Speirs, L., Franco, A., Lehner, B., Veltman, K., & Hodges, J. (2020). Spatial variability of ecosystem exposure to home and personal care chemicals in Asia. *Environment International*, *134*, 105260. https://doi.org/10.1016/j.envint.2019.105260

Kaboré, H. A., Vo Duy, S., Munoz, G., Méité, L., Desrosiers, M., Liu, J., Sory, T. K., & Sauvé, S. (2018). Worldwide drinking water occurrence and levels of newly-identified perfluoroalkyl and polyfluoroalkyl substances. *Science of The Total Environment*, *616*, 1089-1100. https://doi.org/10.1016/j.scitotenv.2017.10.210

Khamesi, A., Khademi, H., & Zeraatpisheh, M. (2020). Biomagnetic monitoring of atmospheric heavy metal pollution using pine needles: The case study of Isfahan, Iran. *Environmental Science and Pollution Research*, *27*, 31555-31566. https://doi.org/10.1007/s11356-020-09247-5

Kim, J. H., Kwak, B. K., Shin, C. B., Jeon, W. J., Park, H. S., Choi, K., & Yi, J. (2010). Spatial distribution multimedia fate model: Numerical aspects and ability for spatial analysis. *Applied Mathematical Modelling*, *34*(9), 2279-2290. https://doi.org/10.1016/j.apm.2009.10.036

Kim, W., Lee, Y., & Kim, S. D. (2017). Developing and applying a site-specific multimedia fate model to address ecological risk of oxytetracycline discharged with aquaculture effluent in coastal waters off Jangheung, Korea. *Ecotoxicology and Environmental Safety*, *145*, 221-226. https://doi.org/10.1016/j.ecoenv.2017.07.038

Kong, X., Liu, W., He, W., Xu, F., Koelmans, A. A., & Mooij, W. M. (2018). Multimedia fate

modeling of perfluorooctanoic acid (PFOA) and perfluorooctane sulphonate (PFOS) in the shallow lake Chaohu, China. *Environmental Pollution*, *237*, 339-347. https://doi.org/10.1016/j.envpol.2018.02.026

Kumar, V., Parihar, R. D., Sharma, A., Bakshi, P., Singh Sidhu, G. P., Bali, A. S., Karaouzas, I., Bhardwaj, R., Thukral, A. K., Gyasi-Agyei, Y., & Rodrigo-Comino, J. (2019). Global evaluation of heavy metal content in surface water bodies: A meta-analysis using heavy metal pollution indices and multivariate statistical analyses. *Chemosphere*, *236*, 124364. https://doi.org/10.1016/j.chemosphere.2019.124364

Kunacheva, C., Fujii, S., Tanaka, S., Seneviratne, S. T. M. L. D., Lien, N. P. H., Nozoe, M., Kimura, K., Shivakoti, B. R., & Harada, H. (2012). Worldwide surveys of perfluorooctane sulfonate (PFOS) and perfluorooctanoic acid (PFOA) in water environment in recent years. *Water Science and Technology*, *66*(12), 2764-2771. https://doi.org/10.2166/wst.2012.518

Kundu, S., Khare, D., & Mondal, A. (2017). Past, present and future land use changes and their impact on water balance. *Journal of Environmental Management*, *197*, 582-596. https://doi.org/10.1016/j.jenvman.2017.04.018

Lammel, G., Klöpffer, W., Semeena, V., Schmidt, E., & Leip, A. (2007). Multicompartmental fate of persistent substances. *Environmental Science and Pollution Research-International*, *14*(3), 153-165. http://www.dx.doi.org/10.1065/espr2006.11.363

Lanza, H. A., Cochran, R. S., Mudge, J. F., Olson, A. D., Blackwell, B. R., Maul, J. D., Salice, C. J., & Anderson, T. A. (2017). Temporal monitoring of perfluorooctane sulfonate accumulation in aquatic biota downstream of historical aqueous film forming foam use areas. *Environmental Toxicology and Chemistry*, *36*(8), 2022-2029. https://doi.org/10.1002/etc.3726

Leung, H. W., Jin, L., Wei, S., Tsui, M. M. P., Zhou, B., Jiao, L., Cheung, P. C., Chun, Y. K., Murphy, M. B., & Lam, P. K. S. (2013). Pharmaceuticals in tap water: Human health risk assessment and proposed monitoring framework in China. *Environmental Health Perspectives*, *121*(7), 839-846. https://doi.org/10.1289/ehp.1206244

Li, N., Zhang, X., Wu, W., & Zhao, X. (2014). Occurrence, seasonal variation and risk assessment of antibiotics in the reservoirs in North China. *Chemosphere*, *111*, 327-335. https://doi.org/10.1016/j.chemosphere.2014.03.129

Li, P., Feng, X., Liang, P., Man Chan, H., Yan, H., & Chen, L. (2013). Mercury in the seafood and human exposure in coastal area of Guangdong province, South China. *Environmental Toxicology and Chemistry*, *32*(3), 541-547. https://doi.org/10.1002/etc.2113

Li, W., Shi, Y., Gao, L., Liu, J., & Cai, Y. (2012). Occurrence of antibiotics in water, sediments, aquatic plants, and animals from Baiyangdian Lake in North China. *Chemosphere*, *89*(11), 1307-1315. https://doi.org/10.1016/j.chemosphere.2012.05.079

Li, Z., Ma, Z., van der Kuijp, T. J., Yuan, Z., & Huang, L. (2014). A review of soil heavy metal pollution from mines in China: Pollution and health risk assessment. *Science of The Total Environment*, *468-469*, 843-853. https://doi.org/10.1016/j.scitotenv.2013.08.090

Lim, D. H., & Lastoskie, C. M. (2011). A dynamic multimedia environmental and bioaccumulation model for brominated flame retardants in Lake Huron and Lake Erie, USA. *Environmental Toxicology and Chemistry*, *30*(5), 1018-1025. https://doi.org/10.1002/etc.482

Lindim, C., van Gils, J., & Cousins, I. T. (2016). A large-scale model for simulating the fate & transport of organic contaminants in river basins. *Chemosphere*, *144*, 803-810. https://doi.org/10.1016/j.chemosphere.2015.09.051

Liu, B., Xie, L., Zhang, H., Li, J., Wang, X., & Dong, W. (2019). Spatial distribution of perfluorinated compounds in atmosphere of the Pearl River Delta, China. *Archives of Environmental Contamination and Toxicology*, *77*(2), 180-187. https://doi.org/10.1007/s00244-019-00637-6

Liu, B., Zhang, H., Xie, L., Li, J., Wang, X., Zhao, L., Wang, Y., & Yang, B. (2015). Spatial distribution and partition of perfluoroalkyl acids (PFAAs) in rivers of the Pearl River Delta, southern China. *Science of The Total Environment*, *524-525*, 1-7. https://doi.org/10.1016/j.scitotenv.2015.04.004

Liu, S., Lu, Y., Wang, T., Xie, S., Jones, K. C., & Sweetman, A. J. (2014). Using gridded

multimedia model to simulate spatial fate of Benzo[α]pyrene on regional scale. *Environment International*, *63*, 53-63. https://doi.org/10.1016/j.envint.2013.10.015

Liu, S., Yang, R., Yin, N., Wang, Y. L., & Faiola, F. (2019). Environmental and human relevant PFOS and PFOA doses alter human mesenchymal stem cell self-renewal, adipogenesis and osteogenesis. *Ecotoxicology and Environmental Safety*, *169*, 564-572. https://doi.org/10.1016/j.ecoenv.2018.11.064

Liu, S., Yin, N., & Faiola, F. (2018). PFOA and PFOS disrupt the generation of human pancreatic progenitor cells. *Environmental Science & Technology Letters*, *5*(5), 237-242. https://doi.org/10.1021/acs.estlett.8b00193

Liu, X., Steele, J. C., & Meng, X. Z. (2017). Usage, residue, and human health risk of antibiotics in Chinese aquaculture: A review. *Environmental Pollution*, *223*, 161-169. https://doi.org/10.1016/j.envpol.2017.01.003

Liu, X., Zhang, G., Liu, Y., Lu, S., Qin, P., Guo, X., Bi, B., Wang, L., Xi, B., Wu, F., Wang, W., & Zhang, T. (2019). Occurrence and fate of antibiotics and antibiotic resistance genes in typical urban water of Beijing, China. *Environmental Pollution*, *246*, 163-173. https://doi.org/10.1016/j.envpol.2018.12.005

Liu, Z., Lu, Y., Wang, P., Wang, T., Liu, S., Johnson, A. C., Sweetman, A. J., & Baninla, Y. (2017). Pollution pathways and release estimation of perfluorooctane sulfonate (PFOS) and perfluorooctanoic acid (PFOA) in central and eastern China. *Science of The Total Environment*, *580*, 1247-1256. https://doi.org/10.1016/j.scitotenv.2016.12.085

Lu, H. J., Luan, M. T., & Zhang, J. L. (2011). Study on transport of Cr(VI) through the landfill liner composed of two-layer soils. *Desalination*, *266*(1), 87-92. https://doi.org/10.1016/j.desal.2010.08.006

Lu, J., Wu, J., Zhang, C., Zhang, Y., Lin, Y., & Luo, Y. (2018). Occurrence, distribution, and ecological-health risks of selected antibiotics in coastal waters along the coastline of China. *Science of The Total Environment*, *644*, 1469-1476. https://doi.org/10.1016/j.scitotenv.2018.07.096

Lu, S., & Xu, Q. (2009). Competitive adsorption of Cd, Cu, Pb and Zn by different soils of Eastern China. *Environmental Geology*, *57*(3), 685-693. DOI: 10.1007/s00254-008-1347-4

Lu, X., & Que, H. (2007). *Investigation on the trend and cause of hydrological elements in Yongding River Basin.* Paper presented at West coast of the strait anti - typhoon flood rescue and relief BBS, Fujian, China.

Luo, Y., Xu, L., Rysz, M., Wang, Y., Zhang, H., & Alvarez, P. J. (2011). Occurrence and transport of tetracycline, sulfonamide, quinolone, and macrolide antibiotics in the Haihe River Basin, China. *Environmental Science & Technology*, *45*(5), 1827-1833. https://doi.org/10.1021/es104009s

Mackay, D. (1979). Finding fugacity feasible. *Environmental Science & Technology*, *13*(10), 1218-1223. https://doi.org/10.1021/es60158a003

Mackay, D. (2001). *Multimedia environmental models: the fugacity approach*. CRC press.

Mackay, D., Paterson, S., Cheung, B., & Neely, W. B. (1985). Evaluating the environmental behavior of chemicals with a level III fugacity model. *Chemosphere*, *14*(3), 335-374. https://doi.org/10.1016/0045-6535(85)90061-X

MacLeod, M., Woodfine, D. G., Mackay, D., McKone, T., Bennett, D., & Maddalena, R. (2001). BETR North America: A regionally segmented multimedia contaminant fate model for North America. *Environmental Science and Pollution Research,* *8*(3), 156. https://doi.org/10.1007/BF02987379

MacLeod, M., Scheringer, M., McKone, T. E., & Hungerbuhler, K. (2010). The state of multimedia mass-balance modeling in environmental science and decision-making. *Environmental Science & Technology*, *44*(22), 8360-8364. https://doi.org/10.1021/es100968w

MacLeod, M., von Waldow, H., Tay, P., Armitage, J. M., Wöhrnschimmel, H., Riley, W. J., McKone, T. E., & Hungerbuhler, K. (2011). BETR global–A geographically-explicit global-scale multimedia contaminant fate model. *Environmental Pollution*, *159*(5), 1442-1445. https://doi.org/10.1016/j.envpol.2011.01.038

Massmann, C., & Holzmann, H. (2012). Analysis of the behavior of a rainfall–runoff model using

three global sensitivity analysis methods evaluated at different temporal scales. *Journal of Hydrology*, *475*, 97-110. https://doi.org/10.1016/j.jhydrol.2012.09.026

McGoldrick, D. J., & Murphy, E. W. (2016). Concentration and distribution of contaminants in lake trout and walleye from the Laurentian Great Lakes (2008–2012). *Environmental Pollution*, *217*, 85-96. https://doi.org/10.1016/j.envpol.2015.12.019

Meng, J., Wang, T., Song, S., Wang, P., Li, Q., Zhou, Y., & Lu, Y. (2018). Tracing perfluoroalkyl substances (PFASs) in soils along the urbanizing coastal area of Bohai and Yellow Seas, China. *Environmental Pollution*, *238*, 404-412. https://doi.org/10.1016/j.envpol.2018.03.056

Ministry of Water Resources the People's Republic of China (MWR). (2009). Chinese river sediment bulletin. Retrieved June 17, 2019 from http://www.mwr.gov.cn/sj/tjgb/zghlnsgb/201612/t20161222_776064.html

Mishra, S. (2009). Uncertainty and sensitivity analysis techniques for hydrologic modeling. *Journal of Hydroinformatics*, *11*(3-4), 282-296. https://doi.org/10.2166/hydro.2009.048

Moreau, P., Viaud, V., Parnaudeau, V., Salmon-Monviola, J., & Durand, P. (2013). An approach for global sensitivity analysis of a complex environmental model to spatial inputs and parameters: A case study of an agro-hydrological model. *Environmental Modelling & Software*, *47*, 74-87. https://doi.org/10.1016/j.envsoft.2013.04.006

Morris, M. D. (1991). Factorial sampling plans for preliminary computational experiments. *Technometrics*, *33*(2), 161-174.

National Meteorological Information Center. (2012). *Daily data set of surface climatological data for China (V3.0).* Retrieved June 18, 2019 from http://data.cma.cn/data/cdcdetail/dataCode/SURF_CLI_CHN_MUL_DAY_V3.0.html

Nilsson, B., Sidle, R. C., Klint, K. E., Bøggild, C. E., & Broholm, K. (2001). Mass transport and scale-dependent hydraulic tests in a heterogeneous glacial till–sandy aquifer system. *Journal of Hydrology*, *243*(3), 162-179. https://doi.org/10.1016/S0022-1694(00)00416-9

Pan, C. G., Wang, Y. H., Yu, K. F., Zhang, W., Zhang, J., & Guo, J. (2020). Occurrence and

distribution of perfluoroalkyl substances in surface riverine and coastal sediments from the Beibu Gulf, south China. *Marine Pollution Bulletin*, *150*, 110706. https://doi.org/10.1016/j.marpolbul.2019.110706

Pan, C. G., Ying, G. G., Liu, Y. S., Zhang, Q. Q., Chen, Z. F., Peng, F. J., & Huang, G. Y. (2014). Contamination profiles of perfluoroalkyl substances in five typical rivers of the Pearl River Delta region, South China. *Chemosphere*, *114*, 16-25. https://doi.org/10.1016/j.chemosphere.2014.04.005

Pan, C. G., Zhao, J. L., Liu, Y. S., Zhang, Q. Q., Chen, Z. F., Lai, H. J., Peng, F. J., Liu, S. S., & Ying, G. G. (2014). Bioaccumulation and risk assessment of per- and polyfluoroalkyl substances in wild freshwater fish from rivers in the Pearl River Delta region, South China. *Ecotoxicology and Environmental Safety*, *107*, 192-199. https://doi.org/10.1016/j.ecoenv.2014.05.031

Pan, L., Wang, Y., Ma, J., Hu, Y., Su, B., Fang, G., Wang, L., & Xiang, B. (2018). A review of heavy metal pollution levels and health risk assessment of urban soils in Chinese cities. *Environmental Science and Pollution Research*, *25*(2), 1055-1069. https://doi.org/10.1007/s11356-017-0513-1

Panhalkar, S. S. (2014). RETRACTED: Hydrological modeling using SWAT model and geoinformatic techniques. *The Egyptian Journal of Remote Sensing and Space Science*, *17*(2), 197-207. https://doi.org/10.1016/j.ejrs.2014.03.001

Pennington, D. W., Margni, M., Ammann, C., & Jolliet, O. (2005). Multimedia fate and human intake modeling: Spatial versus nonspatial insights for chemical emissions in Western Europe. *Environmental Science & Technology*, *39*(4), 1119-1128. https://doi.org/10.1021/es034598x

Pistocchi, A., Sarigiannis, D., & Vizcaino, P. (2010). Spatially explicit multimedia fate models for pollutants in Europe: State of the art and perspectives. *Science of The Total Environment*, *408*(18), 3817-3830. https://doi.org/10.1016/j.scitotenv.2009.10.046

Rai, P. K. (2016). Particulate matter and its size fractionation. In P. K. Rai (Ed.), *Biomagnetic*

Monitoring of Particulate Matter (pp. 1-13). Elsevier. https://doi.org/10.1016/B978-0-12-805135-1.00001-9

Ramírez, N., Cuadras, A., Rovira, E., Borrull, F., & Marcé, R. M. (2012). Chronic risk assessment of exposure to volatile organic compounds in the atmosphere near the largest Mediterranean industrial site. *Environment International*, *39*(1), 200-209. https://doi.org/10.1016/j.envint.2011.11.002

Rankin, K., Mabury, S. A., Jenkins, T. M., & Washington, J. W. (2016). A North American and global survey of perfluoroalkyl substances in surface soils: Distribution patterns and mode of occurrence. *Chemosphere*, *161*, 333-341. https://doi.org/10.1016/j.chemosphere.2016.06.109

Regens, J. L., Obenshain, K. R., Travis, C., & Whipple, C. (2002). Conceptual site models and multimedia modeling: Comparing MEPAS, MMSOILS, and RESRAD. *Human and Ecological Risk Assessment: An International Journal*, *8*(2), 391-403. https://doi.org/10.1080/20028091056971

Resource and Environment Data Cloud Platform. (2015). *Remote sensing monitoring data of land use status in China at 2015.* Retrieved August 12, 2019 from http://www.resdc.cn/data.aspx?DATAID=184

Ruiz, P., Yang, X., Lumen, A., & Fisher, J. (2013). Quantitative structure-activity relationship (QSAR) models, physiologically based pharmacokinetic (PBPK) models, biologically based dose response (BBDR) and toxicity pathways: Computational tools for public health. In B. A. Fowler (Ed.), *Computational Toxicology* (pp. 5-21). Academic Press. https://doi.org/10.1016/B978-0-12-396461-8.00002-6

Saltelli, A., Aleksankina, K., Becker, W., Fennell, P., Ferretti, F., Holst, N., Li, S., & Wu, Q. (2019). Why so many published sensitivity analyses are false: A systematic review of sensitivity analysis practices. *Environmental Modelling & Software*, *114*, 29-39. https://doi.org/10.1016/j.envsoft.2019.01.012

Saltelli, A., & Annoni, P. (2010). How to avoid a perfunctory sensitivity analysis. *Environmental*

Modelling & Software, *25*(12), 1508-1517. https://doi.org/10.1016/j.envsoft.2010.04.012

Sakurai, T., Imaizumi, Y., Kuroda, K., Hayashi, T. I., & Suzuki, N. (2019). Georeferenced multimedia environmental fate of volatile methylsiloxanes modeled in the populous Tokyo Bay catchment basin. *Science of The Total Environment*, *689*, 843-853. https://doi.org/10.1016/j.scitotenv.2019.06.462

Sarigiannis, D. A., Karakitsios, S. P., Gotti, A., Liakos, I. L., & Katsoyiannis, A. (2011). Exposure to major volatile organic compounds and carbonyls in European indoor environments and associated health risk. *Environment International*, *37*(4), 743-765. https://doi.org/10.1016/j.envint.2011.01.005

Schwanz, T. G., Llorca, M., Farré, M., & Barceló, D. (2016). Perfluoroalkyl substances assessment in drinking waters from Brazil, France and Spain. *Science of The Total Environment*, *539*, 143-152. https://doi.org/10.1016/j.scitotenv.2015.08.034

Setegn, S. G., Dargahi, B., Srinivasan, R., & Melesse, A. M. (2010). Modeling of sediment yield from Anjeni-Gauged Watershed, Ethiopia using SWAT model. *Journal of the American Water Resources Association*, *46*(3), 514-526. https://doi.org/10.1111/j.1752-1688.2010.00431.x

Sharafi, K., Yunesian, M., Nodehi, R. N., Mahvi, A. H., & Pirsaheb, M. (2019). A systematic literature review for some toxic metals in widely consumed rice types (domestic and imported) in Iran: Human health risk assessment, uncertainty and sensitivity analysis. *Ecotoxicology and Environmental Safety*, *176*, 64-75. https://doi.org/10.1016/j.ecoenv.2019.03.072

Sheu, T. W. H., & Chen, Y. H. (2002). Finite element analysis of contaminant transport in groundwater. *Applied Mathematics and Computation*, *127*(1), 23-43. https://doi.org/10.1016/S0096-3003(00)00160-0

Shin, H. M., Vieira, V. M., Ryan, P. B., Detwiler, R., Sanders, B., Steenland, K., & Bartell, S. M. (2011). Environmental fate and transport modeling for perfluorooctanoic acid emitted from the Washington Works Facility in West Virginia. *Environmental Science & Technology*,

45(4), 1435-1442. https://doi.org/10.1021/es102769t

Shin, M. J., Guillaume, J. H. A., Croke, B. F. W., & Jakeman, A. J. (2013). Addressing ten questions about conceptual rainfall–runoff models with global sensitivity analyses in R. *Journal of Hydrology*, *503*, 135-152. https://doi.org/10.1016/j.jhydrol.2013.08.047

Sobol, I. M. (1993). Sensitivity analysis for non-linear mathematical models. *Mathematical Modelling and Computational Experiment*, *1*, 407-414.

Song, H. M., & Xu, L. Y. (2011). A method of urban ecological risk assessment: Combining the multimedia fugacity model and GIS. *Stochastic Environmental Research and Risk Assessment*, *25*(5), 713-719. https://doi.org/10.1007/s00477-011-0476-6

Song, S., Su, C., Lu, Y., Wang, T., Zhang, Y., & Liu, S. (2016). Urban and rural transport of semivolatile organic compounds at regional scale: A multimedia model approach. *Journal of Environmental Sciences*, *39*, 228-241. https://doi.org/10.1016/j.jes.2015.12.005

Song, X., Zhang, J., Zhan, C., Xuan, Y., Ye, M., & Xu, C. (2015). Global sensitivity analysis in hydrological modeling: Review of concepts, methods, theoretical framework, and applications. *Journal of Hydrology*, *523*, 739-757. https://doi.org/10.1016/j.jhydrol.2015.02.013

Song, X. M., Kong, F. Z., Zhan, C. S., Han, J. W., & Zhang, X. H. (2013). Parameter identification and global sensitivity analysis of Xin'anjiang model using meta-modeling approach. *Water Science and Engineering*, *6*(1), 1-17. https://doi.org/10.3882/j.issn.1674-2370.2013.01.001

Stahl, L. L., Snyder, B. D., Olsen, A. R., Kincaid, T. M., Wathen, J. B., & McCarty, H. B. (2014). Perfluorinated compounds in fish from U.S. urban rivers and the Great Lakes. *Science of The Total Environment*, *499*, 185-195. https://doi.org/10.1016/j.scitotenv.2014.07.126

Statistics Bureau of Guangdong Province. (2013). *Guangdong statistic yearbook.* Retrieved June 10, 2019 from http://stats.gd.gov.cn/gdtjnj/content/post_1424891.html

Staub, M., Galietti, B., Oxarango, L., Khire, M., & Gourc, J. P. (2018). *Porosity and hydraulic conductivity of MSW using laboratory-scale tests*. Retrieved April 10, 2019 from

http://ce561.ce.metu.edu.tr/files/2013/11/hydraulic-conductivity-waste-2.pdf

Su, C., Jiang, L., & Zhang, W. (2014). A review on heavy metal contamination in the soil worldwide: Situation, impact and remediation techniques. *Environmental Skeptics and Critics*, *3*(2), 24-28.

Su, C., Lu, Y., Wang, T., Lu, X., Song, S., Li, L., Khan, K., Wang, C., & Liang, R. (2018). Dynamic multimedia fate simulation of perfluorooctane sulfonate (PFOS) from 1981 to 2050 in the urbanizing Bohai Rim of China. *Environmental Pollution*, *235*, 235-244. https://doi.org/10.1016/j.envpol.2017.12.045

Su, C., Song, S., Lu, Y., Wang, P., Meng, J., Lu, X., Jürgens, M. D., Khan, K., Baninla, Y., & Liang, R. (2018). Multimedia fate and transport simulation of perfluorooctanoic acid/ perfluorooctanoate in an urbanizing area. *Science of The Total Environment*, *643*, 90-97. https://doi.org/10.1016/j.scitotenv.2018.06.156

Su, C., Zhang, H., Cridge, C., & Liang, R. (2019). A review of multimedia transport and fate models for chemicals: Principles, features and applicability. *Science of The Total Environment*, *668*, 881-892. https://doi.org/10.1016/j.scitotenv.2019.02.456

Sun, J., Zeng, Q., Tsang, D. C. W., Zhu, L. Z., & Li, X. D. (2017). Antibiotics in the agricultural soils from the Yangtze River Delta, China. *Chemosphere*, *189*, 301-308. https://doi.org/10.1016/j.chemosphere.2017.09.040

Sun, T.F. (2017). *Occurrence of perfluorinated compounds in soils and vegetables surrounding the industrial parks in Guangzhou and Foshan* (Master's thesis). Jinan University.

Suzuki, N., Murasawa, K., Sakurai, T., Nansai, K., Matsuhashi, K., Moriguchi, Y., Tanabe, K., Nakasugi, O., & Morita, M. (2004). Geo-referenced multimedia environmental fate model (G-CIEMS): Model formulation and comparison to the generic model and monitoring approaches. *Environmental Science & Technology*, *38*(21), 5682-5693. https://doi.org/10.1021/es049261p

Szabo, D., Coggan, T. L., Robson, T. C., Currell, M., & Clarke, B. O. (2018). Investigating recycled water use as a diffuse source of per- and polyfluoroalkyl substances (PFASs) to

groundwater in Melbourne, Australia. *Science of the Total Environment*, *644*, 1409-1417. https://doi.org/10.1016/j.scitotenv.2018.07.048

Tianjin Municipal Bureau of Statistics. (2010). *Tianjin statistical yearbook 2010.* Retrieved October 10, 2018 from http://stats.tj.gov.cn/nianjian/2010nj/indexch.htm.

Timmermann, C. A. G., Budtz-Jørgensen, E., Jensen, T. K., Osuna, C. E., Petersen, M. S., Steuerwald, U., Nielsen, F., Poulsen, L. K., Weihe, P., & Grandjean, P. (2017). Association between perfluoroalkyl substance exposure and asthma and allergic disease in children as modified by MMR vaccination. *Journal of Immunotoxicology*, *14*(1), 39-49. https://doi.org/10.1080/1547691X.2016.1254306

Tobiszewski, M., Namieśnik, J., & Pena-Pereira, F. (2017). Environmental risk-based ranking of solvents using the combination of a multimedia model and multi-criteria decision analysis. *Green Chemistry*, *19*(4), 1034-1042. DOI: 10.1039/c6gc03424a

Travnikov, O., Ilyin, I. 2005. *Regional model MSCE-HM of heavy metal transboundary air pollution in Europe*. Retrieved April 10, 2018 from http://en.msceast.org/index.php/publications/reports#2005

Trevors, J. T. (2010). What is a global environmental pollution problem? *Water, Air, & Soil Pollution*, *210*(1), 1-2. https://doi.org/10.1007/s11270-010-0337-9

Van Genuchten, M. T., & Alves, W. (1982). *Analytical solutions of the one-dimensional convective-dispersive solute transport equation*. US Department of Agriculture, Agricultural Research Service.

VanGulck, J. F., Rowe, R. K., Rittmann, B. E., & Cooke, A. J. (2003). Predicting biogeochemical calcium precipitation in landfill leachate collection systems. *Biodegradation*, *14*(5), 331-346. https://doi.org/10.1023/A:1025667706695

Vedagiri, U. K., Anderson, R. H., Loso, H. M., & Schwach, C. M. (2018). Ambient levels of PFOS and PFOA in multiple environmental media. *Remediation Journal*, *28*(2), 9-51. https://doi.org/10.1002/rem.21548

Vizcaíno, P., & Pistocchi, A. (2010). A GIS model-based assessment of the environmental

distribution of γ-hexachlorocyclohexane in European soils and waters. *Environmental Pollution*, *158*(10), 3017-3027. https://doi.org/10.1016/j.envpol.2010.07.018

Wang, C., Zhou, S., He, Y., Wang, J., Wang, F., & Wu, S. (2017). Developing a black carbon-substituted multimedia model for simulating the PAH distributions in urban environments. *Scientific reports*, *7*(1), 14548. https://doi.org/10.1038/s41598-017-14789-9

Wang, F., & Shih, K. (2011). Adsorption of perfluorooctanesulfonate (PFOS) and perfluorooctanoate (PFOA) on alumina: Influence of solution pH and cations. *Water Research*, *45*(9), 2925-2930. https://doi.org/10.1016/j.watres.2011.03.007

Wang, H., Du, H., Yang, J., Jiang, H., O, K., Xu, L., Liu, S., Yi, J., Qian, X., Chen, Y., Jiang, Q., & He, G. (2019). PFOS, PFOA, estrogen homeostasis, and birth size in Chinese infants. *Chemosphere*, *221*, 349-355. https://doi.org/10.1016/j.chemosphere.2019.01.061

Wang, L., Ye, M., Fernando Rios, J., Fernandes, R., Lee, P. Z., & Hicks, R. W. (2013). Estimation of nitrate load from septic systems to surface water bodies using an ArcGIS-based software. *Environmental Earth Sciences*, *70*(4), 1911-1926. https://doi.org/10.1007/s12665-013-2283-5

Wang, S. (2016). *Structure of fish food webs and energy flow of ecosystems in the East River* (Doctoral dissertation). Jinan University.

Wannaz, C., Franco, A., Kilgallon, J., Hodges, J., & Jolliet, O. (2018). A global framework to model spatial ecosystems exposure to home and personal care chemicals in Asia. *Science of The Total Environment*, *622-623*, 410-420. https://doi.org/10.1016/j.scitotenv.2017.11.315

Waseem, A., Arshad, J., Iqbal, F., Sajjad, A., Mehmood, Z., & Murtaza, G. (2014). Pollution status of Pakistan: A retrospective review on heavy metal contamination of water, soil, and vegetables. *BioMed Research International*, *2014*, 813206. https://doi.org/10.1155/2014/813206

Webster, E., Mackay, D., Di Guardo, A., Kane, D., & Woodfine, D. (2004). Regional differences in chemical fate model outcome. *Chemosphere*, *55*(10), 1361-1376.

https://doi.org/10.1016/j.chemosphere.2003.10.061

Wei, B., & Yang, L. (2010). A review of heavy metal contaminations in urban soils, urban road dusts and agricultural soils from China. *Microchemical Journal*, *94*(2), 99-107. https://doi.org/10.1016/j.microc.2009.09.014

World Wide Fund for Nature (WWF). (2015). *Toxic Chemicals*. Retrieved August 12, 2019 from http://wwf.panda.org/about_our_earth/teacher_resources/webfieldtrips/toxics/

Wu, S. (2005). *The spatial and temporal change of nitrogen and phosphorus produced by livestock and poultry & their effects on agricultural non-point pollution in China* (Doctoral dissertation). Chinese Academy of Agricultural Science.

Xiao, Y. (2017). *A national action plan to contain antimicrobial resistance in China: Contents, actions and expectations.* Retrieved August 20 2018 from http://resistancecontrol.info/2017/a-national-action-plan-to-contain-antimicrobial-resistance-in-china-contents-actions-and-expectations/

Xie, S., Lu, Y., Wang, T., Liu, S., Jones, K., & Sweetman, A. (2013). Estimation of PFOS emission from domestic sources in the eastern coastal region of China. *Environment International*, *59*, 336-343. https://doi.org/10.1016/j.envint.2013.06.015

Xie, S., Wang, T., Liu, S., Jones, K. C., Sweetman, A. J., & Lu, Y. (2013). Industrial source identification and emission estimation of perfluorooctane sulfonate in China. *Environment International*, *52*, 1-8. https://doi.org/10.1016/j.envint.2012.11.004

Yan, C., Yang, Y., Zhou, J., Liu, M., Nie, M., Shi, H., & Gu, L. (2013). Antibiotics in the surface water of the Yangtze Estuary: Occurrence, distribution and risk assessment. *Environmental Pollution*, *175*, 22-29. https://doi.org/10.1016/j.envpol.2012.12.008

Yang, Q., Li, Z., Lu, X., Duan, Q., Huang, L., & Bi, J. (2018). A review of soil heavy metal pollution from industrial and agricultural regions in China: Pollution and risk assessment. *Science of The Total Environment*, *642*, 690-700. https://doi.org/10.1016/j.scitotenv.2018.06.068

Yang, X., Xu, X., Wei, X., Wan, J., & Zhang, Y. (2019). Biomarker effects in carassius auratus

exposure to ofloxacin, sulfamethoxazole and ibuprofen. *International journal of environmental research and public health*, *16*(9), 1628. https://doi.org/10.3390/ijerph16091628

Yi, X., Lin, C., Ong, E. J. L., Wang, M., & Zhou, Z. (2019). Occurrence and distribution of trace levels of antibiotics in surface waters and soils driven by non-point source pollution and anthropogenic pressure. *Chemosphere*, *216*, 213-223. https://doi.org/10.1016/j.chemosphere.2018.10.087

Yi, X., Zou, R., & Guo, H. (2016). Global sensitivity analysis of a three-dimensional nutrients-algae dynamic model for a large shallow lake. *Ecological Modelling*, *327*, 74-84. https://doi.org/10.1016/j.ecolmodel.2016.01.005

Zhang, M. l., Shen, Y. M., & Guo, Y. (2008). Development and application of a eutrophication water quality model for river networks. *Journal of Hydrodynamics*, *20*(6), 719-726. https://doi.org/10.1016/S1001-6058(09)60007-X

Zhang, Q. Q., Ying, G. G., Pan, C. G., Liu, Y. S., & Zhao, J. L. (2015). Comprehensive evaluation of antibiotics emission and fate in the river basins of China: Source analysis, multimedia modeling, and linkage to bacterial resistance. *Environmental Science & Technology*, *49*(11), 6772-6782. https://doi.org/10.1021/acs.est.5b00729

Zhang, R., Pei, J., Zhang, R., Wang, S., Zeng, W., Huang, D., Wang, Y., Zhang, Y., Wang, Y., & Yu, K. (2018). Occurrence and distribution of antibiotics in mariculture farms, estuaries and the coast of the Beibu Gulf, China: Bioconcentration and diet safety of seafood. *Ecotoxicology and Environmental Safety*, *154*, 27-35. https://doi.org/10.1016/j.ecoenv.2018.02.006

Zhang, R. R., Zhan, C. S., He, Z. P., & Song, X. M. (2012). Review of environmental multimedia models. *Environmental Forensics*, *13*(3), 216-224. https://doi.org/10.1080/15275922.2012.702328

Zhang, Y., Lai, S., Zhao, Z., Liu, F., Chen, H., Zou, S., Xie, Z., & Ebinghaus, R. (2013). Spatial distribution of perfluoroalkyl acids in the Pearl River of Southern China. *Chemosphere*,

93(8), 1519-1525. https://doi.org/10.1016/j.chemosphere.2013.07.060

Zhang, Z., Meng, X., & Lu, Y. (2014). Runoff flood characteristics and arrangement of Yongdingxin River in Haihe River Basin. *Science & Technology Vision, China, 15*, 316-316.

Zhao, S., Breivik, K., Liu, G., Zheng, M., Jones, K. C., & Sweetman, A. J. (2017). Long-term temporal trends of polychlorinated biphenyls and their controlling sources in China. *Environmental Science & Technology*, *51*(5), 2838-2845. https://doi.org/10.1021/acs.est.6b05341

Zhao, Y. G., Wan, H. T., Law, A. Y. S., Wei, X., Huang, Y. Q., Giesy, J. P., Wong, M. H., & Wong, C. K. C. (2011). Risk assessment for human consumption of perfluorinated compound-contaminated freshwater and marine fish from Hong Kong and Xiamen. *Chemosphere*, *85*(2), 277-283. https://doi.org/10.1016/j.chemosphere.2011.06.002

Zheng, W., Shi, H., Fang, G., Hu, L., Peng, S., & Zhu, M. (2012). Global sensitivity analysis of a marine ecosystem dynamic model of the Sanggou Bay. *Ecological Modelling*, *247*, 83-94. https://doi.org/10.1016/j.ecolmodel.2012.08.003

Zhiyan Consulting Group. (2015). *China's antibiotics markets: An in-depth analysis and prospect 2015-2020*. Retrieved November 17 2018 from http://www.chyxx.com/research/201502/306230.html

Zhu, Y., Tao, S., Sun, J., Wang, X., Li, X., Tsang, D. C. W., Zhu, L., Shen, G., Huang, H., Cai, C., & Liu, W. (2019). Multimedia modeling of the PAH concentration and distribution in the Yangtze River Delta and human health risk assessment. *Science of The Total Environment*, *647*, 962-972. https://doi.org/10.1016/j.scitotenv.2018.08.075

Zou, S., Xu, W., Zhang, R., Tang, J., Chen, Y., & Zhang, G. (2011). Occurrence and distribution of antibiotics in coastal water of the Bohai Bay, China: Impacts of river discharge and aquaculture activities. *Environmental Pollution*, *159*(10), 2913-2920. https://doi.org/10.1016/j.envpol.2011.04.037

Zuo, T. T., Jin, H. Y., Zhang, L., Liu, Y. L., Nie, J., Chen, B. l., Fang, C. F., Xue, J., Bi, X. Y., Zhou,

L., Shen, M. R., Shi, S. M, & Ma, S. C. (2020). Innovative health risk assessment of heavy metals in Chinese herbal medicines based on extensive data. *Pharmacological Research*, *159*, 104987. https://doi.org/10.1016/j.phrs.2020.104987

Appendix

A: Solution Techniques

Finite difference method (FDM)

FDM is an efficient method to solve partial differential equations (Sheu & Chen, 2002). It requires a mesh of local coordinate systems and often considers the explicit forward Euler method. The central differentiation method is used to solve the second-order derivative, which requires three points, while the forward Euler differentiation method is used for the first-order derivative, which needs two points.

$$\frac{\partial^2 C}{\partial z^2} = \frac{C_{j+1} - 2C_j + C_{j-1}}{\Delta z^2} + O(\Delta z^2) \tag{A-1}$$

$$\frac{\partial C}{\partial z} = \frac{C_j - C_{j-1}}{\Delta z} + O(\Delta z) \tag{A-2}$$

The solution at time t_{k+1} can be solved explicitly as follows:

$$C_{k+1,j} = (\alpha + \gamma)C_{k,j-1} + (1 - 2\gamma - \alpha)C_{k,j} + \gamma C_{k,j+1} \tag{A-3}$$

where γ and α are defined as,

$$\gamma = \frac{D_E \Delta t}{\Delta z^2} \qquad \alpha = \frac{V_E \Delta t}{\Delta z}$$

Finite element method (FEM)

FEM is a powerful technique for solving engineering problems. The field is firstly divided into a series of finite elements of equal length. The overall governing equation for the fate and transport in the three main zones is provided in equation (3-1).

The test function $w(z)$ is selected to derive the weak form:

$$\int_0^l D\frac{dC}{dz}\frac{dw}{dz} + V\frac{dC}{dz}wdz = DC'(l)w(l) - \int_0^l \frac{dC}{dt}wdz \tag{A-4}$$

The next step is to divide the spatial domain into elements which are assumed to be the same length. Shape functions to interpolate the solution over each element. The approximate solution can be expressed as:

$$\mathrm{C}_{app}(z) = \sum_{j=1}^{N} C_j S_j(z) \tag{A-5}$$

$$S_j(z_j) = \begin{cases} 1 & if\ i = j \\ 0 & if\ i \neq j \end{cases} \tag{A-6}$$

where C_{app} is the approximate solution; N is the number of nodes; C_j and S_j are the unknown value and the shape functions in node j.

Then the weak form could be described as:

$$\int_0^l D\frac{dw}{dz}\left(\sum_{j=1}^{N} C_j \frac{dS_j}{dz}\right) + Vw\left(\sum_{j=1}^{N} C_j \frac{dS_j}{dz}\right)dz = DC'(l)w(l) - \int_0^l \frac{dC}{dt} w dz \tag{A-7}$$

In the framework of the Galerkin method, the test functions are estimated as the same as the shape functions. The equation becomes:

$$\sum_{j=1}^{N}\left[\int_0^l \left(D\frac{dS_i}{dz}\frac{dS_j}{dz} + VS_i\frac{dS_j}{dz}\right)dz\right]C_j = DC'(l)w(l) - \int_0^l \frac{dC}{dt} S_i dz \quad i = 1,2,\ldots,N \tag{A-8}$$

To simplify the equation, the following compact matrix notation is applied:

$$\boldsymbol{KC=B+F} \tag{A-9}$$

where **C** is the vector of nodal unknowns; **K** is the global stiffness matrix; **B** and **F** are the global boundary integral vector and force vector. The boundary integral vector is only evaluated at the boundaries.

These **K** and **F** integrals are evaluated as a sum of separate integrals over individual elements.

$$\boldsymbol{K}=\sum_{k=1}^{N} \boldsymbol{K}^k \tag{A-10}$$

$$\boldsymbol{F}=\sum_{k=1}^{N}\boldsymbol{F}^{k} \tag{A-11}$$

$$\boldsymbol{K}^{k}=\begin{bmatrix} D/h-0.5V & -D/h+0.5V \\ -D/h-0.5V & D/h+0.5V \end{bmatrix} \tag{A-12}$$

$$\boldsymbol{F}^{k}=\begin{vmatrix} \frac{h}{3} & \frac{h}{6} \\ \frac{h}{6} & \frac{h}{3} \end{vmatrix} \begin{vmatrix} \frac{\partial C_i^n}{\partial t} \\ \frac{\partial C_{i+1}^n}{\partial t} \end{vmatrix} \tag{A-13}$$

$\partial\, C_i^n / \partial\, t$ is separated by the backward difference equation:

$$\frac{\partial C_i^n}{\partial t}=\frac{C_i^n-C_i^{n-1}}{\Delta t} \tag{A-14}$$

where C_i^n is the unknown value in node *i* at time *n* and the values at time *n-1* are known as initial conditions or obtained from former simulation.

The matrix equation is easily solvable by various methods such as the Jacobian method, the Gauss–Seidel method or the successive over-relaxation (SOR) method.

Alternating direction implicit method

Alternating direction implicit method is a popular method for solving the large matrix equations that arise in systems theory and can be formulated to construct solutions in a memory-efficient, factored form. The idea of this method is to split the finite difference equations into two: one with the x-derivative taken implicitly and the next with the z-derivative taken implicitly.

From $t = k$ to $t = k+0.5$, we could use the following equations:

$$\alpha_1 C_{i-1,j}^{k+0.5}+\beta_1 C_{i,j}^{k+0.5}-\gamma_1 C_{i+1,j}^{k+0.5}=\delta_1 \tag{A-15}$$

$$\alpha_1=-\frac{D_x}{\Delta x^2}-\frac{V_x}{\Delta x} \tag{A-16}$$

$$\beta_1=2\frac{D_x}{\Delta x^2}+\frac{V_x}{\Delta x}+\frac{2}{\Delta t} \tag{A-17}$$

$$\gamma_1 = -\frac{D_x}{\Delta x^2} \tag{A-18}$$

$$\delta_1 = D_z \frac{C_{i,j+1}^k - 2C_{i,j}^k + C_{i,j-1}^k}{\Delta z^2} - V_z \frac{C_{i,j}^k - C_{i,j-1}^k}{\Delta z} + \frac{2C_{i,j}^k}{\Delta t} \tag{A-19}$$

Similarly, from *t=k+0.5* to *t=k+1*, we could get,

$$\alpha_2 C_{i,j\text{-}1}^{k+1} + \beta_2 C_{i,j}^{k+1} - \gamma_2 C_{i,j+1}^{k+1} = \delta_2 \tag{A-20}$$

$$\alpha_2 = -\frac{D_z}{\Delta z^2} - \frac{V_z}{\Delta z} \tag{A-21}$$

$$\beta_2 = 2\frac{D_z}{\Delta z^2} + \frac{V_z}{\Delta z} + \frac{2}{\Delta t} \tag{A-22}$$

$$\gamma_2 = -\frac{D_z}{\Delta z^2} \tag{A-23}$$

$$\delta_2 = D_x \frac{C_{i+1,j}^{k+0.5} - 2C_{i,j}^{k+0.5} + C_{i-1,j}^{k+0.5}}{\Delta x^2} - V_x \frac{C_{i,j}^{k+0.5} - C_{i-1,j}^{k+0.5}}{\Delta x} + \frac{2C_{i,j}^{k+0.5}}{\Delta t} \tag{A-24}$$

The analytical solution in the source, unsaturated and saturated zone

Since this study case in Chapter 4 concerns the fate and transport of heavy metal, the mass emission rate upwards into the air is negligible. The overall governing equation for the pollutant fate and transport is established as equation (3-1). The fate and transport of leachate are calculated for the unsaturated zone module. The source of the contaminant is the bottom of the source zone. The governing one-dimensional equations for the unsaturated zone soil medium are similar to equation (3-1). The following equations (A-25 to A-27) could serve as the analytical solution for the source and unsaturated zone, with the difference being that the upper boundary conditions vary with time.

The analytical solution is shown as follows (Van Genuchten and Alves 1982):

$$C(z,t) = C_u - (C_0 - C_u)A(z,t) \quad 0 < t < t_0 \tag{A-25}$$

$$C(z,t) = C_u + (C_0 - C_u)A(z,t) - C_0 A(z,t-t_0) \quad t > t_0 \tag{A-26}$$

where

$$A(x,t) = \frac{1}{2} erfc\left[\frac{Rx - vt}{2(DRt)^{1/2}}\right] + \frac{1}{2} erfc\left[\frac{Rx + vt}{2(DRt)^{1/2}}\right] \tag{A-27}$$

where *erfc* is the complementary error function and the other parameters are mentioned above.

In the saturated zone, the mass balance equation describes solute transport in a three-dimensional homogeneous isotropic aquifer with the uniform flow at a velocity V in the x-direction. Domenico (1987) derived a semi-analytical solution for the case of a semi-infinite aquifer ($x \geq 0$) with asymmetrical contaminant sources in the form of an area of size $Y \times Z$. The solution is given as follows:

$$\begin{aligned} C(x,y,z,t) = {} & (C_0/8) erfc\left[x - vt/2(\alpha_x vt)^{1/2}\right] \\ & \left\{erf\left[(y + Y/2)/2(\alpha_y vx)^{1/2}\right] - erf\left[(y - Y/2)/2(\alpha_y vx)^{1/2}\right]\right\} \\ & \left\{erf\left[(z + Z/2)/2(\alpha_z vx)^{1/2}\right] - erf\left[(z - Z/2)/2(\alpha_z vx)^{1/2}\right]\right\} \end{aligned} \tag{A-28}$$

where α_x, α_y and α_z are the dispersivity in the coordinate directions (m) and are defined as the dispersion coefficient divided by the mean seepage velocity.

Finite volume method (FVM)

Finite volume methods (FVM) are one of the most widely used for the solution of the advection-diffusion equations (Merrick et al., 2018). The 3D atmosphere pollutant transport model is numerically solved based on FVM. The first order upwind scheme is applied for calculations of the advection term in space.

The governing equation of atmosphere module (Equation 3-19) is discretized through the central control volume method with a flexible mesh. Control volumes are established around the interior nodes with six control volume faces as shown in Figure A-1. At the ends of the domain are

considered as the boundary control volumes, in which the ghost points are applied based on boundary conditions.

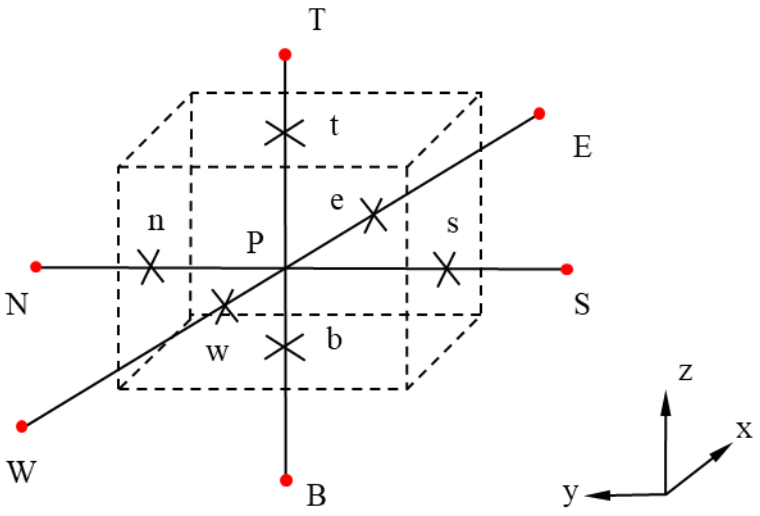

Figure A-1 Control volume for an interior node

Integration of Equation 3-19 in the control volume $N_{i,j,k}$ gives the following equation:

$$\int_t^{t+\Delta t}\int_{\Delta V}\frac{\partial C}{\partial t}dVdt=\int_t^{t+\Delta t}\int_{\Delta V}D\frac{\partial^2 C}{\partial x_i{}^2}dVdt-\int_t^{t+\Delta t}\int_{\Delta V}V\frac{\partial C}{\partial x_i}dVdt-\int_t^{t+\Delta t}\int_{\Delta V}(\mu C+S)dVdt \tag{A-29}$$

The diffusion derivatives can be approximated with the central difference. An upwind approximation is used for the advection derivatives. Taking diffusion and advection approximation in *x*-direction as an example, the equation as shown as follow:

$$\int_t^{t+\Delta t}\int_{\Delta V}D\frac{\partial^2 C}{\partial x_i{}^2}dVdt\approx\int_t^{t+\Delta t}\left(AD_e\frac{C_E-C_P}{\Delta x_{PE}}\right)-\left(AD_w\frac{C_P-C_W}{\Delta x_{WP}}\right)dt \tag{A-30}$$

$$\int_t^{t+\Delta t}\int_{\Delta V}V\frac{\partial C}{\partial x_i}dVdt\approx\int_t^{t+\Delta t}A(V_eC_P-V_wC_W)dt\ ,\ V_e>0,\ V_w>0 \tag{A-31}$$

$$\int_t^{t+\Delta t}\int_{\Delta V}V\frac{\partial C}{\partial x_i}dVdt\approx\int_t^{t+\Delta t}A(V_eC_E-V_wC_P)dt\ \ ,\ V_e<0,\ V_w<0 \tag{A-32}$$

where, subscript *e* and *w* mean the face e and w, subscript *E*, *P* and *W* mean the node *E*, *P* and *W*. *A* is the area of faces, Δx means the length of two interior nodes. The other parameters are mentioned above.

The time discretization of Equation 3-19 is performed by a forward approximation. Combing the previous expression, the FVM solution to the governing equation for n+1 time is obtained:

$$a_P C_P = a_e C_E + a_w C_W + a_s C_S + a_n C_N + a_b C_B + a_t C_T + a_{p0} C_P^n + S - F \tag{A-33}$$

where

$$a_p = \frac{1}{\Delta t} + \frac{\left(D_e + D_w\right)}{\Delta x^2} + \frac{V_e}{\Delta x} + \frac{\left(D_n + D_s\right)}{\Delta y^2} + \frac{V_n}{\Delta y} + \frac{\left(D_t + D_b\right)}{\Delta z^2} + \frac{V_t}{\Delta z} + \mu \tag{A-34}$$

$$a_w = \frac{D_w}{\Delta x^2} + \frac{V_w}{\Delta x}, a_s = \frac{D_s}{\Delta y^2} + \frac{V_s}{\Delta y}, a_b = \frac{D_b}{\Delta z^2} + \frac{V_b}{\Delta z} \tag{A-35}$$

$$a_e = \frac{D_e}{\Delta x^2}, a_n = \frac{D_n}{\Delta y^2}, a_t = \frac{D_t}{\Delta z^2} \tag{A-36}$$

$$a_{p0} = \frac{1}{\Delta t} \tag{A-37}$$

B: Supporting Material for Chapter 7

Table B-1 physical and chemical properties of PFOS (Kong et al., 2018; Lindim et al., 2016; Su, Lu, et al., 2018)

Parameters	Definition	Value
H	Henry's constant	4.75×10^{-4}
$Log(K_{oc})$	Organic-carbon partition coefficients	2.7
$Log(K_{ow})$	Octanol–water partition coefficient	4.49
K_a	Degradation rate in air (1/day)	6.26×10^{-5}
K_w	Degradation rate in water (1/day)	4.36×10^{-6}
K_s	Degradation rate in soil (1/day)	1.66×10^{-7}
K_{se}	Degradation rate in sediment (1/day)	1.41×10^{-6}

Table B-2 Characteristics of the river streams (Hu and Li, 2009; Hydrologic Bureau of the Ministry of Water Resources, China, 2013)

Section No.	Section Name	River	Average width (m)	Depth (m)	Flow rate (10^7 m^3/d)	Velocity (10^3 m/d)
1	DJB-1	Dongjiang	500	5.0	7.81	31.24
2	DJB-2	Dongjiang	500	5.0	5.18	20.74
3	DJB-3	Dongjiang	500	5.0	3.72	14.86
4	DYH	Dongjiang	450	5.0	1.47	6.53
5	DJN-1	Dongjiang	450	5.0	2.63	11.67
6	DJN-2	Dongjiang	300	5.0	1.30	8.64
7	HJD	Dongjiang	300	5.0	1.33	8.87
8	DJN-3	Dongjiang	600	5.0	2.63	8.76
9	BJ-1	Beijiang	600	10	12.36	20.59
10	BJ-2	Beijiang	500	15	10.63	14.17
11	BJ-3	Beijiang	600	7.5	8.38	18.62
12	BJ-4	Beijiang	400	7.5	6.13	20.45
13	XHD	Zhujiang	300	7.5	1.73	7.68
14	QHD-1	Zhujiang	400	7.5	0.86	2.88
15	HHD-1	Zhujiang	450	7.5	0.86	2.56
16	HHD-2	Zhujiang	500	7.5	1.47	3.92
17	GZSD	Zhujiang	400	7.5	0.26	0.86
18	QHD-2	Zhujiang	400	7.5	1.12	3.74

Section No.	Section Name	River	Average width (m)	Depth (m)	Flow rate (10^7 m^3/d)	Velocity (10^3 m/d)
19	HHD-3	Zhujiang	500	7.5	1.21	3.23
20	ZJZG-1	Zhujiang	1000	10	2.33	2.33
21	ZJZG-2	Zhujiang	2000	15	6.05	2.02
22	ZJZG-3	Zhujiang	2000	15	7.52	2.51
23	ZJZG-4	Zhujiang	2000	15	10.14	3.38

Table B-3 Soil compartment area in each subarea (Resource and Environment Data Cloud Platform, 2015)

Subarea	1	2	3	4	5	6	7	8
Soil area (km^2)	180.2	167.7	220.3	180.2	173.0	106.2	235.6	250.5

Table B-4 Properties of soil and air zone (Daggupaty et al., 2006; Mackay et al., 1996; Nobel, 2009; Pennington et al., 2005; Zhang et al., 2015)

Soil zone (Mackay et al., 1996; Zhang et al., 2015)	
Depth (m)	0.1
Solid phase density (kg/m^3)	2400
Volumetric water fraction	0.3
Volumetric air fraction	0.2
Volumetric soil fraction	0.5
Diffusion coefficient from soil to air (m/d)	0.48
Runoff rate of dissolved phase (m/d)	9.36×10^{-4}
Ruoff rate of solids in soil (m/d)	5.52×10^{-7}
Air zone (Daggupaty et al., 2006; Nobel, 2009; Pennington et al., 2005)	
Height (m)	100
Average velocity in x-direction (m/d)	7361
Average velocity in y-direction (m/d)	6510
Eddy diffusivities (m^2/d)	4320
Diffusion coefficient from air to water (m/d)	0.51
Diffusion coefficient from water to air (m/d)	2.43×10^{-5}
Dry deposition velocity (m/d)	1.44×10^{-4}
Normalized scavenging coefficient (d/mm d)	0.79
Precipitation intensity (mm/d)	4.8

Table B-5 Organism properties used for the food web (Hu et al., 2014; R. Sun et al., 2017; Zhang et al., 2010)

Group	V (cm^3)	L	GR(d^{-1})	Fd (d^{-1})	Aw	Ao
Detritus	2.23×10^{-7}	0.005	5.26×10^{-2}	0	5.30×10^{-8}	4
Phytoplankton	2.04×10^{-8}	0.015	1.95×10^{-1}	0	5.30×10^{-8}	4
Zooplankton	2.71×10^{-4}	0.015	9.86×10^{-2}	5.10×10^{-1}	5.30×10^{-8}	4
Macrophyte	1.83×10^{-1}	0.015	8.22×10^{-3}	3.29×10^{-2}	5.30×10^{-8}	3.5
Herbiorous feeders	6.90×10^{3}	0.048	8.22×10^{-3}	4.11×10^{-2}	5.30×10^{-8}	1.5
Crucian carp	2.80×10^{1}	0.04	5.78×10^{-3}	7.13×10^{-2}	5.30×10^{-8}	1.5
Mud carp	3.50×10^{2}	0.03	5.75×10^{-3}	3.84×10^{-2}	5.30×10^{-8}	1.5
Tilapia	2.50×10^{2}	0.035	9.97×10^{-3}	5.86×10^{-2}	5.30×10^{-8}	1.5
Grass carp	5.00×10^{2}	0.045	5.29×10^{-3}	2.93×10^{-2}	5.30×10^{-8}	1.5
Common carp	1.35×10^{3}	0.048	4.58×10^{-3}	3.57×10^{-2}	5.30×10^{-8}	1.5
Leather catfish	7.59×10^{2}	0.028	4.93×10^{-3}	1.43×10^{-2}	5.30×10^{-8}	1.5

Note: V, organism volume; L, lipid volume fraction; GR, growth rate; Fd, feeding rate; Aw, gut absorption efficiency for water; Ao, gut absorption efficiency for lipids.

Table B-6 The monitored PFOS levels in aquatic species (Pan, Zhao, et al., 2014)

	Species	Min	Max	Mean	Standard deviation
G6	Crucian carp	0.63	18.97	5.33	5.6
G7	Mud carp	0.19	0.65	0.43	0.2
G8	Tilapia	0.63	55.00	13.7	12.0
G9	Grass carp	n.d.	10.54	1.73	3.1
G10	Common carp	0.16	79.15	8.70	22.0
G11	Leather catfish	12.5	24.09	17.30	61.0

Note: n.d. means no data.

References:

Daggupaty, S. M., Banic, C. M., Cheung, P., & Ma, J. (2006). Numerical simulation of air concentration and deposition of particulate metals around a copper smelter in northern Quebec, Canada. *Geochemistry: Exploration, Environment, Analysis*, *6*(2-3), 139-146. https://doi.org/10.1144/1467-7873/05-094

Domenico, P. (1987). An analytical model for multidimensional transport of a decaying contaminant species. *Journal of Hydrology*, *91*(1-2), 49-58.

Hu, J., & Li, S. (2009). Modeling the mass fluxes and transformations of nutrients in the Pearl River Delta, China. *Journal of Marine Systems*, *78*(1), 146-167. https://doi.org/10.1016/j.jmarsys.2009.05.001

Hu, Y., Gong, X., Xu, Y., Song, X., Liu, H., Deng, X., & Ru, S. (2014). Risk assessment of butyltins based on a fugacity-based food web bioaccumulation model in the Jincheng Bay mariculture area: I. model development. *Environmental Science: Processes & Impacts*, *16*(8), 1994-2001. DOI: 10.1039/C4EM00219A

Hydrologic Bureau of the Ministry of Water Resources, China (2013). *Annual hydrological report, P.R. China*. Hydrologic Bureau of the Ministry of Water Resources, China.

Kong, X., Liu, W., He, W., Xu, F., Koelmans, A. A., & Mooij, W. M. (2018). Multimedia fate modeling of perfluorooctanoic acid (PFOA) and perfluorooctane sulphonate (PFOS) in the shallow lake Chaohu, China. *Environmental Pollution*, *237*, 339-347. https://doi.org/10.1016/j.envpol.2018.02.026

Lindim, C., van Gils, J., & Cousins, I. T. (2016). A large-scale model for simulating the fate & transport of organic contaminants in river basins. *Chemosphere*, *144*, 803-810. https://doi.org/10.1016/j.chemosphere.2015.09.051

Mackay, D., Di Guardo, A., Paterson, S., & Cowan, C. E. (1996). Evaluating the environmental fate of a variety of types of chemicals using the EQC model. *Environmental Toxicology and Chemistry: An International Journal*, *15*(9), 1627-1637. https://doi.org/10.1002/etc.5620150929

Merrick, D. G., Malan, A. G., & van Rooyen, J. A. (2018). A novel finite volume discretization method for advection–diffusion systems on stretched meshes. *Journal of Computational Physics*, *362*, 220-242. https://doi.org/10.1016/j.jcp.2018.02.025

Nobel, P. S. (2009). Plants and fluxes. In P. S. Nobel (Ed.), *Physicochemical and Environmental Plant Physiology (Fourth Edition)* (pp. 438-505). Academic Press. https://doi.org/10.1016/B978-0-12-374143-1.00009-0

Van Genuchten, M. T., & Alves, W. (1982). *Analytical solutions of the one-dimensional convective-dispersive solute transport equation*. US Department of Agriculture, Agricultural Research Service.

Pan, C. G., Zhao, J. L., Liu, Y. S., Zhang, Q. Q., Chen, Z. F., Lai, H. J., Peng, F. J., Liu, S. S., & Ying, G. G. (2014). Bioaccumulation and risk assessment of per- and polyfluoroalkyl substances in wild freshwater fish from rivers in the Pearl River Delta region, South China. *Ecotoxicology and Environmental Safety*, *107*, 192-199. https://doi.org/10.1016/j.ecoenv.2014.05.031

Pennington, D. W., Margni, M., Ammann, C., & Jolliet, O. (2005). Multimedia fate and human intake modeling: Spatial versus nonspatial insights for chemical emissions in Western Europe. *Environmental Science & Technology*, *39*(4), 1119-1128. https://doi.org/10.1021/es034598x

Resource and Environment Data Cloud Platform. (2015). *Remote sensing monitoring data of land use status in China at 2015.* Retrieved August 12, 2019 from http://www.resdc.cn/data.aspx?DATAID=184

Sheu, T. W. H., & Chen, Y. H. (2002). Finite element analysis of contaminant transport in groundwater. *Applied Mathematics and Computation*, *127*(1), 23-43. https://doi.org/10.1016/S0096-3003(00)00160-0

Su, C., Lu, Y., Wang, T., Lu, X., Song, S., Li, L., Khan, K., Wang, C., & Liang, R. (2018). Dynamic multimedia fate simulation of Perfluorooctane Sulfonate (PFOS) from 1981 to 2050 in the urbanizing Bohai Rim of China. *Environmental Pollution*, *235*, 235-244.

https://doi.org/10.1016/j.envpol.2017.12.045

Sun, R., Luo, X., Tang, B., Chen, L., Liu, Y., & Mai, B. (2017). Bioaccumulation of short chain chlorinated paraffins in a typical freshwater food web contaminated by e-waste in south china: Bioaccumulation factors, tissue distribution, and trophic transfer. *Environmental Pollution*, *222*, 165-174. https://doi.org/10.1016/j.envpol.2016.12.060

Zhang, B. Z., Ni, H. G., Guan, Y. F., & Zeng, E. Y. (2010). Occurrence, bioaccumulation and potential sources of polybrominated diphenyl ethers in typical freshwater cultured fish ponds of South China. *Environmental Pollution*, *158*(5), 1876-1882. https://doi.org/10.1016/j.envpol.2009.10.043

Zhang, Q. Q., Ying, G. G., Pan, C. G., Liu, Y. S., & Zhao, J. L. (2015). Comprehensive evaluation of antibiotics emission and fate in the river basins of China: Source analysis, multimedia modeling, and linkage to bacterial resistance. *Environmental Science & Technology*, *49*(11), 6772-6782. https://doi.org/10.1021/acs.est.5b00729